The two level system under the influence of non-commuting fluctuations

Timo Palm

Hamburg
2020

The two level system under the influence of non-commuting fluctuations

Dissertation
zur Erlangung des Doktorgrades
an der Fakultät für Mathematik, Informatik,
Naturwissenschaften
Fachbereich Physik
der Universität Hamburg

vorgelegt von
Timo Palm
aus Norderstedt

Hamburg
2020

Gutachter der Dissertation:	Prof. Dr. Peter Nalbach Prof. Dr. Michael Thorwart
Zusammensetzung der Prüfungskommission:	Prof. Dr. Peter Nalbach Prof. Dr. Michael Thorwart Prof. Dr. Robert Blick Prof. Dr. Daniela Pfannkuche Prof. Dr. Alexander Lichtenstein
Datum der Disputation:	19.10.2020
Vorsitzender Fach-Promotionsausschuss PHYSIK:	Prof. Dr. Günter Hans Walter Sigl
Leiter des Fachbereichs PHYSIK:	Prof. Dr. Wolfgang Hansen
Dekan an der Fukultät MIN:	Prof. Dr. Heinrich Graener

Contents

I think it's much more interesting to live not knowing than to have answers which might be wrong. I have approximate answers and possible beliefs and different degrees of uncertainty about different things, but I am not absolutely sure of anything and there are many things I don't know anything about, such as whether it means anything to ask why we're here. I don't have to know an answer. I don't feel frightened not knowing things, by being lost in a mysterious universe without any purpose, which is the way it really is as far as I can tell.

Richard P. Feynman

Abstract

This thesis is investigating the different influences of correlated and uncorrelated environmental fluctuations on a two level system. These correlations are of quantum mechanical nature, since they are the result of non-commuting operators coupled to the dynamics of the degrees of freedom from a bath or multiple ones. This model has a wide variety of applications which are highly relevant modern research topics. The most prominent example is a qubit, where the dissipative properties are of up most importance. Negligence of one of the non-commuting fluctuations only allows for an insufficient description of the noise sources and thereby inhibit the attempt to correctly identify which of the ones are important and possibly reduce their influence. The correlated as well as uncorrelated fluctuations are relevant in the description of voltage gates, used to control quantum dots, but also to correctly describe the influence of electromagnetic fields, lasers and crystals defining the various realisations of qubits.

In the first half of this thesis I show the relevant theoretical foundations and extend them to arrive at a correct description of non-commuting fluctuations. Therein, I first discuss the system-bath model and its fundamental concepts, show the solution of the dynamics of an isolated two level system in Liouville space and use them to introduce two methods. First I present RESPET, a perturbative theory, through the derivation of the dephasing rate in the Spin-Boson model. Then, I extend RESPET by introducing a master equation to model an additional, pure dephasing bath effectively. Afterwards I show the resulting propagator for two fully correlated, non-commuting fluctuations and then continue on to analyse two uncorrelated, non-commuting fluctuations. Here, I find a contribution of the pure dephasing fluctuations to the relaxation rate, thereby showing the presence of a second uncorrelated bath can change fundamental properties of a bath. Next an introduction in the numerically exact method called QUAPI is given, which I then combine with a master equation approach. Afterwards I derive an extension of QUAPI for two non-correlated fluctuations, which I then simplify to model one of the baths influences by pure dephasing fluctuations and the other by relaxational fluctuations.

In the second half of this thesis I give a detailed investigation of the models used. Here, I first show how an extension of RESPET and QUAPI by a simple master equation yield fundamental problems, since both models start to diverge drastically. There after I use the simplified QUAPI scheme for uncorrelated fluctuations as well as the original QUAPI scheme for fully correlated fluctuations and discover severe differences. I analyse whether and when in which regimes both fluctuations can be treated as additive. I observe differences between fully correlated and uncorrelated fluctuations at all temperatures investigated. Fully correlated fluctuations result in a transition of the two level system to the overdamped regime at lower temperatures and bath coupling strengths then additive as well as uncorrelated fluctuations. At low temperatures the dephasing rate is enhanced for fully correlated fluctuations, compared to additive ones, for certain strengths of pure dephasing fluctuations. The uncorrelated fluctuations consistently decrease the dephasing rate at low temperatures. Next I investigate the relaxation of the two level system under these influences. Both fully correlated and uncorrelated fluctuations consistently lower the relaxation rate for increased pure dephasing fluctuations, thus additive fluctuations fail to model either uncorrelated or fully correlated fluctuations. Uncorrelated fluctuations show higher order effects even at weak to moderate coupling strengths of the dephasing fluctuations. These higher order effects can even be reduced by increasing the relaxational coupling strength. This shows the introduction of a second bath can modify the scale of a bath, thereby making an interpretation of regime as weak more complicated. Finally, I study a symmetric two level system under the influence of polarized baths for an Ohmic pure dephasing bath and a relaxational bath that is either sub-Ohmic or Ohmic. Such a model is a description for superconduction charge qubits being cooled to low temperatures, thereby polarizing the environment. I find a polarized relaxational bath creates an effective asymmetry in the two level system, while a polarized dephasing bath creates a shift in the oscillation frequency.

Zusammenfassung

In dieser Dissertation werden die unterschiedlichen Einflüsse von korrelierten und unkorrelierten Umgebungsfluktuation, auf ein Zwei-Niveau-System untersucht. Diese Korrelationen sind quantenmechanischer Natur, da sie aus nicht kommutierenden Operatoren stammen, die an die Dynamik der Freiheitsgrade eines oder mehrere Bäder gekoppelt sind. Dieses Modell hat eine große Breite an Anwendungen, die hoch relevante, moderne Forschungsthemen sind. Das hervorstechenste Beispiel ist das Qubit, dessen dissipative Eigenschaften von enormer Bedeutung sind. Ein Vernachlässigen einer der nicht kommutierenden Fluktuationen erlaubt nur eine unzureichende Beschreibung der Rauschquellen und verhindert dadurch den Versuch der korrekten Idenifikation, welche der Rauschquellen signifikant sind und ob es möglich ist deren Einfluss zu verringern. Korrelierte wie unkorrelierte Fluktuationen sind relevant in der Beschreibung der Spannungs-Gates, die in der Kontrolle von Quantenpunkten genutzt werden, ebenso wie in der korrekten Beschreibung des Einflusses von elektromagnetischen Feldern, Lasern und Kristallen, die die unterschiedlichen Realiserungen von Qubits bestimmen.

Im ersten Teil der Dissertation präsentiere ich das notwendige theoretische Fundament und erweitere es, um eine korrekte Beschreibung von nicht kommutierenden Fluktuationen zu erreichen. Dabei diskutiere ich erst das System-Bad-Modell und seine grundlegenden Eigenschaften, zeige die Lösung der Dynamik eines isolierten Zwei-Niveau-Systems im Liouvilleraum und nutze dies um zwei Methoden einzuführen. Zunächst stelle ich RESPET, eine störungstheoretische Technik, anhand der Herleitung der Dephasierungsrate im Spin-Boson-Modell vor. Danach erweitere ich RESPET, indem eine Mastergleichung eingeführt wird, die ein zusätzliches, pures Dephasierungbad effektiv modelliert. Hiernach zeige ich den resultierenden Propagator für zwei voll korrelierte, nicht kommutierende Fluktuationen und fahre dann fort mit der Analyse zweier unkorrelierter, nicht kommutierender Fluktuationen. Dabei finde ich einen Beitrag von pur dephasierende fluktuationen zu der Relaxationsrate, wodurch gezeigt wird, dass die Gegenwart eines zweiten, unkorrelierten Bades die fundamentalen Eigenschaften eines Bades ändern kann. Als nächstes führe ich die numerisch exakte Methode QUAPI ein, welche ich dann mit einer Mastergleichung Methode kombiniere. Danach leite ich die Erweiterung von QUAPI für zwei nicht kommutierende Fluktuationen

her, die ich dann vereinfache, um den Einfluss eines der Bäder als pur dephasierende Fluktuationen und den des anderen Bades als relaxationierende Fluktuationen zu modellieren.

Im zweiten Teil der Dissertation präsentiere ich eine detailierte Untersuchung der benutzten Modelle. Ich zeige zunächst, wie eine Erweiterung von RESPET und QUAPI mit einer simplen Mastergleichung zu fundamentalen Problemen führt, da beide Modelle anfangen drastisch voneinander abzuweichen. Dann nutze ich die vereinfachte QUAPI-Erweiterung für nicht korrelierte Fluktuationen, sowie die ursprüngliche QUAPI Methode für voll korrelierte Fluktuationen und entdecke gravierende Unterschiede. Ich analysiere ob und wenn in welchen Regimen die beiden Fluktuationen additiv behandelt werden können. Ich stelle Unterschiede zwischen voll und unkorrelierten Fluktuationen bei allen untersuchten Temperaturen fest. Voll korrelierte Fluktuationen resultieren in einem Übergang des Zwei-Niveau-Systems in das überdämpfte Regime bei niedrigeren Temperaturen und System-Bad-Kopplungsstärken als sowohl unkorrelierte Fluktuationen als auch additiv behandelte Fluktuationen. Bei niedrigen Temperaturen wird die Dephasierungsrate von voll korrelierten Fluktuationen erhöht, verglichen mit additiven Fluktuatonen, in bestimmten Bereichen der Kopplungstärke der pur dephasierenden Fluktuationen. Unkorrelierte Fluktuationen reduzieren die Dephasierungsrate durchweg bei niedrigen Temperaturen. Als nächstes untersuche ich die Relaxation des Zwei-Niveau-Systems unter diesen Einflüssen. Sowohl voll korrelierte, als auch unkorrelierte Fluktuationen reduzieren durchgängig die Relaxationsrate für anwachsende Kopplungsstärken pur dephasierender Fluktuationen, daher versagen additive Fluktuationen bei der Beschreibung von sowohl unkorrelierten, als auch von voll korrelierten Fluktuationen. Unkorrelierte Fluktuationen zeigen höhere Ordnungseffekte bereits bei schwachen und moderaten Kopplungsstärken pur dephasierender Fluktuationen. Diese höheren Ordnungseffekte können reduziert werden durch ein Erhöhen der Kopplungsstärke der relaxierenden Fluktuationen. Dies zeigt, dass das Einführen eines zweiten Bades kann die Skala eines Bades modifizieren und dadurch die Interpretation eines Regimes als schwaches Kopplungsregime komplizierter machen. Zum Ende studiere ich ein symmetrisches Zwei-Niveau-System unter dem Einfluss polarisierter Bäder mit einem ohmschen, puren Dephasierungsbad und einem relaxierendem Bad, das entweder ohmsch oder sub-ohmsch ist. Ein solches Modell beschreibt das Kühlen supraleitender Ladungsqubits zu niedrigen Temperaturen, wodurch die Umgebung polarisiert wird. Ich stelle fest, dass ein polarisiertes relaxierendes Bad eine effektive Asymmetrie erzeugt, während ein polarisierendes Dephasierungsbad eine Verschiebung der Oszillationsfrequenz erzeugt.

Chapter 1

Introduction

We have been observing the tides in the oceans for millennia and have understood the gravitational force of the solar system as their source some centuries ago. Similarly, humans have used boiling water to make otherwise indigestible supplies of food useful, without understanding how the exposure to a heat bath breaks down molecule bonds and fundamentally changes the structure of the proteins. More recently, most households have a fridge, here food is stored in a cold box and the surrounding temperature cools the organic matter. Thereby, the molecular processes are slowed down and decay is inhibited. These are examples of a system of interest such as the oceans or proteins, being exposed to a larger system, such as the solar system or an external heating or cooling source. Such a larger system is considered an environment or a bath. System-bath models are useful for a wide variety of applications and play an important role in understanding physical phenomena. The idea is to effectively describe, how these environments act on a system of interest without treating the whole environment explicitly, such that the gravitational force on the ocean is modelled without describing the dynamics of the planets in detail or to model the exchange of temperature between the proteins and their bath without a precise description of the atoms of neither the boiling water nor the cold air in the freezer.

Physicists started describing the exposure to heat/cold baths in static scenarios in greater detail in the context of thermodynamics in the 19.-th century. This resulted in the description of systems as micro-canonical, canonical and great canonical ensembles, introducing the bath concept in theoretical physics. Derived from these thermodynamical concepts is the idea of the partition function and, deeply connected to it, the density matrix. The latter, in equilibrium, connects the temperature of a system to the energy of its underlying micro states and thereby describes their population via the Boltzmann distribution. Thus, allowing a detailed description of an infinite system, continuous as well as discrete. When quantum mechanics was newly developed in the 1920's, these two concepts were incorporated into it, first by Landau in 1927 [1] and shortly afterwards by von Neumann [2]. Whereas non-equilibrium dynamics were partially already discussed in the early days of thermodynamics, the Carnot process immediately comes to mind as well as the second law of thermodynamics, a detailed, microscopic description of how a small quantum system reaches equilibrium, came to be much later. Even though Dirac introduced Fermi's Golden rule in 1927 [3, 4], describing the transition from a quantum state into a continuum of states, it took until the 50's and 60's, when non-equilibrium dynamics were formalised by the introduction of **open quantum dynamics** [5–8].

Open quantum dynamics are employed to discuss a vast range of modern physical problems. A few prominent examples are the description of relaxation and decoherence of quantum systems due to fluctuations induced by their environment, such as quantum dots [9–11] or lasers [12–14], charge or energy transport dynamics in crystal structures or, in the form of exciton dynamics, along molecules [15–17] as well as spectroscopy in molecular systems [18].

Qubits [19, 20] are a research topic of high interest, they are the quantum mechanical equivalent of the bit, the basis of the modern computer. The classical bit is created by transistors and has two possible states. Either a current flows through the transistor or not, which translates into one or zero and is used to encode information. A qubit allows to circumvent this limitation of classical transistors. This can improve computer processors in unprecedent ways, leading towards a new age of computational power which can drastically influence human life. A theoretical description, as accurate as possible, is therefore of immense importance on the way to quantum computing. In general, a qubit is a quantum two level system. It allows to go beyond a binary system of only ones and zeros and instead use amplitudes of quantum mechanical states, e. g. complex numbers, to store information. Experimental realisations of the qubit have been proposed in various ways.

The main realisations of qubits, which are being investigated at this time, are: Qubits based on optical coherent states, which can be used over large distances, though photon-photon-interaction is weak and therefore manipulation of these states is problematic [21–26]. Qubit systems based on ion traps have been realized with up to 20 qubits in a chain and are a promising candidate for quantum computing. Such qubits are arranged in a lattice defined by electromagnetic fields in vacuum [27–32]. Qubits composed of nuclear spins can be created, which are difficult to interact with experimentally but therefore experience relatively long coherence times [33–38]. Qubits are also realized through superconducting quantum interference devices (SQUIDS) based on Josephson junctions. There have been systems of ten qubits with full control realized and even systems of 72 qubits with limited control [39–44]. Majorana Fermions, which were demonstrated experimentally in 2012 [45], are an exiting application for qubits [46–50]. Their topological protection might allow for longer coherence times but also make them hard to interact with experimentally. Another realisation of qubits are based on quantum dots [51], which can be used as two types of qubits, either as spin qubits [52–55] or as charge qubits [56–59]. The advantage lies in highly precise manipulation of the dots by voltage gates with the downside of relatively short lived coherence times.

There are multiple ideas combining a few of these approaches. Since nuclear spin qubits are difficult to manipulate, it was proposed to use them as storage for qubits based on quantum dots [60]. Another interesting combination of ideas is the usage of quantum dots to interact with Majorana Fermions. The Majorana edge modes in a superconducting nanowire are brought into contact with a quantum dot, which in turn is used to prepare and measure the amplitude of the edge mode [61,62]. A recent proposal, in cooperation with Microsoft, uses this idea [63]. In combinations like these with quantum dots, the decoherence of the two level system is dominated by dissipative properties of the dot.

All qubit realisations are subject to environmental fluctuations which induce dissipation in these systems. A major challenge is to control and reduce the decoherence time of the qubits. Thus, a two level system in connection with an environment is a relevant model for all qubits, regardless of their type. In most cases the dissipative influence is modelled either via an effective flcutuation of one bath or via additive fluctuations of multiple baths. However, in many cases experimentalist find long relaxation times while the dephasing times are short. This gave rise to the idea that there are more dephasing then relaxation channels. To understand how such different fluctuations are created, the focus is going to be on quantum dot qubits. These incredible quantum mechanical systems have many practical uses besides qubits such as lasers, solar cells and single electron transistors [64–67], and they all have dephasing and relaxation environments [68].

A quantum dot is subject to multiple environmental fluctuations coupled to **non-commuting** system-bath operators. Since these fluctuations do not commute, they can be non-additive. It is not clear, if these fluctuation interfere with each other constructively or destructively and in what ways set up schemes of quantum dots could be modified to minimize the decoherence rate. For temperature $T = 0$ a competing behaviour in relaxation to the eigenbasis of the respective fluctuation has been demonstrated [69]. At finite temperature such a behaviour might explain longer relaxation times. While one can consider multiple fluctuations from different sources, such as the phonons of the underlying crystal structure or the electron scattering on defects, it already suffices to focus on the fluctuations in the voltage gates controlling the quantum dot to see non-commuting fluctuations arise. A closer look at an experimental set-up of a quantum dot will help to see this in detail.

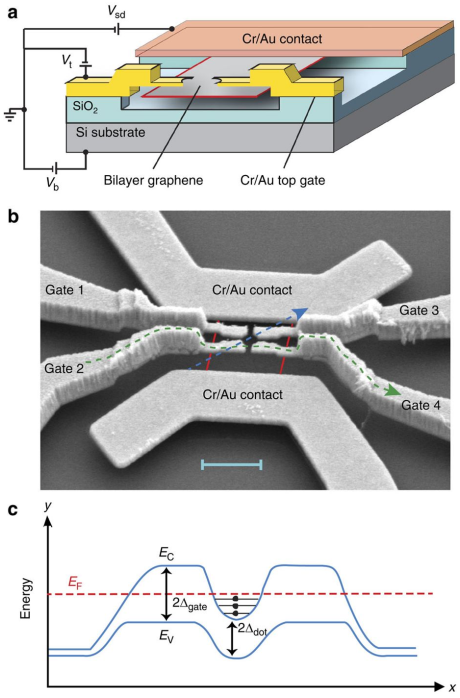

Figure 1.1: In (a) the schematic cross-section of a suspended gate-defined bilayer graphene quantum dot is shown. Graphene is deposited on a thermally grown SiO_2 layer followed by electron-beam litography steps to define Cr/Au electrodes, an evaporated SiO_2 spacer layer and local top gates. The electric field and carrier density profiles are controlled with back and top gate voltages V_b and V_t. In (b) a scanning electron micrograph of a similar quantum dot device is shown. The green line represents a cross-sectional cut through the device corresponding to visualisation in (a) while the clue line represents one corrsepong to (c). In (c) the quantum dot formation is illustrated in a cross-sectional cut of energy vs position at magnetic field $B = 0$. E_C and E_V mark the edges of the conductance and valence bands. This figure is taken from [70] .

The quantum dot set-up, which will serve as an example, was done by M.T. Allen et al. in reference [70] and is shown in Figure 1.1. Here, the electric field effect in bilayer graphene is used in the production of quantum confined structures by applying an external electric field and inducing a bandgab in graphene. Local gating further distorts the band structure such that a potential well, and thus the quantum dot, is created [71]. The local voltage gates determine the depth of the potential well and thus play an important role for electron transport on and from the dot, effectively controlling a tunnel barrier. A scanning electron micrograph of a similar set-up of gates is shown in Figure 1.1 b). Additionally, the energy level splitting in the potential well is tunable via separate voltage gates. This distorted band structure is schematically shown in Figure 1.1 c). If the level splitting is chosen large enough, only a single bound state is possible in the potential well. By further introducing a magnetic field B a spin qubit can be created, allowing only one electron on the quantum dot. The energy vs position sketch then has multiple potential wells, corresponding to the induced Landau levels. If done correctly, only two states are possible with either an electron on the dot or not. Thus, a Two-Level-System (TLS) describes the system Hamiltonian accurately. The induced bandgap is further manipulated by two additional gates, called top and back gate, with voltages V_t and V_b. These gates are illustrated in Figure 1.1 a). Allen et al. give a relationship between their voltages and the energy level splitting Δ as $\Delta \propto E = (\alpha V_t - \beta V_b)/2e\epsilon_0$. Thus, the voltage fluctuations in the level splitting are independent of the fluctuations in the tunnel barrier while they both do not commute. A good microscopic description of the system would be in the form of the asymmetric TLS: $\Delta\sigma_x + \epsilon\sigma_z$, where $\epsilon\sigma_z$ describes the tunnel barrier. In this picture it is is easy to see how the fluctuations do not commute since they contribute to different Pauli matrices. Furthermore, if one considers a further simplification to a symmetric TLS by neglecting the tunnel barrier, the top and back gate only contribute to the decoherence of the dot states and not their relaxation. The neglect of the tunnel barrier would be an aim for the Mayorana-quantum dot combination [63]. This is achievable by setting the energy level of the single bound state as close as possible to the maximum potential of the well. Thereby, a level splitting which is large against the tunnel barrier is created. This allows for a high possibility of electron exchange between the edge mode and the dot, as desired. In this set up the top and back voltages create pure dephasing noise, while they induce no additional relaxation. They can be interpreted as additional dephasing channels and will be called **pure dephasing baths** throughout this thesis. The gates controlling the depth of the potential well induce coherence as well as relaxation, such baths will be called **relaxational baths**.

Therefore, non-commuting fluctuations are in general a relevant source of decoherence in this kind of qubit realisation. Where the case of additional pure dephasing fluctuations are of special interest to control the dissipative properties. Gaining a better understanding of these sources of noise is going to be the main goal of this thesis.

The question remains how to model such scenarios in terms of the system-bath formalism. The coupling between the system and the bath is commonly modelled as bilinear [6]. In many cases, the Markov approximation is sufficient. It assumes a separation of time scales, thus environmental correlations to decay rapidly in comparison with the correlations of the system. Also, it assumes an environment which does not change meaningfully with time due to the interaction with the system. One example for a physical scenario where this approach was employed successfully, is the description of atom lasers [12,72], where the photon field is the environment and a single atom is modelled as a discrete system. For cases where the approximation is valid, the system dynamics can be simulated by master equations, which modify the von- Neumann equation. Popular and widely used are the Lindblad equations [73–75]. In this form, the master equation ensures positivity of the density matrix, preventing probabilities from becoming negative and thus illogical. Additionally the conservation of the trace is ensured thereby keeping the sum over all probabilities in the system equal to one. With new experimental techniques to create and manipulate nanosystems, approaches beyond the Markov approximation have become increasingly necessary to accurately describe them. In quantum dots but also in exciton dynamics in biological systems non-Markovian dynamics are evident. A good example for a typical relevant system environment situation, where the separation of the time scales fails, is the environment in semi conductors. It is sub-Ohmic, e.g. 1/f type noise, and therefore has long lived correlations [76–79]. Non-Makovian master equations have been proposed and used to accurately describe such scenarios [80,81]. A non-Markovian approach, essential for this thesis, is the path integral one done by Feynman and Vernon [6], which integrates out the environmental influence and relates it to the Feynman-Vernon influence functional. This approach is exact and has been applied in a wide variety of work [82–88]. The method called hierarchical equations of motion (HEOM) [84] and the closely related hierarchy of pure states (HOPS) [89], are based on the influence functional. They are both numerically exact but can not use arbitrary spectral densities. Problematic spectral densities are modelled by a sum of treatable spectral densities, usually exponentials, instead. HEOM derives auxiliary density operators which are coupled via differential equations and the reduced density matrix of the system is obtained by solving these differential equations. HOPS couples pure states of the system in such a hierarchy of differential equations instead. The Keldysh formalism is another alternative [90, 91], in which contour integrals are solved, to analytically derive expressions for Greens' functions, which are then solved numerically . Another method is called the stochastic Schrödinger equations, in which Monte Carlo simulations are employed [92, 93] to treat a vector of states in the Hilbertspace of the system and propagate it. In this thesis the method called QUAPI, also based on the Feynman-Vernon influence functional, is used for exact numerical simulations. QUAPI discretizes the Feynman-Vernon influence functional and employs an iterative tensor propagation scheme. The numerical cost is related to the size of the tensor and the convergence investigation. While in general, numerically more expensive than the HEOM approach, it allows to include arbitrary spectral densities. Additionally,it is possible to add a large numbers of baths, as long as their system-bath coupling operators commute with each other [94] with negligible additional numerical costs. This can also be applied to non-commuting system-bath operators, as long the additional fluctuations commute with one of the non-commuting fluctuations. Practically, in the example of Allen et al. the top and the back gate can be treated as two such commuting fluctuations, assuming they act only on the level splitting Δ, while the other gates are treated as commuting with each other as well, assuming these only act on the barrier strength ϵ.

In the first chapters of this thesis, the theoretical groundwork is done to derive the methods used. In chapter 2 a brief introduction to system-bath description is depicted. In chapter 3, the dynamics of an isolated TLS is solved, using and introducing the Liouville formalism of quantum mechanics.

Chapter 4 uses the framework of the previous chapters to show how to derive the perturbative treatment called RESPET and utilize it, to gain some insight into the effect of non-commuting fluctuations resulting from two different baths on the symmetric TLS. Additionally, the influence of two non-commuting fluctuations coupled to a single bath on the symmetric TLS is studied.

This allows for a comparison between fully correlated and fully uncorrelated fluctuations. Also, RESPET and master equations are combined in a form called Hybrid-RESPET. In chapter 4 the derivation of the QUAPI scheme, as proposed by Makri et al in 1995 [83] [95], with an initial short detour to its basis done by Grabert et al. in 1988 [82], is given as well as the known extension to multiple, commuting baths [96]. Afterwards, the extension of QUAPI for multiple non-commuting fluctuations is derived, in the general case and for a pure dephasing bath. This allows to simulate pure dephasing channels and the resulting method was published in reference [97]. Furthermore, the combination of QUAPI and Lindblad equations into a Hybrid-QUAPI is shown as well.

In Chapter 6, Hybrid-QUAPI and Hybrid-RESPET are compared. Here a problem emerged, the resulting decoherence rate of both methods diverge drastically with increased weight of the Lindblad equation in the model. This was the motivation for deriving a numerically exact method beyond a combination of master equations. These results have been published in reference [98].

In chapter 7, the derived QUAPI form for pure dephasing and relaxational fluctuations is used to investigate the decoherence and relaxation properties of the TLS for multiple temperatures and multiple system-bath coupling strengths for Ohmic spectral densities. These findings are compared to fully correlated fluctuations, which have the same form of system operators coupled to a single bath and to additive fluctuations. These results will be published soon [99].

In Chapter 8 we study a TLS under the influence of a sub-Ohmic pure dephasing bath with either an Ohmic or a sub-Ohmic relaxational bath. This reflects a typical environment of a superconducting phase qubit. Cooling protocols of such devices leave the baths polarized, thus we investigate polarized baths in such an environment. Our findings have been published in reference [100].

Chapter 2

Non-equilibirum physics: The system-bath model

There are different approaches to include dissipation in quantum physics. The one used throughout this work is a system of interest coupled to a bath of infinite uncoupled harmonic oscillators, which are kept in thermal equilibrium at a fixed temperature T. It is assumed that the interaction with the system can not change this temperature. The generic Hamiltonian is given by:

$$\begin{aligned} H_{gen} &= H_S + \sum_j \left\{ \frac{p_j^2}{2m_j} + \frac{1}{2} m_j \omega_j^2 \left(x_j - \frac{c_j O}{m_j \omega_j^2} \right)^2 \right\} \qquad (2.1) \\ &= H_S + \sum_j \left\{ \frac{p_j^2}{2m_j} + \frac{1}{2} m_j \omega_j^2 x_j^2 - c_j O x_j + \frac{c_j^2 O^2}{m_j \omega_j^2} \right\} \quad . \end{aligned}$$

Throughout this work $\sum_j \equiv \sum_{j=1}^{N_{bath}}$ denotes the sum over all N_{bath} oscillators that make up the bath. H_{gen} consists of four parts. A system part H_S, which contains the information of the quantum system of interest subjected to fluctuations. An often used case is that of a free particle in a potential with $H_S = \frac{p_S^2}{2m_S} + V_S$, where p is the momentum of the particle, m_S the mass of the particle and V_S the potential it is subjected to. Another part of H_{gen} is $H_B = \left\{ \sum_j \frac{p_j^2}{2m_j} + \frac{1}{2} m_j \omega_j^2 x_j^2 \right\}$, which is called the bath Hamiltonian. It consists of uncoupled bath oscillators with positions x_j, momenta p_j, frequencies ω_j and mass m_j of the j.-th oscillator. The number of oscillators N_{bath} is usually large and often the limit $N \to \infty$ is taken. The interaction between the bath oscillators and the system is modelled with a bilinear coupling as $H_{SB} = -O \sum_j c_j x_j$, where O is an operator on the system Hilbert space. Intuitively, one would believe this to be sufficient to model the interaction between two such systems. It is, however, necessary to include the counter term $H_{counter} = \frac{c_j^2 O^2}{m_j \omega_j^2}$ to ensure the potential given by V_S remains unchanged by the bath, such that the properties one wishes to include in the microscopic model are unchanged. To illustrate this, consider a Hamiltonian $H_{gen,int} = H_S + H_B + H_{SB}$, without $H_{counter}$, such that:

$$H_{gen,int} = H_S + \sum_j \frac{1}{2} m_j \omega_j^2 \left(x_j - \frac{c_j O}{m_j \omega_j^2} \right)^2 - \frac{c_j^2 O^2}{m_j \omega_j^2} \quad . \tag{2.2}$$

Since the bath is assumed to be in thermal equilibrium, the oscillators, its composed of, should be in their respective potential minima [101]. This way, one finds a correction to the system Hamiltonian, giving a new potential $\widetilde{V_S} = V_S - \frac{c_j^2 O^2}{m_j \omega_j^2}$, which in principle can change the fundamental behaviour of the system one wishes to investigate. To illustrate this, one might consider a particle in a harmonic potential (harmonic oscillator) as the system with $H_S = \frac{p_S^2}{2m_S} + \frac{1}{2}\omega_S^2 m_S x_S^2$ which is coupled via its position $O = X_s$ the potential would become $\widetilde{V_S} = (\omega_S^2 - \sum_j \frac{c_j^2}{m_j \omega_j^2}) x_S = \widetilde{\omega}_S^2 X_S^2$. Depending on the choice of the bath parameter $\widetilde{\omega}_S^2 < 0$ is possible. In this limit the model description becomes unphysical. This particle would not simply be a free particle, but one which experiences an infinitely decreasing potential and would be accelerated even for $x_S \to \pm\infty$. The bath would generate infinite energy in the system, creating a perpetuum mobile. While this is an extreme example to show problems that might occur, in many cases with the right choice of bath parameters, this effect is less drastic. To deal with this problem within our model description the simplest way possibly is to simply subtract the correction of the system potential from $H_{gen,int}$, giving rise to the fourth term in H_{gen} the counter term $H_{counter}$ with $H_{gen} = H_{gen,int} + H_{counter}$, countering the correction of the system potential in way, that in the potential minimum of the bath the system potential is given by V_S.

2.1 Quantum Langevin Equation

The generic Hamiltonian can be used to derive a quantum Langevin equation. The classical generalized Langevin equation describes a stochastic force acting on a Brownian particle and thus creates dissipation for the particle [8]. A bath system can exert as such a stochastic force on the system. Analogously a Brownian particle coupled to a bath via its position $O = x_S$ in a general position dependent potential $V(x_S)$ is considered here. By using the definition $p_\alpha(t) = m_\alpha \dot{x}_\alpha$ coupled differential equations can be derived for x_S and the x_j's from the Heisenberg equation of motion:

$$m_S\ddot{x}_S = -\frac{d}{dx_S}V(x_S) - \sum_j c_j(\frac{c_j}{m_j\omega_j^2}x_S - x_j) \ , \tag{2.3}$$

and

$$m_j\ddot{x}_j = -m_j\omega_j^2 x_j - c_j x_S \ . \tag{2.4}$$

Equation (2.4) is an inhomogeneous differential equation with solutions $x_j(t) = x_{j,hom}(t) + x_{j,inh}(t)$, which, inserted in Equation (2.3), give:

$$\begin{aligned} m_S\ddot{x}_S + \int_0^t ds\left(\sum_j \frac{c_j^2}{m_j\omega_j^2}\cos(\omega_j(t-s))\right)\dot{x}_S(s) + \frac{d}{dx_S}V(x_S) \\ = \sum_j c_j\left[x_j(0)\cos(\omega_j t) + \frac{\dot{x}_j(0)}{\omega_j}\sin(\omega_j t) - \frac{c_j}{m_j\omega_j^2}x_S(0)\cos(\omega_j t)\right] \ . \end{aligned} \tag{2.5}$$

It is now possible to introduce a damping kernel $\gamma(t) = \frac{1}{m_S}\sum_j \frac{c_j^2}{m_j\omega_j^2}\cos(\omega_j t)$ and an operator-valued force $\Gamma(t) = \sum_j c_j\left[x_j(0)\cos(\omega_j t) + \frac{\dot{x}_j(0)}{\omega_j}\sin(\omega_j t)\right]$, giving Equation (2.5) the form:

$$m_S\ddot{x}_S + m_S\int_0^t ds\gamma(t-s)\dot{x}_S(s) + \frac{d}{dx_S}V(x_S) = \Gamma(t) - m_S\gamma(t)x_S(0) \ . \tag{2.6}$$

The Equation of motion (2.6) is a generalized Langevin equation, extended by an inhomogeneous term $m_S\gamma(t)x_S(0)$, which is an initial slip. Further evaluation makes a discussion of initial conditions of the bath necessary, since the random force $\Gamma(t)$ is dependent on the initial conditions of the bath $x_j(0)$ and $p_j(0)$. A useful and physically meaningful choice is, to assumes the bath to be at thermal equilibrium, $\rho_B = \exp(-\beta H_B)/Z_B$, with $Z_B = \mathrm{Tr}_B\left\{\exp(-\beta H_B)\right\}$. The expectation value of the bath is defined as $\langle O\rangle_B = \mathrm{Tr}_B\left\{O\exp(-\beta H_B)\right\}$. The force $\Gamma(t)$ thus becomes a stochastic force and its bath expectation is value zero. For the autocorrelation function $L(t-s)$ follows:

$$\begin{aligned}L(t-s) &= \langle\Gamma(t)\Gamma(s)\rangle_B = \langle\Gamma(t-s)\Gamma(0)\rangle_B \\ &= \hbar\sum_j \frac{c_j^2}{2m_j\omega_j}\left[\coth(\hbar\omega_j\beta/2)\cos(\omega_j(t-s)) - i\sin(\omega_j(t-s))\right] \ .\end{aligned} \tag{2.7}$$

It is convenient to define the spectral density $J(\omega)$ as:

$$J(\omega) = \frac{\pi}{2}\sum_j \frac{c_j^2}{m_j\omega_j}\delta(\omega-\omega_j) \ , \tag{2.8}$$

such that

$$\langle\Gamma(t)\Gamma(s)\rangle_B = \frac{\hbar}{\pi}\int_0^\infty d\omega J(\omega)\left[\coth(\hbar\omega\beta/2)\cos(\omega(t-s)) - i\sin(\omega(t-s))\right] \ . \tag{2.9}$$

It is also possible to express the damping kernel $\gamma(t)$ in terms of the spectral density:

$$\gamma(t) = \frac{2}{m_s\pi}\int_0^\infty d\omega\frac{J(\omega)}{\omega^2}\cos(\omega t) \ . \tag{2.10}$$

All of the influence of the bath on the system can be expressed via $J(\omega)$. This becomes obvious, if one looks at Equation (2.3) and notes that the sum over the bath degrees of freedom is now expressed by a general integral over all possible frequencies ω, which are sampled by the spectral density. A bath can therefore be described in terms of its spectral density.

In the limit $N_{bath} \to \infty$ and with the assumption that the eigenfequencies ω_j's are so dense as to form a continuous spectrum, the spectral density $J(\omega)$ becomes a smooth function of ω. The form used throughout this work is:

$$J(\omega) = \gamma\omega_c^{1-s}\omega^s f_{cut-off}(\omega,\omega_c) \ . \tag{2.11}$$

Where the constant γ is called the coupling strength of the bath, $f_{cut-off}(\omega,\omega_c)$ is a dimensionless cut-off function. The cut-off frequency ω_c limits the energies of the bath, such that larger frequencies are suppressed, while introducing a short-time scale ω_c^{-1}. This spectral density is called sub Ohmic for $s < 1$, Ohmic for $s = 1$ and super Ohmic for $s > 1$, each case describes different physical situations. The transition between these regimes can play an important role in the description of environments. A spectral density describing acoustic phonons in semi conductors such as Ga/As can be modelled for low frequencies as super-Ohmic with $J(\omega) \propto \omega^3$, while for high frequencies the behaviour is sub-Ohmic with $J(\omega) \propto \omega^{-1}$ [102]. Sub Ohmic noise is of high interest for qubits, since it is generic for all disordered materials and common in single electron devices [76–79].

2.2 Master equations

Master equations are a powerful and widely used approach to simulate quantum mechanical many body interactions such as in quantum optics [12], condensed matter physics [103], quantum chemistry [104] as well as quantum thermodynamics [105]. They can be derived for a huge variety of situations. One of the earliest known examples is Landau's paper from 1927 describing emmission [1]. Very prominent are the Redfield equations [101] and the Lindblad equations [73], both are markovian and have been used for an astonishing number of publications, more recently works beyond these approaches such as non-Markovian master equations [80] and non-additive master equations [106] have been published. Here the focus will be on master equations in Lindblad form, since they were employed in this project [98]. This approach modifies the von Neumann equation by introducing additional terms:

$$\frac{\partial}{\partial t}\rho = \frac{i}{\hbar}[\rho, \mathrm{H}] + \Gamma\rho = \mathcal{L}_{Lind}\rho \quad . \tag{2.12}$$

Where $\Gamma\rho = \sum_j V_j^\dagger \rho V_j - \frac{1}{2}\{V_j^\dagger V_j, \rho\}$ and V_j a system operator. This form ensuress the conservation of the trace and the positivity of all diagonal elements of ρ. The dynamics becomes Liovillian instead of Hamiltonian, which inclines one to use superoperators. The modified von Neumann equation can be solved, yielding a new system time evolution operator $U_{S,M}$. We combine the master equation approach with a numerically exact simulation method, Hybrid-QUAPI for details see chapter 5.3, and with a perturbative theory, Hybrid-RESPET for details see chapter 4.4.

Chapter 3

The Two Level System in Liouville space

The Two Level System (TLS) is one of the simplest systems imaginable, consisting only of two states. It has been investigated intensively [7] and is a widely used toy model with applications in broad spectrum of modern physics, such as description of a spin, polarized photons, atomic lasers and of course qubits and the mixing of states. It is often used in connection with other systems, such as in the description of masers in the Jaymes-Cummings-Model [107], where it is used to model an atom in connection with a photon field. More recently the TLS has been used to model defects in glasses [108, 109], quantum dots in interaction with their environment [63, 110] as well as molecules in fluids [111, 112]. The TLS Hamiltonian is given by:

$$H_{asym.TLS} = \frac{1}{2}\Delta\sigma_x + \frac{1}{2}\epsilon\sigma_z \ . \tag{3.1}$$

This is called the asymmetric TLS, while for either $\Delta = 0$ or $\epsilon = 0$ this is called the symmetric TLS.

3.1 The Liouville space: Introduction

The Liouville space is a formulation of quantum mechanics in which operators are represented as vectors and superoperators, which act as matrices on operators are introduced. To understand what superoperators are, it is helpful to look at the underlying tensor structure of quantum mechanics. For a Hilbert space with basis vectors e_i and scalar product $e_i(e^j) = \delta_i^j$. The Hilbert space of the TLS has dimension 2 and any eigenstates consists of two vectors, for example e_1 and e_2. Operators like the position x or momentum p are matrices acting on the basis elements of the Hilbert space. Mathematically speaking they are (1,1)-tensors which have basis elements $e_i \otimes e^j$. A superoperator is a (2,2)-tensor acting on the operators of the Hilbert space, they have basis elements $e_i \otimes e_j \otimes e^k \otimes e^l$. Propose an operator $A = e_a \otimes e^b$ and a superoperator $S = e^c \otimes e^d \otimes e_f \otimes e_g$. The convention used in this thesis is: $S(A) = e^c \otimes e^d \otimes e_f \otimes e_g(e_a \otimes e^b) \equiv e^c \otimes e^d(e_a) \otimes e_f \otimes e_g(e^b) = e^c \otimes e_f \delta^d_a \delta^b_g$. To differentiate between the vectors of the Hilbert space, f.e. $|a\rangle$ for an eigenvector of an operator A, in this theses the convention $|A)$, for the operator A itself, is used. The scalar product of Liouville space is defined as $(A|B) = \mathrm{Tr}\{A^\dagger B\}$. Two important examples of superoperators are the response operator of an operator O: $\widetilde{O} = i[O,.]$, and the correlation operator of O: $\overline{O} = \frac{1}{2}\{O,.\}$.

$$\widetilde{A}|B) = |i[A,B]) \ . \tag{3.2}$$

For the TLS a useful basis for the operators are the three Pauli matrices and the identity matrix. In tensor algebra they are represented as $\sigma_x = e_1 \otimes e^2 + e_2 \otimes e^1$, $\sigma_y = i(-e_1 \otimes e^2 + e_2 \otimes e^1)$,$\sigma_z = e_1 \otimes e^1 - e_2 \otimes e^2$ and $\mathbb{1} = e_1 \otimes e^1 + e_2 \otimes e^2$. For the Pauli matrices $[\sigma_1, \sigma_2] = 2i\sigma_3\epsilon_{123}$ with $(123) \equiv (xyz)$ and ϵ_{123} the Levi-Civita-Symbol. The convention used here is $|O) = O_{\mathbb{1}}\mathbb{1} + O_x\sigma_x + O_y\sigma_y + O_z\sigma_z \equiv (O_{\mathbb{1}}, O_x, O_y, O_z)^T$.

Often one is interested in correlation and response functions, the representation in Liouville space is the following. For the response function:

$$R_{AB}(t,0) = i\langle A(t)B(0) - B(0)A(t)\rangle = (\mathbb{1}|\overline{A}\mathcal{U}\widetilde{B}|\rho(0)) \ . \tag{3.3}$$

For the correlation function:

$$C_{AB}(t,0) = \frac{1}{2}\langle A(t)B(0) + B(0)A(t)\rangle = (\mathbb{1}|\overline{A}\mathcal{U}\overline{B}|\rho(0)) \ . \tag{3.4}$$

Notice $\langle A(t)B(0)\rangle = 2C_{AB}(t,0) - iR_{AB}(t,0)$

3.1.1 Dynamics of the TLS in Liouville space

The dynamics of the TLS is given by the von-Neumann equation:

$$\frac{d}{dt}|\rho) = -i[H,\rho] = -\widetilde{H}|\rho) = -\frac{\Delta}{2}\widetilde{\sigma}_x|\rho) =: L|\rho) \ , \tag{3.5}$$

where L is called the Liovillian super operator. A formal solution of the von-Neumann equation can be obtained with the following steps:

$$|\rho(t)) = \mathcal{U}(t)\rho(0) \ . \tag{3.6}$$

Thus

$$\frac{d}{dt}\mathcal{U}(t) = L\mathcal{U}(t) \ , \tag{3.7}$$

giving the solution

$$\mathcal{U}(t) = \mathcal{T}\exp\left[\int_0^t L(s)ds\right] \ , \tag{3.8}$$

where $\mathcal{T}$ is the time ordering operator. Since H_{TLS} does not depend on time it follows that:

$$\mathcal{U}(t) = \exp\left[-\frac{\Delta * t}{2}\widetilde{\sigma}_x\right] \ . \tag{3.9}$$

For Hermitian dynamics the identity $\mathcal{U}(t)|\rho(0)) = U(t)\rho(0)U^{-1}(t)$ holds. Calculation of $\exp[\frac{\Delta}{2}\widetilde{\sigma}_x]$ is straightforward. First one has to find a matrix form of $\widetilde{\sigma}_x$. It is easy to calculate how $\widetilde{\sigma}_x$ acts on $|\rho(t))$:

$$\begin{aligned}\widetilde{\sigma}_x|\rho(t)) &= \widetilde{\sigma}_x[\rho_{\mathbb{1}}(t)|\mathbb{1}) + \rho_x(t)|\sigma_x) + \rho_y(t)|\sigma_y) + \rho_z(t)|\sigma_z)] = i(\rho_y(t)|[\sigma_x,\sigma_y]) + \rho_z(t)|[\sigma_x,\sigma_z])) \\ &= (0, 0, 2\rho_z(t), -2\rho_y(t))^T \ .\end{aligned} \tag{3.10}$$

In matrix form thus:

$$\widetilde{\sigma}_x \begin{pmatrix} \rho_{\mathbb{1}}(t) \\ \rho_x(t) \\ \rho_y(t) \\ \rho_z(t) \end{pmatrix} = \begin{pmatrix} 0 \\ 0 \\ 2\rho_z(t) \\ -2\rho_y(t) \end{pmatrix} \ , \tag{3.11}$$

therefore

$$\widetilde{\sigma}_x = \begin{pmatrix} 0 & 0 & 0 & 0 \\ 0 & 0 & 0 & 0 \\ 0 & 0 & 0 & 2 \\ 0 & 0 & -2 & 0 \end{pmatrix} . \tag{3.12}$$

Now the super operator propagator can be calculated:

$$\begin{aligned} \mathcal{U}(t) = \exp\left[-\frac{\Delta * t}{2}\widetilde{\sigma}_x\right] &= \sum_{j=0}^{\infty}\left(-\frac{\Delta * t}{2}\right)^{j}\frac{\widetilde{\sigma}_x^{j}}{j!} = \sum_{j=0}^{\infty}\left(-\frac{\Delta * t}{2}\right)^{2j+1}\frac{-\widetilde{\sigma}_x^{2j+1}}{(2j+1)!} + \sum_{j=0}^{\infty}\left(-\frac{\Delta * t}{2}\right)^{2j}\frac{\widetilde{\sigma}_x^{2j}}{2j!} \\ &= \begin{pmatrix} 1 & 0 & 0 & 0 \\ 0 & 1 & 0 & 0 \\ 0 & 0 & -\cos[\Delta * t] & \sin[\Delta * t] \\ 0 & 0 & -\sin[\Delta * t] & -\cos[\Delta * t] \end{pmatrix} . \end{aligned} \tag{3.13}$$

This form of $\mathcal{U}(t)$ allows a few important statements to be made. A fundamental property of the density matrix is $\mathrm{Tr}\{\rho\} = 1$ for all times. For the trace of all Pauli matrices is zero except for the identity:$\mathrm{Tr}\{\mathbb{1}\} = 2$, therefore $\rho_{\mathbb{1}} = \frac{1}{2}$. Since this has to hold for all times, the first row in $\widetilde{U}(t)$ can only contain zero's at off-diagonal elements. The eigenstates of the σ_x are the two vectors $\frac{1}{\sqrt{2}}(1,1)$ and $\frac{1}{\sqrt{2}}(1,-1)$, the corresponding density matrix elements are $\frac{1}{2}(\mathbb{1} + \rho_x\sigma_x)$ and $\frac{1}{2}(\mathbb{1} - \rho_x\sigma_x)$ respectively. Since the second row of $\mathcal{U}(t)$ also only contains 0 at off-diagonal elements, it follows that ρ_x is constant and thus also the population of the eigenstates remains constant. This shows a fundamental property of the von-Neumann equation: in pure quantum dynamics there is no dissipation but infinite coherent oscillations with no change of the population of the energy states. The Liouville formulation now allows for simple manipulations to introduce relaxation and decoherence by changing L. While the first row always has to be a zero vector, the second row can be changed to introduce relaxation, $L_{22} < 0$ and $L_{21} \rightarrow const.$ for $t \rightarrow \infty$ and to mix decoherence and relaxation $L_{23} \neq 0$ and $L_{24} \neq 0$. By introducing changes in the third and fourth row one can introduce pure dephasing rates, see for example [98], if one limits oneself to the third and fourth column. Introducing non-zero values in the second column mixes the population dynamics into the dephasing, while introducing non zero values into the first column, σ_z and σ_y do not vanish any more in the equilibrium. Thus the eigenbasis of the physical problem changes.

Chapter 4

RESPET: The dissipating two level system in a perturbative treatment

4.1 Spin-Boson model: The 1-loop approximation

RESPET is a resumed perturbative approach in Liouville space. This introduction of RESPET is along the line of thought of the derivation done by Nalbach and Thorwart in [113]. Continuing with the formalism of the previous chapter, the connotation is changed such that the U introduced before will be renamed into U_S, from now on the pure system propagator. To model the TLS in an environment that introduces dissipation the **Spin-Boson model** (SBM) [7] has been developed. The generic system-bath Hamiltonian of Equation (2.1) for the SBM reads:

$$H = H_S + H_{SB} + H_B + H_{counter} = \frac{\Delta}{2}\sigma_x + \frac{\sigma_z}{2}\sum_j c_j x_j + \frac{1}{2}\sum_j \frac{p_j^2}{m_j} + m_j\omega_j^2 x_j^2 + \frac{c_j^2}{4m_j\omega_j^2} \quad . \tag{4.1}$$

Note the counter term is proportional to $\sigma_z^2 = \mathbb{1}$, thus commutes with the density matrix $W(t)$, therefore does not contribute to L and can be neglected in the following derivation. Now interpret $H_{SB} = \frac{\sigma_z}{2}\sum_j c_j x_j$ as a perturbation of $H_0 = H_B + H_S = \frac{\Delta}{2}\sigma_x + \frac{1}{2}\sum_j \frac{p_j^2}{m_j} + m_j\omega_j^2 x_j^2$. The formal solution of the Liouvillian is given by $\mathcal{U} = Te^{\int_0^t dsL*s}$, following $L = L_0 + L_{SB}$ and $\mathcal{U}_0 = Te^{\int_0^t dsL_0*s} = \mathcal{U}_S \otimes \mathcal{U}_B$. If one assumes a system initially uncorrelated with the bath, then: $\rho(0) = \rho_S(0) \otimes \rho_B^{Boltz}(0)$. It holds that $\langle \mathcal{U}_0(t,0)\rangle_B = \mathrm{Tr}_{bath}\{\mathcal{U}_0(t,0)\rho_B^{Boltz}(0)\} = \mathcal{U}_S(t,0)$, where $\langle . \rangle_B$ denotes the expectation value of the bath, obtained by tracing out the bath degrees of freedom. Now it is possible to write down a Dyson equation for this Hamiltonian. Using $\mathcal{U}(a,b) = \mathcal{U}(a-b)$, one finds:

$$\begin{aligned}\mathcal{U}(t) &= \mathcal{U}_0(t) + \int_0^t ds \mathcal{U}_0(t-s) L_{SB} \mathcal{U}(s) \\ &= \mathcal{U}_0(t) + \int_0^t ds \mathcal{U}_0(t-s) L_{SB} \mathcal{U}_0(s) + \int_0^t \int_0^s ds ds' \mathcal{U}_0(t-s) L_{SB} \mathcal{U}_0(s-s') L_{SB} \mathcal{U}(s') \ .\end{aligned} \tag{4.2}$$

Assuming a large enough bath, such that the energy Δ is negligibly small against the sum of the energy of all the bath oscillators, it can also be assumed that the $\mathcal{U}_S$ is affected by the bath, while $\mathcal{U}_B$ is not affected by the system. Thus the propagator of interest is the effective system propagator, obtained by $\langle \mathcal{U}(t,0) \rangle_B$. Calculating the bath expectation value of the Dyson equation one obtains:

$$\begin{aligned}\mathcal{U}_{eff}(t) =& \mathcal{U}_S(t) + \int_0^t ds \langle \mathcal{U}_0(t-s) L_{SB} \mathcal{U}_0(s) \rangle_B \\ &+ \int_0^t \int_0^s ds ds' \langle \mathcal{U}_0(t-s) L_{SB} \mathcal{U}_0(s-s') L_{SB} \mathcal{U}(s') \rangle_B \ .\end{aligned} \tag{4.3}$$

The second term vanishes since:

$$\int_0^t ds \langle \mathcal{U}_0(t-s) L_{SB} \mathcal{U}_0(s) \rangle_B \propto \sum_j \langle x_j(s) \rangle_B = 0 \ . \tag{4.4}$$

Here the cyclic permutation of the trace was used and $\rho_B(s) = \rho_B(0)$, since ρ_B is assumed to be initially in equilibrium, as well as $\langle x_k \rangle = 0$ for harmonic oscillators at equilibrium, hence oscillators that are not displaced. Equation (4.3) is a one loop Dyson equation, where 'loop' denotes expectation values of the type $\langle x_j(t_1) x_j(t_2) \rangle$ as fundamental objects. These can be viewed as a form of irreducable Feynman diagrams. Hence, all correlation functions are expressed in these objects, such that higher order correlations of the type $\langle x_j(t_1) x_j(t_2) \rangle \langle x_j(t_3) x_j(t_4) \rangle$, for $t_1 < t_2 < t_3 < t_4$, are considered, while $\langle x_j(t_1) x_j(t_3) \rangle \langle x_j(t_2) x_j(t_4) \rangle$ are not. The treatment of the third term makes an approximation necessary.

$$\int_0^t \int_0^s ds ds' \langle \mathcal{U}_0(t-s) L_{SB} \mathcal{U}_0(s-s') L_{SB} \mathcal{U}(s') \rangle_B = \int_0^t \int_0^s ds ds' \mathcal{U}_S(t-s) \mathcal{M}(s-s') \mathcal{U}_{eff}(s') \ . \tag{4.5}$$

Where $M(s-s') = \langle L_{SB} \mathcal{U}_0(s-s') L_{SB} \rangle_B$ and a mean-field type approximation is employed according to [114]. Application of a Laplace transformation allows to solve the integrals in this equation. A short reminder of the Laplace transformation: $LT[f(t)] = i\int_0^\infty dte^{izt}f(t) \equiv f(z)$ is the transformation of the function $f(t)$. The back-transformation is defined as $f(t) = \frac{1}{2\pi i}\int_{-\infty}^{\infty} dte^{-izt}f(z)$, with the conditions that $f(z)$ is an analytical function and $Im(z) > 0$ as well as $f(t \to \infty) < \infty$. Now one can make use of the convolution theorem for the Laplace transformation: $LT[\int_0^t dsf(t-s)g(s)] = -iLT[f(t)]LT[g(t)]$:

$$\begin{aligned} LT[\mathcal{U}_{eff}(t)] = \mathcal{U}_{eff}(z) &= \mathcal{U}_S(z) - \mathcal{U}_S(z)M(z)\mathcal{U}_{eff}(z) \\ &= (\mathcal{U}_S^{-1}(z) + \mathcal{M}(z))^{-1} \ . \end{aligned} \tag{4.6}$$

$\mathcal{U}_S(t)$ was calculated in the previous chapter, performing the Laplace transformation one finds:

$$\mathcal{U}_S(z) = \begin{pmatrix} -z^{-1} & 0 & 0 & 0 \\ 0 & -z^{-1} & 0 & 0 \\ 0 & 0 & \frac{-z}{z^2-\Delta^2} & \frac{i\Delta}{z^2-\Delta^2} \\ 0 & 0 & \frac{-i\Delta}{z^2-\Delta^2} & \frac{-z}{z^2-\Delta^2} \end{pmatrix} \quad \text{and} \quad \mathcal{U}_S^{-1}(z) = \begin{pmatrix} -z & 0 & 0 & 0 \\ 0 & -z & 0 & 0 \\ 0 & 0 & -z & -i\Delta \\ 0 & 0 & i\Delta & -z \end{pmatrix} \ . \tag{4.7}$$

Now only $\mathcal{M}(z)$ is left to obtain, therefore L_{SB} has to be analyzed in more detail: $L_{SB} = -\widetilde{H_{SB}} = -\frac{1}{2}\sum_j c_j\widetilde{\sigma_z x_k} = -\frac{1}{2}\sum_j c_j\,(\widetilde{\sigma}_z\overline{x_k} + \overline{\sigma_z}\widetilde{x}_k)$ with this:

$$\begin{aligned} 4\mathcal{M}(s-s') &= \overline{\sigma_z}U_S(s-s')\overline{\sigma_z}\sum_{jk} c_jc_k\langle\widetilde{x}_jU_B(s-s')\widetilde{x}_k\rangle_B + \overline{\sigma_z}U_S(s-s')\widetilde{\sigma}_z\sum_{jk} c_jc_k\langle\widetilde{x}_jU_B(s-s')\overline{x}_k\rangle_B \\ &\quad + \widetilde{\sigma}_zU_S(s-s')\overline{\sigma_z}\sum_{jk} c_jc_k\langle\overline{x}_jU_B(s-s')\widetilde{x}_k\rangle_B + \widetilde{\sigma}_zU_S(s-s')\widetilde{\sigma}_z\sum_{jk} c_jc_k\langle\overline{x}_jU_B(s-s')\overline{x}_k\rangle_B \\ &= \widetilde{\sigma}_zU_S(s-s')\overline{\sigma_z}\sum_{j} c_j^2\langle\overline{x}_jU_B(s-s')\widetilde{x}_j\rangle_B + \widetilde{\sigma}_zU_S(s-s')\widetilde{\sigma}_z\sum_{j} c_j^2\langle\overline{x}_jU_B(s-s')\overline{x}_j\rangle_B \\ &= \widetilde{\sigma}_zU_S(s-s')\overline{\sigma_z}\sum_{j} c_j^2R_{qq,j}(s-s') + \widetilde{\sigma}_zU_S(s-s')\widetilde{\sigma}_z\sum_{j} c_j^2C_{qq,j}(s-s') \ . \end{aligned} \tag{4.8}$$

where $R_{qq,j}(t) = \frac{1}{m_j\omega_j}\Theta(t)\sin(\omega_jt)$ is the response function of the k-th bath oscillator and $C_{qq,j}(t) = \frac{1}{2m_j\omega_j}\cos(\omega_jt)\coth(\beta\frac{\omega_j}{2})$ and $\langle\widetilde{x}_jA\rangle_B = 0$, for arbitrary A. After a change to the continuum representation for sufficiently large N_{bath}, with $\sum_k \to \int_0^\infty d\omega$, the correlation and response functions of the bath can be expressed by the spectral density $J(\omega)$, introduced in chapter 2.1 . This leads to the bath response function $\sum_j c_j^2 R_{qq,j}(s-s') = \int_0^\infty \frac{d\omega}{4\pi} 2J(\omega)\sin(\omega(s-s')) \equiv R_{qq}$ and the bath correlation function $\sum_j c_j^2 C_{qq,j}(s-s') = \int_0^\infty \frac{d\omega}{4\pi} J(\omega)\coth(\beta\omega/2)\cos(\omega(s-s')) \equiv C_{qq}(s-s')$. The kernel $M(t)$ thus has the form:

$$\mathcal{M}(s-s') = \begin{pmatrix} 0 & 0 & 0 & 0 \\ 2R_{qq}(s-s')\sin(\Delta(s-s')) & -4C_{qq}(s-s')\cos(\Delta(s-s')) & 0 & 0 \\ 0 & 0 & -4C_{qq}(s-s') & 0 \\ 0 & 0 & 0 & 0 \end{pmatrix}, \quad (4.9)$$

which is in Laplace space:

$$\mathcal{M}(z) = \begin{pmatrix} 0 & 0 & 0 & 0 \\ \Xi(z) & \chi(z) & 0 & 0 \\ 0 & 0 & \Theta(z) & 0 \\ 0 & 0 & 0 & 0 \end{pmatrix}. \quad (4.10)$$

with $\Xi(z) = B_R(z)^{\omega-\Delta} - B_R(z)^{\omega+\Delta}$, $\chi(z) = 2(B_C(z)^{\omega-\Delta} + B_C(z)^{\omega+\Delta})$ and $\Theta(z) = -4B_C(z)$. With $B_R(z) = LT\{R_{qq}(t)\}$ and $B_C(z) = LT\{C_{qq}(t)\}$. The upper index in $B^\alpha_{R/C}$ indicates a change of ω in the argument of cos or sin, such that $R^\alpha_{qq}(t) = \int_0^\infty \frac{d\omega}{4\pi} 2J(\omega)\sin(\alpha t)$ and correspondingly in C_{qq}. This result together with Equation (4.7) allows to calculate the inverse in Equation (4.6).

$$\mathcal{U}_{eff}(z) = \begin{pmatrix} -z^{-1} & 0 & 0 & 0 \\ a(z) & b(z) & 0 & 0 \\ 0 & 0 & \frac{z}{p(z)} & \frac{-i\Delta}{p(z)} \\ 0 & 0 & \frac{i\Delta}{p(z)} & \frac{z+\Theta(z)}{p(z)} \end{pmatrix}, \quad (4.11)$$

with $a(z) = \frac{\Xi(z)}{\chi(z)} \frac{-\chi(z)}{z(z+\chi(z))}$, $b(z) = -(z+\chi(z))^{-1}$ and $p(z) = \Delta^2 - z^2 - 2z\Gamma(z)$. The one loop characteristic becomes apparent if one analyses the components of $U_{eff}(z)$ on the basis of Equation (4.6), which can be rewritten as $\mathcal{U}_{eff}(z) = \mathcal{U}_S(z)(1 + \mathcal{U}_S(z)\mathcal{M}(z))^{-1} = \mathcal{U}_S(z)(1 + \alpha(z))^{-1}$. The corresponding Taylor series in $\alpha(z)$ gives: $\mathcal{U}_{eff}(z) = \mathcal{U}_S(z)\sum_{m=0}^\infty (-1)^m \alpha^m(z)$. Since α consists of 1-loops, α^m is a product of m such 1-loops.

$\mathcal{U}_{eff}$ allows the calculation of the expectation value of any given system operator in the given approximation for any choice of $\rho_S(0)$. The expectation value for an operator O is given by:

$$\begin{aligned}\langle O(z)\rangle &= \Big(\mathbb{1}\,\big|\overline{O}\mathcal{U}_{eff}(z)\big|\,\rho_S(0)\Big) \\ &= \Big(\mathbb{1}\,\big|\overline{O}\big| - \frac{1}{2}z^{-1}\mathbb{1} + (\frac{1}{2}a(z) + b(z)\rho_x(0))\sigma_x\Big) \\ &+ \Big(\mathbb{1}\,\big|\overline{O}\big|\,p(z)^{-1}(z\rho_y(0) - i\Delta\rho_z(0))\sigma_y + p^{-1}(z)(i\Delta\rho_y(0) + (z+\Theta(z))\rho_z(0))\sigma_z\Big) \\ &= -z^{-1}O_{\mathbb{1}} + 2(\frac{1}{2}a(z) + b(z)\rho_x(0))O_x + 2p^{-1}(z)(z\rho_y(0) - i\Delta\rho_z(0))O_y \\ &+ 2p^{-1}(z)(i\Delta\rho_y(0) + (z+\Theta(z))\rho_z(0))O_z \ .\end{aligned} \tag{4.12}$$

To investigate the dissipation of the TLS the relevant expectation values are $P_z \equiv \langle\sigma_z\rangle$ and $P_x \equiv \langle\sigma_x\rangle$. To study decoherence the time evolution P_z has to be analysed while to study relaxation P_x is the quantity of interest. For relaxation a system initially in an excited stated is sensible, implying the choice $\rho_S(0) = 0.5(\mathbb{1} + \sigma_x)$, with this initial condition the resulting expectation value becomes: $P_x(z) = 0.5(a(z) + b(z))$. A useful choice for the initial density matrix to investigate decoherence is $\rho_S(0) = 0.5(\mathbb{1} + \sigma_z)$, implying a state of full coherence with equal population in ground and excited state. Then the expectation value is given by: $P(z) = \frac{z+2\Theta(z)}{p(z)}$. Even in Laplace space these results are quite useful. The dynamics are decoupled in two sectors. The $\mathbb{1}\sigma_x$ sector governs the relaxation dynamics, while the $\sigma_y\sigma_z$ sector covers decoherence dynamics. The first line in $U_{eff}(z)$ can only contain an element at $(\mathcal{U}_{eff}(z))_{\mathbb{1}\mathbb{1}}$, otherwise the conservation of the trace is violated.

Normally one wishes to discuss the dynamics in time space. The back transformation of $U_{eff}(z)$ however is highly non trivial and depends on the choice of the spectral density. To give an impression of the necessary steps a closer look to $P_z(z)$ with the initial conditions of factorized bath and system density matricces is useful. The back transformation is formally given by:

$$P(t) = \frac{1}{2\pi i}\int_{-\infty}^{\infty} dz e^{-izt}\frac{z+\Theta(z)}{p(z)} \ . \tag{4.13}$$

This integral has to be solved by complex integration. A first simple approximation is to evaluate each residuum at the bare system poles, yielding results which are equivalent to the Bloch equations. Additional corrections become substantial for larger system-bath couplings γ, which make the consideration of branch cuts and shifted system frequencies necessary. These steps are shown in a rigorous and detailed manner in the 2010 paper by Nalbach et al [113]. Neglecting all terms of order $O(\gamma^4)$ the result reads:

$$P(z) \simeq \cos(\Delta t)e^{-\Gamma_P t} \ \text{ with the rate } \ \Gamma_P = 2\pi J(\Delta)\coth(\beta\frac{\Delta}{2}) \ . \tag{4.14}$$

4.2 RESPET: The asymmetric two level system

As mentioned before, by diagonalization any asymmetric TLS can be transformed to a symmetric TLS, if the TLS is in contact with a bath, this basis change will reflect in the system-bath coupling operators. Thereby, effectively simplifying a system Hamiltonian for the cost of a more complex system-bath coupling operator. Performing this transformation gives:

$$\begin{aligned} H_{RBM} &= \frac{\Delta}{2}\sigma_x + \frac{\epsilon}{2}\sigma_z - a_{RBM}\sigma_z \sum_j c_j x_j + \frac{1}{2}\sum_j \frac{p_j^2}{m_j} + m_j\omega_j^2 x_j^2 + \frac{c_j^2}{4m_j\omega_j^2} \\ &= \frac{\Omega}{2}\tau_x + (a_x\tau_x + a_z\tau_z)\sum_j c_j x_j + \frac{1}{2}\sum_j \frac{p_j^2}{m_j} + m_j\omega_j^2 x_j^2 + \frac{c_j^2}{4m_j\omega_j^2} \ . \end{aligned} \tag{4.15}$$

Where $a_{RBM} = 1/2$, $\Omega = \sqrt{\Delta^2 + \epsilon^2}$, $a_z = \frac{\Delta}{2\Omega}$ and $a_x = \frac{\epsilon}{2\Omega}$ with the rotation $\sigma_z = a_x\tau_x + a_z\tau_z$ and $\sigma_x = a_z\tau_x - a_x\tau_z$, such that τ_x and τ_z are Pauli matrices in the eigenbasis of H_S. Hereafter this model will be referred to as the **Rotated Bath Model** (RBM). The RBM can be interpreted as two **fully correlated** fluctuations, one being in $a_x\tau_x$ and the other in $a_z\tau_z$, fully correlated since both fluctuation result from the same bath. For example, a voltage fluctuation in one of the gates of the connection set up for a quantum dot might cause a fluctuation in the energy splitting of the levels $\delta\Delta$ as well as a fluctuation in the depth of the potential well $\delta\epsilon$, see chapter 1. This feature would be well represented by the RBM, with the choice of a_x and a_z reflecting whether the gate influences the Δ or ϵ with different strengths.

With the diagonalized version of H_{RBM} the derivation for the symmetric TLS can be followed up to Equation (4.8). After some algebra one obtains:

$$\begin{aligned} 4\mathcal{M}(s-s') = &\{\mu\widetilde{\tau_z}\mathcal{U}_S(s-s')(\mu\overline{\tau_z} + \nu\overline{\tau_x}) + \nu\mu\widetilde{\tau_x}\mathcal{U}_S(s-s')\overline{\tau_z}\}\sum_j c_j^2 R_{qq,j}(s-s') \\ &+ (\mu\widetilde{\tau_z} + \nu\widetilde{\tau_x})\mathcal{U}_S(s-s')(\mu\widetilde{\tau_z} + \nu\widetilde{\tau_x})\sum_j c_j^2 C_{qq,j}(s-s') \ , \end{aligned} \tag{4.16}$$

and

$$\begin{aligned}\mathcal{M}(z) &= \mathcal{M}_{\tau_x} + \mathcal{M}_{\tau_z} + \mathcal{M}_{mix} \\ &= a_x^2 \begin{pmatrix} 0 & 0 & 0 & 0 \\ 0 & 0 & 0 & 0 \\ 0 & 0 & \chi(z) & \chi_2(z) \\ 0 & 0 & -\chi_2(z) & \chi(z) \end{pmatrix} + a_z^2 \begin{pmatrix} 0 & 0 & 0 & 0 \\ \Xi(z) & \chi(z) & 0 & 0 \\ 0 & 0 & \Theta(z) & 0 \\ 0 & 0 & 0 & 0 \end{pmatrix} \\ &+ a_x a_z \begin{pmatrix} 0 & 0 & 0 & 0 \\ 0 & 0 & 0 & 0 \\ \Sigma(z) & 0 & 0 & 0 \\ \Phi(z) & 0 & 0 & 0 \end{pmatrix} + \mu\nu \begin{pmatrix} 0 & 0 & 0 & 0 \\ 0 & 0 & \zeta_2(z) & \zeta(z) \\ 0 & \zeta_2(z) & 0 & 0 \\ 0 & \zeta(z) & 0 & 0 \end{pmatrix} .\end{aligned} \tag{4.17}$$

Here the index 2 indicates a change from sin to cos and correspondingly in the definition of the bath correlation function $C_{qq}(t)$ and bath response function $R_{qq}(t)$, such that $\chi_2(z) = 2(B_{C2}^{\omega-\Delta}(z) + B_{C2}^{\omega+\Delta}(z))$, with $B_{C2}(z) = LT\{C_{qq2}(t)\}$ and $C_{qq2}(t) = \int_0^\infty \frac{d\omega}{4\pi} J(\omega)\coth(\beta\omega/2)\sin(\omega t)$. Furthermore the definitions $\Sigma(z) = 2(B_R^{\omega+\Delta}(z) + B_R^{\omega-\Delta}(z) - B_R(z))$, $\Phi(z) = 2(B_{R2}^{\omega+\Delta}(z) - B_{R2}^{\omega-\Delta}(z))$ and $\zeta(z) = 2(B_C^{\Delta-\omega}(z) + B_C^{\Delta+\omega}(z))$ have been used.

The part of $\mathcal{M}(z)$ proportional to a_x^2 only influences the dephasing dynamics. For $a_z = 0$ the system-bath coupling operator would only be τ_x, sharing the same eigenbasis as the system Hamiltonian. Thus, $\langle\psi_{\tau_x}|[H,\rho]|\psi_{\tau_x}\rangle = 0 = \dot{\rho}_{\psi_{\tau_x},\psi_{\tau_x}}$ with ψ_{τ_x} being the eigenstates for τ_x. Physically this holds dramatic meaning: The population of the eigenstates does not change over time, the initial preparation of these states given by the density matrix ρ_0 will never change and no relaxation can happen. In the way system-bath Hamiltonians were introduced in chapter 2, this holds for any system-bath model in which H_{SB} commutes with H_S. All these baths are pure dephasing baths, in this project the focus is on the dynamics of the TLS, therefore the model in which $H_{SB} \propto \tau_x$ will be called the **Pure Dephasing Model**. For $a_x = 0$ the result for the SBM is recovered. The mix terms with $\mu\nu$ are more interesting, the bath response function now also gives equilibrium contributions in ρ_y and ρ_z, corresponding to the additional terms in the first row in $\mathcal{M}(z)$. The bath correlation function now mixes the relaxation and the dephasing dynamics. It is straight forward but tedious to calculate $\mathcal{U}_{eff}(z)$, its form is shown in appendix A.1.

4.3 The symmetric TLS for two uncorrelated non-commuting baths

While the RBM is a useful description to model fluctuation in ϵ and Δ stemming from the same source, it is not applicable if the two fluctuations have different sources. As mentioned in the introduction this is far from a purely theoretical discussion, but has many real world counter parts. In this section two completely **uncorrelated** fluctuations are considered and RESPET is derived for two uncoupled baths. The Hamiltonian investigated here couples the system via $\frac{\sigma_x}{2}\sum_j c_{j,1}x_{j,1}$ to the first bath and via $\frac{\sigma_z}{2}\sum_j c_{j,2}x_{j,2}$ to the second bath. From here on this model is called the **Two Bath Model** (TBM). The generic Hamiltonian for the TBM reads:

$$\begin{aligned} H &= H_S + H_{SB,1} + H_{B,1} + H_{counter,1} + H_{SB,2} + H_{B,2} + H_{counter,2} \\ &= \frac{\Delta}{2}\sigma_x + \sum_{e=1,2}\sum_j \frac{p_{j,e}^2}{2m_{j,e}} + \frac{1}{2}m_{j,e}\omega_{j,e}^2\left(x_{j,e} - \frac{c_{j,e}O_e}{m_{j,e}\omega_{j,e}^2}\right)^2 \quad . \end{aligned} \tag{4.18}$$

With $O_1 = \frac{\sigma_x}{2}$ and $O_2 = \frac{\sigma_z}{2}$. Each of the counter terms is proportional to $\mathbb{1}$ and can be ignored. To calculate the reduced density matrix the trace over all degrees of freedom for both baths has to be performed. Since both baths are uncorrelated in absence of the system-bath couplings many of the previous considerations still hold but are slightly modified:$L = L_0 + L_{SB,1} + L_{SB,2}$, factorized initial condition: $W(0) = \rho_S(0) \otimes \rho_{B1}^{Boltz}(0) \otimes \rho_{B2}^{Boltz}(0)$, both at equilibrium with Boltzmann type density matrix and $\mathcal{U}_0 = \mathcal{U}_S \otimes \mathcal{U}_{B,1} \otimes \mathcal{U}_{B,2}$. In the Dyson equation (4.3) simply L_{SB} has to be substituted with $L_{SB,1} + L_{SB,2}$ and the second term still vanishes. Continuing the previous steps one arrives at a new integral kernel:

$$\mathcal{M} = \langle [L_{SB,1} + L_{SB,2}]\mathcal{U}_0(s-s')[L_{SB,1} + L_{SB,2}]\rangle_{B1+B2} \quad , \tag{4.19}$$

where $\langle A\rangle_{B1+B2} = \mathrm{Tr}_B\{A\rho_{B1}^{Boltz}(0) \otimes \rho_{B2}^{Boltz}(0)\}$. Every term in M that mixes $L_{SB,1}$ and $L_{SB,2}$ is proportional to:

$$\begin{aligned} \mathcal{M}_{mix} &\propto \mathrm{Tr}_B\{\alpha\sum_j c_j x_{j,1}\mathcal{U}_{B1} \otimes \mathcal{U}_{B1}\sum_k c_k x_{k,2}\rho_{B1}^{Boltz}(s') \otimes \rho_{B2}^{Boltz}(s')\} \\ &\propto \alpha\sum_j c_j \sum_k c_k \mathrm{Tr}_{B1}\{\mathcal{U}_{B1}(s-s')x_{j,1}\rho_{B1}^{Boltz}(s')\}\mathrm{Tr}_{B2}\{\mathcal{U}_{B2}(s-s')x_{k,2}\rho_{B2}^{Boltz}(s')\} \\ &\propto \alpha\langle x_{j1}\rangle_{B1}\langle x_{j2}\rangle_{B2} = 0 \quad . \end{aligned} \tag{4.20}$$

The result for $\mathcal{M}(z)$ can actually be obtained from the asymmetric TLS result (A.1) by dropping the terms proportional to $a_x a_z$ and identifying: $a_z^2(C/R)_{qq}(t) = (C/R)_{qq,1}(t)$ and $a_x^2(C/R)_{qq}(t) = (C/R)_{qq,2}(t)$. Therefore in the 1-loop approximation the kernel is simply the sum of both kernels: $\mathcal{M} = \mathcal{M}_{\sigma_x} + \mathcal{M}_{\sigma_z}$. While the dephasing dynamics become somewhat more complex, the relaxation dynamics actually are entirely unchanged compared to the SBM. For stronger coupling this is not true since higher order differences occur. To understand this in greater detail a two-loop Dyson equation has to be used.

4.3.1 Two-loop approximation

The two loop Dyson equation for the reduced density matrix reads:

$$\begin{aligned}\mathcal{U}_{eff}(t) = U_S(t) + \int_0^t \int_0^s ds ds' \mathcal{U}_S(t-s)\mathcal{M}(s-s')\mathcal{U}_S(s') \\ + \int_0^t \int_0^s \int_0^{s'} \int_0^{s''} ds ds' ds'' ds''' \mathcal{U}_S(t-s)\mathcal{V}(s-s', s'-s'', s''-s''')\mathcal{U}_{eff}(s''') \ .\end{aligned} \tag{4.21}$$

By performing the bath trace additionally to the terms $\propto L_{SB}$ also the terms $\propto L_{SB}^3$ vanish after some algebra, mainly employing a form of the Wick theorem for superoperators, since they are either proportional to $\langle x_{j,1}\rangle$ or $\langle x_{j,2}\rangle$. Transformed to Laplace space the equation reads:

$$\mathcal{U}_{eff}(z) = \mathcal{U}_S(z) - \mathcal{U}_S(z)\mathcal{M}(z)\mathcal{U}_S(z) + \mathcal{U}_S(z)\mathcal{V}(z)\mathcal{U}_{eff}(z) \ , \tag{4.22}$$

which is formally solved by:

$$\mathcal{U}_{eff}(z) = (\mathcal{U}_S^{-1}(z) - \mathcal{V}(z))^{-1}(\mathbb{1} - M(z)U_S(z)) \ , \tag{4.23}$$

where $\mathcal{V}(s-s', s'-s'', s''-s''')$ is the two loop kernel, which has the form:

$$\mathcal{V} = \langle L_{SB}\mathcal{U}_0(s-s')L_{SB}\mathcal{U}_0(s'-s'')L_{SB}\mathcal{U}_0(s''-s''')L_{SB}\rangle_B \ , \tag{4.24}$$

with $L_{SB} = L_{SB,1} + L_{SB,2}$. Note that in $\mathcal{V}$ the first non vanishing terms mixing $L_{SB,1}$ and $L_{SB,2}$ occur. As mentioned before, even in 1-loop approximation, the dephasing becomes rather complex. After a lot of tedious algebra one finds contributions to the relaxation rate in this kernel. In this chapter the overall form of $\mathcal{V}(z)$ is given, but explicitly only the element $\mathcal{V}_{(22)}(z)$ is discussed, since it is the relevant entry for relaxation. In Appendix A.3 all elements are shown.

First a deeper look in the structure of both factors in Equation (4.23) is necessary, the right bracket has the form:

$$\mathbb{1} - M(z)U_S(z) = \begin{pmatrix} 1 & 0 & 0 & 0 \\ D_1 & D_2 & 0 & 0 \\ 0 & 0 & D_3 & D_4 \\ 0 & 0 & D_5 & D_6 \end{pmatrix} , \tag{4.25}$$

with $D_1 - D_6$ being complex numbers. For the left bracket one finds:

$$\mathcal{U}_S^{-1}(z) + \mathcal{V}(z) = \frac{-1}{z} \begin{pmatrix} 1 & 0 & 0 & 0 \\ a & b & 0 & 0 \\ 0 & 0 & c & d \\ 0 & 0 & e & f \end{pmatrix} , \tag{4.26}$$

with $a - f$ being complex numbers. Then

$$(\mathcal{U}_S^{-1}(z) + \mathcal{V}(z))^{-1} = \begin{pmatrix} I_1 & 0 & 0 & 0 \\ I_2 & I_3 & 0 & 0 \\ 0 & 0 & I_4 & I_5 \\ 0 & 0 & I_6 & I_7 \end{pmatrix} = \frac{-z}{b(cf - ed)} \begin{pmatrix} b(cf - ed) & 0 & 0 & 0 \\ -a(cf - ed) & cf - ed & 0 & 0 \\ 0 & 0 & bf & -bd \\ 0 & 0 & -be & bc \end{pmatrix} . \tag{4.27}$$

The overall form of $\mathcal{U}_{eff}(z)$ then is:

$$U_{eff}(z) = \begin{pmatrix} I_1 & 0 & 0 & 0 \\ I_2 + I_3 D_1 & I_3 D_2 & 0 & 0 \\ 0 & 0 & I_4 D_3 + I_5 D_5 & I_4 D_4 + I_5 D_6 \\ 0 & 0 & I_6 D_3 + I_7 D_5 & I_6 D_4 + I_7 D_6 \end{pmatrix} . \tag{4.28}$$

Therefore the form of $U_{eff}(z)$ remains unchanged and no additional equilibrium values for $\langle \sigma_y \rangle$ and $\langle \sigma_z \rangle$ are obtained. The dephasing and relaxation dynamics are not mixed in contrast to the RBM. Now focus on $\mathcal{V}_{(22)}(z) = I_3 D_2$, where one finds $I_3 = \frac{-z}{b}$ and $D_2 = 1 + \frac{\chi_{\sigma_z}(z)}{z}$, with the index σ_z showcasing that this is the $\chi(z)$ for the bath coupled via σ_z to system . Now a closer look into b is necessary to evaluate the influence of the baths on the relaxation rate. Regarding the structure of the system super operators four terms can contribute to b in principle. Two terms result only from the σ_z bath, these are :

$$\begin{aligned} Z_1 &= \widetilde{\sigma}_z \mathcal{U}_S(s-s')\widetilde{\sigma}_z \mathcal{U}_S(s'-s'')\widetilde{\sigma}_z \mathcal{U}_S(s''-s''')\widetilde{\sigma}_z \\ &\times \sum_{ijkl} c_i c_j c_k c_l \langle \overline{x}_{i,2} \mathcal{U}_{B,2}(s-s')\overline{x}_{j,2} \mathcal{U}_{B,2}(s'-s'')\overline{x}_{k,2} \mathcal{U}_{B,2}(s''-s''')\overline{x}_{l,2}\rangle \\ &= 16 \begin{pmatrix} 0 & 0 & 0 & 0 \\ 0 & c_1^\Delta c_3^\Delta & 0 & 0 \\ 0 & 0 & c_2^\Delta & 0 \\ 0 & 0 & 0 & 0 \end{pmatrix} \sum_{ijkl} c_i c_j c_k c_l \langle \overline{x}_{i,2} \mathcal{U}_{B,2}(s-s')\overline{x}_{j,2} \mathcal{U}_{B,2}(s'-s'')\overline{x}_{k,2} \mathcal{U}_{B,2}(s''-s''')\overline{x}_{l,2}\rangle \ , \end{aligned} \tag{4.29}$$

where $c_1^\Delta = \cos(\Delta(s-s'))$, $c_2^\Delta = \cos(\Delta(s'-s''))$ and $c_3^\Delta = \cos(\Delta(s''-s'''))$.
The second term is:

$$\begin{aligned} Z_2 &= \widetilde{\sigma}_z \mathcal{U}_S(s-s')\overline{\sigma}_z \mathcal{U}_S(s'-s'')\overline{\sigma}_z \mathcal{U}_S(s''-s''')\widetilde{\sigma}_z \\ &\times \sum_{ijkl} c_i c_j c_k c_l \langle \overline{x}_{i,2} \mathcal{U}_{B,2}(s-s')\widetilde{x}_{j,2} \mathcal{U}_{B,2}(s'-s'')\widetilde{x}_{k,2} \mathcal{U}_{B,2}(s''-s''')\overline{x}_{l,2}\rangle \\ &= 4 \begin{pmatrix} 0 & 0 & 0 & 0 \\ 0 & s_1^\Delta s_3^\Delta & 0 & 0 \\ 0 & 0 & 0 & 0 \\ 0 & 0 & 0 & 0 \end{pmatrix} \sum_{ijkl} c_i c_j c_k c_l \langle \overline{x}_{i,2} \mathcal{U}_{B,2}(s-s')\widetilde{x}_{j,2} \mathcal{U}_{B,2}(s'-s'')\widetilde{x}_{k,2} \mathcal{U}_{B,2}(s''-s''')\overline{x}_{l,2}\rangle \ , \end{aligned} \tag{4.30}$$

where s indicates sin and otherwise the same notation as above.
To evaluate $\langle \overline{x}_i \mathcal{U}_{B,2}(s-s')\overline{x}_j \mathcal{U}_{B,2}(s'-s'')\overline{x}_k \mathcal{U}_{B,2}(s''-s''')\overline{x}_l\rangle$ the action of the superoperators on the density matrix has to be performed, the details are shown in appendix A.2. This allows to a representation in terms of two point correlation functions, the result reads:

$$\begin{aligned} \langle \overline{x}_{i,2} \mathcal{U}_{B,2}(s-s')\overline{x}_{j,2} \mathcal{U}_{B,2}(s'-s'')\overline{x}_{k,2} \mathcal{U}_{B,2}(s''-s''')\overline{x}_{l,2}\rangle &= \langle \overline{x}_{i,2} \mathcal{U}_{B,2}(s-s')\overline{x}_{j,2}\rangle \langle \overline{x}_{k,2} \mathcal{U}_{B,2}(s''-s''')\overline{x}_{l,2}\rangle \\ &+ \langle \overline{x}_{i,2} \mathcal{U}_{B,2}(s-s'')\overline{x}_{k,2}\rangle \langle \overline{x}_{j,2} \mathcal{U}_{B,2}(s'-s''')\overline{x}_{l,2}\rangle + \langle \overline{x}_{i,2} \mathcal{U}_{B,2}(s-s''')\overline{x}_{l,2}\rangle \langle \overline{x}_{j,2} \mathcal{U}_{B,2}(s'-s'')\overline{x}_{k,2}\rangle \end{aligned} \tag{4.31}$$

and

$$\langle \overline{x}_{i,2} \mathcal{U}_{B,2}(s-s')\widetilde{x}_{j,2} \mathcal{U}_{B,2}(s'-s'')\widetilde{x}_{k,2} \mathcal{U}_{B,2}(s''-s''')\overline{x}_{l,2}\rangle = 0 \ . \tag{4.32}$$

Therefore only Z_1 actually contributes to b, the sum over the bath degrees of freedom can be performed, yielding a contribution to b in time space with:

$$\begin{aligned} b_1 &= 16\cos(\Delta(s-s'))\cos(\Delta(s''-s''')) \\ &\quad\times\left(C_{qq,\sigma_z}(s-s')C_{qq,\sigma_z}(s''-s''')+C_{qq,\sigma_z}(s-s'')C_{qq,\sigma_z}(s'-s''')+C_{qq,\sigma_z}(s-s''')C_{qq,\sigma_z}(s'-s'')\right)\ . \end{aligned} \tag{4.33}$$

Note that $C_{qq,\sigma_z}(s-s')C_{qq,\sigma_z}(s''-s''')$ is a contribution covered by the one loop approximation. The other two contributions to b result from the mixing of the two baths. They are:

$$\begin{aligned} Mix_1 &= \widetilde{\sigma}_z U_1 \widetilde{\sigma}_x U_2 \widetilde{\sigma}_x U_3 \widetilde{\sigma}_z \sum_{ijkl} c_{i,2}c_{j,1}c_{k,1}c_{l,2}\langle \overline{x}_{j,1}\mathcal{U}_{B,1}(s'-s'')\overline{x}_{k,1}\rangle\langle \overline{x}_{i,2}\mathcal{U}_{B,2}(s-s''')\overline{x}_{l,2}\rangle \\ &= 16\begin{pmatrix} 0 & 0 & 0 & 0 \\ 0 & c_3^\Delta(c_1^\Delta c_2^\Delta - s_1^\Delta s_2^\Delta) - s_3^\Delta(c_1^\Delta s_2^\Delta + s_1^\Delta c_2^\Delta) & 0 & 0 \\ 0 & 0 & 0 & 0 \\ 0 & 0 & 0 & 0 \end{pmatrix} C_{qq,\sigma_z}(s-s''')C_{qq,\sigma_x}(s'-s'')\ , \end{aligned} \tag{4.34}$$

and

$$\begin{aligned} Mix_2 &= \widetilde{\sigma}_z U_1 \widetilde{\sigma}_x U_2 \overline{\sigma}_z U_3 \overline{\sigma}_x \sum_{ijkl} c_{i,2}c_{j,1}c_{k,2}c_{l,1}\langle \overline{x}_{j,1}\mathcal{U}_{B,1}(s'-s''')\widetilde{x}_{l,1}\rangle\langle \overline{x}_{i,2}\mathcal{U}_{B,2}(s-s'')\widetilde{x}_{k,2}\rangle \\ &= 4\begin{pmatrix} 0 & 0 & 0 & 0 \\ 0 & c_1^\Delta c_2^\Delta - s_1^\Delta s_2^\Delta & 0 & 0 \\ 0 & 0 & 0 & 0 \\ 0 & 0 & 0 & 0 \end{pmatrix} R_{qq,\sigma_z}(s-s'')R_{qq,\sigma_x}(s'-s''')\ . \end{aligned} \tag{4.35}$$

Therefore, contributions to the relaxation rate from both the bath correlation function and the bath response function of the σ_x bath contribute through irreducible 2-loop diagrams. Additionally, the bath response function of the σ_z bath also contributes to the relaxation rate, while in one loop approximation only the bath correlation does. It is to be expected that these contributions become especially prominent for large system-bath coupling and temperatures in the region of system energy difference Δ. While the Laplace transformation of the contributions to b is very tedious, it is also straightforward.

For the purpose of this thesis we will restrain ourselves from giving the transformed $b(z)$ or any other contributions or elements of $U_{eff}(z)$. The Laplace back transformation is highly non-trivial, an example for integrals occurring is:

$$\int_0^\infty d\omega_1 \int_0^\infty d\omega_2 \int_{-\infty}^\infty dz J_{\sigma_x}(\omega_1) J_{\sigma_z}(\omega_2) e^{-izt} \frac{-z(\Delta+\omega_1+\omega_2)(\omega_2+\Delta)}{(z^2-\omega^2)(z^2-(\Delta+\omega_1+\omega_2)^2(z^2-(\Delta+\omega_2)^2)}. \tag{4.36}$$

By performing a partial fraction decomposition this can be further simplified. One of the terms occurring in Equation (4.36) is:

$$\int_0^\infty d\omega_1 \int_0^\infty d\omega_2 \int_{-\infty}^\infty dz J_{\sigma_x}(\omega_1) J_{\sigma_z}(\omega_2) e^{-izt} \frac{i(\Delta+\omega_1+\omega_2)(\Delta+\omega_1+\omega_2)(\omega_2+\Delta)}{z+i(\Delta+\omega_1+\omega_2)}. \tag{4.37}$$

For Equation (4.37) no analytical solution is known ad we did not find one. One could try to solve these integrals numerically or employ drastic simplifications. Self consistency methods to obtain a form U_{eff} might also circumvent the problem of calculating these integrals. In this thesis instead the numerical method called Quasi Adiabatic Path Integral was extended, to simulate and investigate the dynamics of the two level system under the influence of two non-commuting baths, while including higher loops.

4.4 Hybrid-RESPET

Alternatively one can try to study two baths by treating one phenomenologically and the other completely, either perturbatively or numerically exact. An approach to include a second bath phenomenological is to modify the von-Neumann equation with a set of Lindblad operators, see 2.2. This allows to keep the above derivation for the first bath, since only the solution of the $\mathcal{U}_S$ is affected.

The bare evolution is still $\mathcal{U}_0(t, t_0) = e^{\mathcal{L}_0(t-t_0)}$, here $\mathcal{L}_0 = -i[H_S + H_B, .] + \Gamma_L$ with the Lindblad type superoperator $\Gamma_L = (0, 0, -\gamma_D, -\gamma_D) \otimes \mathbb{1}_B$. This choice of Γ_L ensures only dephasing contributions to the system dynamics, therefore modelling a PDB. Furthermore $\mathcal{L}_{SB} = -i[H_{SB}, .]$ with $H_{SB} = -\sigma_z \sum_\alpha c_\alpha x_\alpha$. Hence in Hybrid-RESPET the σ_x-bath is included in the bare propagation U_0, this is illustrated diagrammatically in Figure 4.1. The effective Dyson equation keeps its previous form and thus reads:

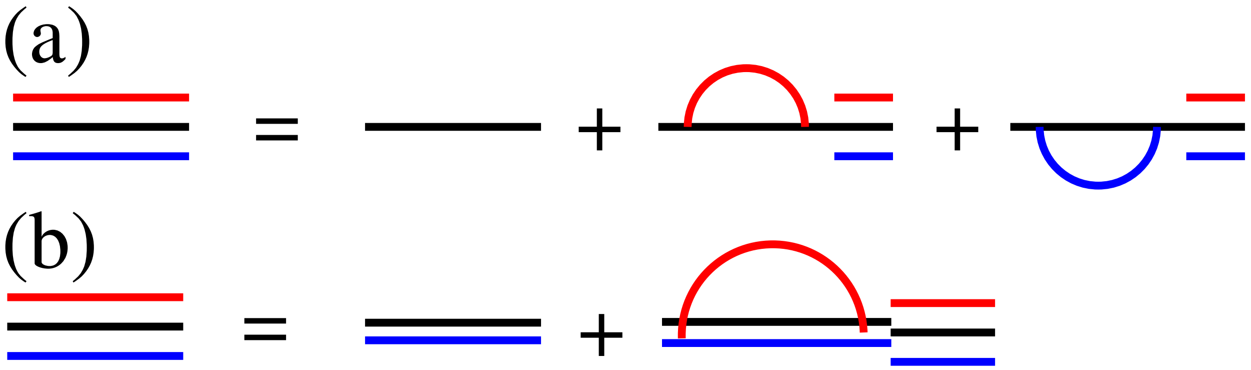

Figure 4.1: This figure shows a diagramtic representation of the Dyson Equation. In (a) both baths are treated via the RESPET formalism, while in (b) the effect of one bath (blue) is absorbed into the system propagation and the other bath (red) is treated via RESPET.

$$\mathcal{U}_{eff}(t-t_0) = \mathcal{U}_S(t-t_0) + \int_{t_0}^{t}\int_{t_0}^{s} ds ds' \mathcal{U}_S(t,s)\mathcal{M}(s,s')\mathcal{U}_{eff}(s',t_0) \ . \tag{4.38}$$

Therein, $\mathcal{U}_S(t,t_0) = e^{\mathcal{L}_S(t-t_0)}$ with $\mathcal{L}_S = -i[H_S,.] + \Gamma_D$. In this lowest order perturbative treatment the memory kernel $\mathcal{M}(s,s')$ is given as $\mathcal{M}(s,s') = \langle \mathcal{L}_I \mathcal{U}_0(s,s') \mathcal{L}_I \rangle_B$. Therefore, if one includes a rate in this form, there are already effectively mixing effects between baths in lowest order. The rest in analogous to the above derivation, where one arrives in the end at the same 1-loop form of $P(z)$:

$$P(z) \simeq \cos(\Delta t) e^{-\Gamma_P t} \ .$$

For an initial system state $\rho_S(0) = 0.5(\mathbb{1} + \sigma_z)$ the modified rate reads:

$$\begin{aligned}\Gamma_P = \gamma_D - \int_{-\infty}^{\infty} d\omega J(\omega) \coth\left(\frac{\beta\omega}{2}\right) \frac{\gamma_D}{(\Delta-\omega)^2 + \gamma_D^2} \\ +2\pi \mathrm{Re}\left\{ J(\Delta - i\gamma_D) \coth\left(\beta \frac{\Delta - i\gamma_D}{2}\right)\right\} \ .\end{aligned} \tag{4.39}$$

Chapter 5

The Quasi Adiabatic Path Integral

The method called Quasi Adiabatic Path Integral (QUAPI) was first proposed by Nancy Makri et al. in 1995 [83, 95]. It is a highly successful numerical exact simulation method, which has been used extensively over the past decades [115]. This chapter first introduces the original method and then goes on with deriving the extension to multiple non-commuting baths as well as the less general extension, which is used for the results later on in this dissertation. The start is from the generic system-bath Hamiltonian as introduced in Equation (2.1):

$$H_{gen} = H_S + \sum_j \left\{ \frac{p_j^2}{2m_j} + \frac{1}{2} m_j \omega_j^2 \left(x_j - \frac{c_j O}{m_j \omega_j^2} \right)^2 \right\}. \tag{5.1}$$

First the essential steps of Grabert et al.'s derivation of $\rho_{red}(t)$ will be followed, explicitly focusing on the ones necessary for integrating out the bath degrees of freedom. Afterwards, this chapter will showcase the developing of Makri's method QUAPI and its iterative scheme. Thereafter a combination of master equations and QUAPI are shown, for which the scheme is rewritten in terms of super operators. Then the chapter goes on to derive the extension, essential for treating multiple non-commuting fluctuations in terms of baths. In the earlier parts of this project, the general case for arbitrary system operators O_j was developed, but due to numerical costs, was not usable in a sensible way. With the emergence of that issue a solution was found by restricting the choice of system operators, such that one set of operators fulfills $[H_S, O_j] = 0$. The reasons for the increase in numerical cost, compared to the original method, and the choice of the restriction can only be understood fully if one takes a closer look into the influence functional. The influence functional describes an effective bath dynamics via time non-local correlations in the system operators O_j of H_{SB}. To achieve the necessary insight it is useful to start with the basics.

5.1 A formal solution of the Feynman-Vernon Influence functional

In this section the formal solution of the Feynman-Vernon influence functional as effective system dynamics, as proposed by Grabert et al., is derived. The main steps follow therefore the paper "Quantum Brownian Motion: The functional integral approach" of Grabert et al. [82] starting with the original form Feynman and Vernon proposed in 1963 [6]. For comparability $H_S = \frac{p^2}{2m_0} + V_0$ is used here, as it is done in the paper.

5.1.1 Real time functional integral

A system, initially prepared in a pure state $\Psi(o_i, \bar{x}_i, t = 0)$, with $\bar{x}_i = (x_{1_i}, ..., x_{N_i})$, evolves in time as:

$$\Psi(o_f, \bar{x}_f, t) = \int do_i d\bar{x}_i U(o_f, \bar{x}_f, t; o_i, \bar{x}_i, 0)\Psi(o_i, \bar{x}_i, 0), \tag{5.2}$$

where $U(o_f, \bar{x}_f, t; o_i, \bar{x}_i, 0) = \langle o_f, \bar{x}_f, t|\exp[-iHt/\hbar]|o_i, \bar{x}_i, 0\rangle$ is the coordination representation of the time evolution operator. This may in turn also be represented as a functional integral [116–118]:

$$\int \mathcal{D}o\mathcal{D}\bar{x} \exp\left[\frac{i}{\hbar}S(o, \bar{x})\right]. \tag{5.3}$$

This integral is over all possible paths $o(s)$, $\bar{x}(s)$,$0 \leq s \leq t$ with boundary conditions $o(0) = o_i$, $\bar{x}(0) = \bar{x}_i$, $o(t) = o_f$ and $\bar{x}(t) = \bar{x}_f$. The path probability is weighted according to the action:

$$S(o, \bar{x}) = \int_0^t ds\mathcal{L}(o, \dot{o}, \bar{x}, \dot{\bar{x}}, s), \tag{5.4}$$

as in the case of the full Hamiltonian H the full action $\mathcal{L}$ may be viewed as composition of system, bath and system-bath parts. In contrast to Grabert's paper, the equilibrium contributions and therefore the imaginary time integrals will not be discussed in detail. While they are an important representation of the equilibrium density matrix and allow for more general initial conditions, explicitly they allow for a prepared density matrix $W_0 = \sum_j P_j W_\beta P'_j$ instead of a factorized density matrix$W_0 = \rho_S(0)\rho_{bath}^{equil}(0)$ with $W_\beta = Z_\beta^{-1}\exp[-\beta H]$ and P_j,P'_j system operators. The equilibrium contributions are neglected, since they are of no importance for the derivation of the nonequilibrium dynamics and additionally the QUAPI scheme constraints the models investigated to the factorized initial condition. Applied this yields: $\mathcal{L}_S = \frac{1}{2}M\dot{o}^2 - V(o, s)$, $\mathcal{L}_B = \sum_j \frac{1}{2}m_j\dot{x}_j{}^2 - \frac{1}{2}m_j\omega_j^2 x_j^2$ and $\mathcal{L}_{SB} = \sum_j qc_j x_j$. Putting all this together, using the fundamental relation $\rho(t) = |\Psi(o_f, \bar{x}_f, t\rangle\langle\Psi(o'_f, \bar{x}'_f, t|$ for time evolved initial pure states, one arrives at $W(t)$:

$$W(o_f,\bar{x}_f,o'_f,\bar{x}'_f,t) = \int do_i do'_i d\bar{x}_i d\bar{x}'_i U(o_f,\bar{x}_f,t;o_i,\bar{x}_i,0) \times W(o_i,\bar{x}_i,o'_i,\bar{x}'_i,0) U^{-1}(o'_f,\bar{x}'_f,t;o'_i,\bar{x}'_i,0) \ , \tag{5.5}$$

which leads to the following representation:

$$W(o_f,\bar{x}_f,o'_f,\bar{x}'_f,t) = \int do_i do'_i d\bar{x}_i d\bar{x}'_i \int \mathcal{D}o\mathcal{D}\bar{x}\mathcal{D}o'\mathcal{D}\bar{x}' \exp\left[\frac{i}{\hbar}\{S(o,\bar{x}) - S(o',\bar{x}')\}\right] \ . \tag{5.6}$$

Equation (5.6) sums over all paths $o(s)$, $o'(s)$, $\bar{x}(s)$ and $\bar{x}'(s)$ for $0 \le s \le t$.

5.1.2 The reduced density matrix: How to trace out the bath

In the coordinate representation the trace becomes an integral over the bath coordinates. The reduced density matrix is:

$$\rho_{red}(o_f,o'_f,t) = \int d\bar{x}_f W(o_f,\bar{x}_f,o'_f,\bar{x}_f,t) \ . \tag{5.7}$$

This equation can be rewritten using the previous definitions and by separating the integrals over the system coordinates and the bath coordinates :

$$\rho_{red}(o_f,o'_f,t) = \int dq_i dq'_i \int \mathcal{D}q\mathcal{D}q' \exp\left[\frac{i}{\hbar}\{S_S(o,\bar{x}) - S_S(o',\bar{x}')\}\right] F_{FV}(q,q') \ , \tag{5.8}$$

now the whole influence of the bath is in F_{FV}, the Feynman-Vernon influence functional,

$$\mathrm{F}_{FV}(o,o') = \int d\bar{x}_i d\bar{x}'_i d\bar{x}_f \int \mathcal{D}\bar{x}\mathcal{D}\bar{x}' \exp\left[\frac{i}{\hbar}\{S_B(\bar{x}) + S_{SB}(o,\bar{x}) - S_B(\bar{x}') - S_{SB}(o',\bar{x}')\}\right] \ . \tag{5.9}$$

This equation is analytically solvable. First the path integrals of the coordinates for each bath oscillator may be performed separately:

$$\mathrm{F}_{FV}(o,o') = \int d\bar{x}_i d\bar{x}'_i d\bar{x}_f \prod_j \widetilde{\mathrm{F}}_j(o,x_{j_f},x_{j_i}) \widetilde{\mathrm{F}}^*_j(o',x'_{j_f},x'_{j_i}) \ , \tag{5.10}$$

where each $\widetilde{\mathrm{F}}_j$ includes the whole influence of the j.-th bath oscillator. They are naturally defined by:

$$\widetilde{\mathrm{F}}_j(o,x_{j_f},x_{j_i}) = \int \mathcal{D}x_j \exp\left[\frac{i}{\hbar}\int_0^t ds \left\{\frac{1}{2}m_j\dot{x}_j^2 - \frac{1}{2}m_j\omega_j^2\left(x_j - \frac{c_j o}{m_j\omega_j^2}\right)^2\right\}\right] \quad . \tag{5.11}$$

It should be noted that, in contrast to Equation (5.1) the momenta of the bath oscillators are not written as p_j but $m_j\dot{x}_j$. In the path integral formulation as introduced by Feynman and Vernon the momenta p_j are rewritten as $p_j(t) = m_j\frac{x_j(t+dt)-x_j(t)}{dt} = m_j\dot{x}_j(t)$ [116–118]. The outer integral is a Gaussian functional integral over all paths $x_j(s)$ with conditions as introduced before. This can be solved exactly and most of the required steps can be found in appendix A of Grabert et al.'s paper [82]. The solution reads: $\widetilde{\mathrm{F}}_j(o,x_{j_f},x_{j_i}) = \left(\frac{m_j\omega_j}{2\pi i\hbar sin(\omega_j t)}\right)^2 \exp\left[\frac{i}{\hbar}\Phi_j(o,x_{j_f},x_{j_i})\right]$, with a real phase $\Phi_j(o,x_{j_f},x_{j_i})$, which is quadratic in x_{j_f} and x_{j_i}. The remaining integral over $d\bar{x}_i$, $d\bar{x}_i'$ and $d\bar{x}_f$ therefore also become Gaussian. One arrives at:

$$\begin{aligned}
\mathrm{F}_{FV} &= \exp\left[-\frac{1}{\hbar}\int_0^t ds\int_0^s dr(o(s)-o'(s))(L(s-r)o(r)-L^*(s-r)o'(r))\right] \\
&\times \exp\left[-\frac{i}{2\hbar}\int_0^t ds\,\mu(o^2(s)-o'^2(s))\right] \\
&= \exp\left[-\frac{1}{\hbar}\int_0^t ds\int_0^s dr(o(s)-o'(s))(\eta(s-r)o(r)-\eta^*(s-r)o'(r))\right] \quad .
\end{aligned} \tag{5.12}$$

With $L(t-t')$ being the correlation function of the bath defined in Equation (2.7). The factor in the second line arises from the counter term, here $\mu = \sum_j \frac{c_j^2}{m_j\omega_j} = \int_0^\infty \frac{d\omega}{\pi}J(\omega)\frac{2}{\pi}$ for infinitely many harmonic oscillators. This also allows the redefining of the integral kernel as: $\eta(t-t') = L(t-t') + \frac{i\mu}{2}\delta(t-t')$. Equation (5.8) and Equation (5.12) are the starting point for Makri et al.'s development of the scheme.

5.2 QUAPI

For a numerical evaluation of the path integral defined in Equation (5.8) instead of a continuous path, the path of the system eigenvalues of O has to be discretized. To achieve this, the propagator $U(o_f,x_f,t;o_i,x_i,0)$ has to be sliced into short time propagators. Assuming a time independent

Hamiltonian the propagator is given by:

$$U = \exp[-iHt/\hbar] = \prod_{j=1}^{N} \exp[-iHdt/(N\hbar)] \ , \tag{5.13}$$

for $t = Ndt$. This splitting of the propagators is trivially justified, since $U(t_a - t_b) = U(t_a - t_c)U(t_c - t_b)$ for $t_a > t_c > t_b$. A splitting of the bath and system parts, as in the continuous path integral formulation, is however not trivial. In the path integral formalism the limes $dt \to 0$ allows a splitting, as if the $[H_S, H_B + H_{SB}] = 0$, since $e^{(A+B)dt} = e^{Adt}e^{Bdt} + [A, B]dt^2$ in lowest order. Thus, the discretized version of the path integral generates an error that is proportional to the square of the time slices for each time slice. To achieve even higher accuracy a symmetric Trotter splitting can be employed, giving: $e^{(A+B)dt} = e^{Adt/2}e^{Bdt}e^{Adt/2} + [A, [A, B]]dt^3$. This holds an advantage in the final scheme, where all the errors accumulate. The overall error, in contrast to the error of a single slice, becomes $\propto Ndt^3 = t * dt^2$ and a judgement whether the error is large in regards to dt can be made by investigating its increase, while for the normal Trotter splitting the overall error is $\propto dt$, thus with constant increase.

To split the system and bath dynamics the obvious choice is $A = H_{SB} + H_B = H_{env}$ and $B = H_S$. The propagator then reads:

$$U = \exp[-iH_{env}dt/(2\hbar)] \left(\prod_{j=1}^{N} \exp[-iH_S dt/\hbar] \exp[-iH_{env}dt/\hbar] \right) \exp[iH_{env}dt/(2\hbar)] \ . \tag{5.14}$$

This means, first the environment is propagated over half a time slice dt, then the propagation of system and environment over a time slice dt alternate until the whole propagation finishes with one last propagation of the environment over half a time slice. To evaluate Equation (5.5) numerically, it is necessary to insert the completeness relation of the full Hilbert space

$$\mathbb{I} = \int do |o\rangle\langle o| \prod_{l} \int dx_l |x_l\rangle\langle x_l| \ , \tag{5.15}$$

after each system propagation. Therefore the k.-th system propagation is surrounded by two $\mathbb{I}$, let the one after the propagation be called $\mathbb{I}_k$. Note that from here on it is necessary to label the system eigenvalues o according to the number of propagations used before the identity relation was inserted. Thus for the initial and final eigenvalues: $o_i = o_0$, $o'_i = o'_0$, $o_f = o_N$ and $o'_f = o'_N$.

$$\begin{aligned}
&\mathbb{I}_k \exp[-iH_S dt/\hbar]\exp[-iH_{env} dt/\hbar]\mathbb{I}_{k-1} \\
&\quad = \int do_k |o_k\rangle\langle o_k| \prod_l \int dx_{k,l} |x_{k,l}\rangle\langle x_{k,l}| \exp[-iH_S dt/\hbar]\exp[-iH_{env} dt/\hbar] \\
&\quad \times \int do_{k-1} |o_{k-1}\rangle\langle o_{k-1}| \prod_m \int dx_{k-1,m} |x_{k-1,m}\rangle\langle x_{k-1,m}| \\
&\quad = \int do_k \int do_{k-1} |o_k\rangle\langle o_{k-1}| \prod_l \int dx_{k,l} \prod_m \int dx_{k-1,m} |x_{k,l}\rangle\langle x_{k-1,m}| \\
&\quad \times \langle o_k|\exp[-iH_S dt/\hbar]|o_{k-1}\rangle\langle x_{k,l}|\exp[-iH_{env}(o_{k-1}) dt/\hbar]|x_{k-1,m}\rangle \ .
\end{aligned} \tag{5.16}$$

Applying this to the definition of the reduced density matrix, with the now necessary factorized initial condition $W(0) = \rho_S(0) \otimes \rho_{bath}(0)$ to separate bath and system initially, one finds:

$$\begin{aligned}
&\rho_{red}(o_N, o'_N, t) = \int do_0 \int do_1 ... \int do_N \int do'_0 \int do'_1 .... \int do'_N \\
&\times \langle o_N|\exp[-iH_S dt/\hbar]|o_{N-1}\rangle ... \langle o_1|\exp[-iH_S dt/\hbar]|o_0\rangle\langle o_0|\rho_S(0)|o'_0\rangle \\
&\times \langle o'_0|\exp[iH_S dt/\hbar]|o'_1\rangle ... \langle o_{N-1}|\exp[iH_S dt/\hbar]|o'_N\rangle \\
&\times \prod_l \int dx_{N,l} \int dx'_{N,l} \delta(x'_{N,l} - x_{N,l}) .... \int dx_{0,l} \int dx'_{0,l} \langle x_{0,l}|\rho_{bath}(0)|x'_{0,l} \\
&\times \prod_{m=1}^{N-2} \langle x_{m+1,l}|\exp[-iH_{env}(o_m) dt/\hbar]|x_{m,l}\rangle\langle x'_{m,l}|\exp[iH_{env}(o'_m) dt/\hbar]|x'_{m+1,l}\rangle \\
&\times \langle x_{N,l}|\exp[-iH_{env}(o_N) dt/2\hbar]|x_{N-1,l}\rangle\langle x'_{N-1,l}|\exp[iH_{env}(o'_N) dt/2\hbar]|x'_{N,l}\rangle\rangle \\
&\times \langle x_{1,l}|\exp[-iH_{env}(o_0) dt/2\hbar]|x_{0,l}\rangle\langle x'_{0,l}|\exp[iH_{env}(o'_0) dt/2\hbar]|x'_{1,l}\rangle\rangle \ .
\end{aligned} \tag{5.17}$$

The last four lines in Equation (5.17) represent the influence functional. A shift back to a continuous path integral formulation is now possible for bath integrals. They can be expressed by:

$$\begin{aligned}
&\prod_l \int dx_{N,l} \int dx_{0,l} \int dx'_{0,l} \langle x_{N,l}|\exp\left[-i \int_0^t H_{env}(\overline{o}) ds/\hbar\right]|x_{0,l}\rangle \\
&\quad \times \langle x_{0,l}|\rho_{bath}(0)|x'_{0,l}\rangle\langle x'_{0,l}|\exp\left[i \int_0^t H_{env}(\overline{o'}) ds/\hbar\right]|x_{N,l}\rangle \ ,
\end{aligned} \tag{5.18}$$

with the definition of a "path distribution" $\widetilde{o}$ as:

$$\begin{aligned}\widetilde{o} =& o_0(1 - \Theta[t - dt/2]) + \sum_{m=1}^{N-1} o_m(\Theta[t - dt(k - 1/2)] - \Theta[t - dt(k + 1/2)]) \\ &+ o_N\Theta[t - dt(N - 1/2)] \ .\end{aligned} \tag{5.19}$$

Note the property of the symmetric Trotter splitting and, following from it, an initial and a final propagation with H_{env} over half a time slice dt, shows itself in the first and last term of Equation (5.19). These two terms are only different from zero in a time window of $\frac{dt}{2}$. The reason for that is, initially the system operators are only propagated after the bath was propagated by half a time slice and afterwards all the propagation are over full time slices dt, until another propagation of the bath at the very end of the time evolution again only over half a time slice.

Equation (5.18) is fairly similar to Equation (5.9) and from there one arrives at the form of the Feynman-Vernon influence functional in Equation (5.12). The distribution $\widetilde{o}$ plugged into Equation (5.12) gives a discretized version:

$$\mathrm{F}_{FV,dis} = \exp\left[-\frac{1}{\hbar}\sum_{k=0}^{N}\sum_{k'=0}^{k}(o_k - o'_k)(\eta_{kk'}o_{k'} - \eta^*_{kk'}o'_{k'})\right] \ . \tag{5.20}$$

The $\eta_{kk'}$ are calculated in appendix B.1.1. Essential for the following discussion is the relationship with the spectral density function $J(\omega)$ through the function $Q(t - t')$, which is the second integral of the bath correlation function $L(t - t')$, specified by the conditions $F_{FV,dis} = 0$ for $t = t_0$ and $Q(t) = Q(-t)^\dagger$. The connection is given by: $\eta_{kk'} = \eta(t_k - t_{k'}) \propto Q(t - t')$. For a rapidly decaying $J(\omega)$, for instance with an exponential cut off function or with a Debye cut off function, the resulting bath response function L is also fast decaying, if $T \neq 0$, and thus is Q. This allows to neglect the time non-local coupling between the eigenvalues of O for sufficiently large time distances. Let $\tau = Kdt$ with K being an integer and τ the maximum memory defined by the number of time slices after which the correlations between the system coupling operators are decayed, then for $t - t' = dt(k - k') > \tau$ the coupling $\eta_{kk'} = 0$, obviously this is equivalent of the $k - k' > K$. With this follows for Equation (5.20):

$$\begin{aligned} \mathrm{F}_{FV,\tau} &= \exp\left[-\frac{1}{\hbar}\sum_{k=0}^{N}\sum_{\max\{0,k-K\}}^{k}(o_k - o'_k)(\eta_{kk'}o_{k'} - \eta^*_{kk'}o'_{k'})\right] \\ &= \prod_{k'=0}^{N}\prod_{k=k'}^{\min\{N,k'+K\}}\exp\left[-\frac{1}{\hbar}(o_k - o'_k)(\eta_{kk'}o_{k'} - \eta^*_{kk'}o'_{k'})\right] \\ &= \prod_{k'=0}^{N}\widetilde{I}_{k';K}(o_{k'},...,o_{k'+K}) \ . \end{aligned} \tag{5.21}$$

This rearrangement of the sum in the exponential is necessary for the iterative scheme, since it allows to integrate out, e.g. numerically sum over, all possible eigenstates of $o_{k'}$ and $o'_{k'}$, starting with the earliest times. Each $\widetilde{I}_{k';K}(o_{k'},...,o_{k'+K})$ contains all correlations from a time $t_{k'}$ until a future time $t_{k'+K}$. In this notation if $k = \widetilde{k} + k' > N$ the difference $o_k - o'(k)$ is set to 0. It should be pointed out, that $\eta_{kk'}$ has special values for $k = 0, N$ and $k' = 0, N$.
For final times $t_f \leq \tau$ the whole path integral of Equation (5.17) has to be evaluated to get the reduced density matrix, for times $t_k > \tau$ two tensors need to be defined to achieve this:

$$A_{k+1}(o_{k+1},o'_{k+1},...,o_{k+K},o'_{k+K}) = \int do_k \int do_{k'} \Lambda_k(o_k,o'_k,....o_{k+K},o'_{k+K})A_k(o_k,o'_k,...,o_{k+K-1},o'_{k+K-1}) \ , \tag{5.22}$$

and

$$\Lambda_k(o_k,o'_k,....o_{k+K},o'_{k+K}) = \langle o_{k+1}|\exp[-iH_S dt/\hbar]|o_k\rangle\langle o'_k|\exp[iH_S dt/\hbar]|o'_{k+1}\rangle\widetilde{I}_{k;K}(o_k,...,o_{k+K}) \ , \tag{5.23}$$

with initial condition

$$A_0(o_0,o'_0,....o_{K-1},o'_{K-1}) = \langle o_0|\rho(t_0)|o_0\rangle \ . \tag{5.24}$$

Λ_0 contains η_{00} and η_{k0}, while all other Λ_k are constructed only with $\eta_{kk'}$ and η_{kk}. To obtain the reduced density matrix as in Equation (5.17), the tensor A_k has to be integrated over all its coordinates and multiply with the last $K\,\widetilde{I}_{k';K}(o_{k'},...,o_{k'+K})$, containing η_{Nk} and η_{NN} and the corresponding system propagations. With o_f=o_{k+K}:

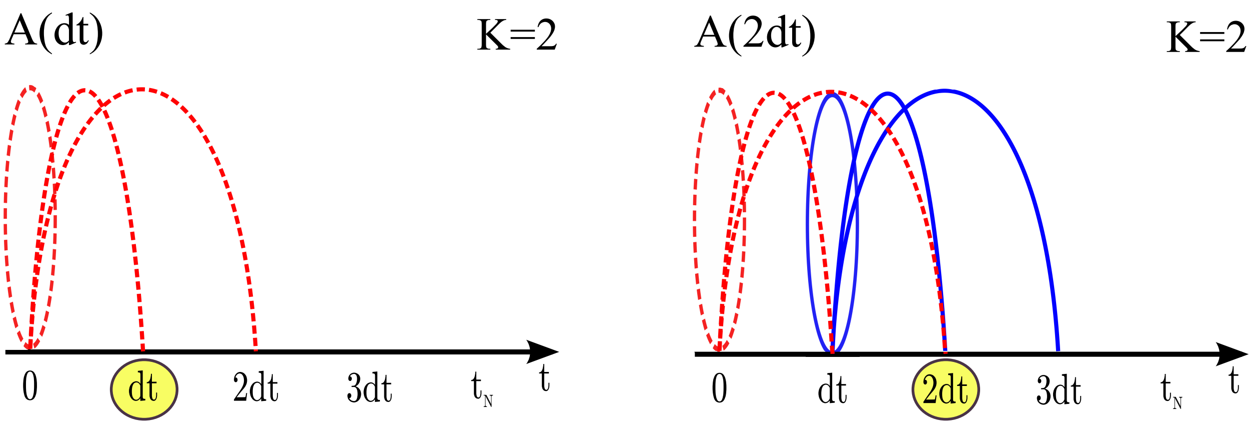

Figure 5.1: Here two different A tensors are shown. The red lines represent the unique correlations between the starting point at $t = 0$ (η_{k0}) and endpoint $t = t_N$ (η_{Nk}) of the simulation. The blue lines stand for the $\eta_{kk'}$, being used throughout most of the simulation. On the left side the first tensor $A(dt)$ calculated from the initial condition shown in Equation (5.24). This first A tensor calculated out of the starting conditions only contains η_{k0}. The yellow circle represents the system propagations and integrations that have taken place.

$$\begin{aligned}\rho_{red}(o_f, o'_f,) = &\int do_k \int do'_k .... \int do_{k+K-1} \int do_{k+K-1} A_k(o_k, ..., o'_{k+K-1}) \\ &\times \langle o_f | \exp[-iH_S dt/\hbar] | o_{k+K-1}\rangle .... \langle o_{k+1} | \exp[-iH_S dt/\hbar] | o_k \rangle \\ &\times \langle o'_k | \exp[iH_S dt/\hbar] | o'_{k+1}\rangle .... \langle o'_{k+K-1} | \exp[iH_S dt/\hbar] | o'_f \rangle \\ &\times \widetilde{I}_{k;K}(o_k, ..., o'_{o_f}) \widetilde{I}_{k;K}(o_{k+1}, ..., o'_{o_f}, 0, 0) .... \widetilde{I}_{k;K}(o_f, o'_f, 0, ..., 0) \quad .\end{aligned} \tag{5.25}$$

An example for the iterative scheme is given Figure 5.1, where the A tensor is shown at two different times dt and $2dt$. The red lines represent the unique correlations between the starting point at $t = 0$ and the k.-th time slice, the $\eta'_{k0}s$ as well as the correlations between the k.-th time slice and the endpoint $t = t_N$, the $\eta'_{Nk}s$. The blue lines stands for the correlations between the k.-th time slice and the k'.-th time slice, $\eta'_{kk'}s$, with $k, k \neq o, N$. The $\eta_{kk'}$ are usually being used throughout most of the simulation, since the final time is normally multiples of τ. On the left side the first tensor $A(dt)$ calculated from the initial condition given in Equation (5.24). This first A tensor calculated out of the starting conditions only contains η_{k0}. The yellow circle represents the system propagations and integrations that have taken place. On the right side the second tensor $A(2dt)$ is calculated from $A(dt)$. All new correlations, given by Equation 5.22, are of $\eta_{kk'}$ type and thus represented by blue lines. On the left side the system was propagated from $t = 0$ to $t = dt$ and the system coordinates o_0, o'_0 have been integrated out. While on the right side the system was propagated from $t = 0$ to $t = 2dt$ and the system coordinates o_0, o'_0,o_1, o'_1 have been integrated out. Both objects allow the calculation of two different reduced density matrices, the left one at $t = 3dt$ and the right on at $t = 4dt$. To achieve this Equation (5.25) has to be evaluated, for $A(2dt)$ this gives the density matrix with $K = 2$ shown in Figure 5.2.

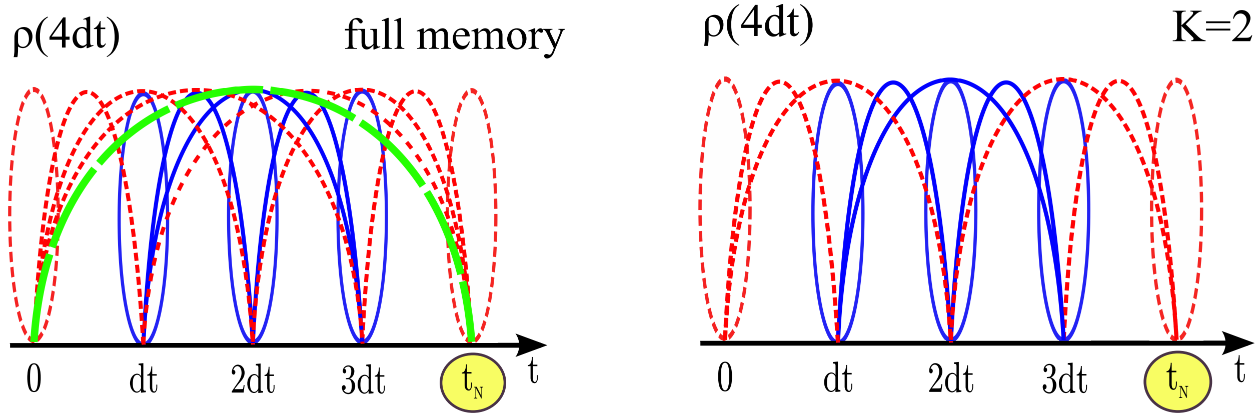

Figure 5.2: This figure shows a sketch of the density matrix at $t_N = 4dt$ for full memory (left) and memory a restriction of $\tau = 2dt$. The yellow circle around a time symbolizes that all integrations up to that time have been performed and all system propagations have been done until said time. The red lines represent the unique correlations between the starting point at $t = 0$, the $\eta'_{k0}s$ and endpoint $t = t_N$, the $\eta'_{Nk}s$, of the scheme. The green line marks the correlation between starting point and endpoint, η_{N0}.

In Figure 5.2 two reduced density matrices are shown, the one on the left has full memory, while the one on the right has the memory restricted to $\tau = 2dt$, hence $K = 2$. Again, the yellow circle around a time symbolizes that all integrations up to that time have been performed and all system propagations have been done until said time. As before the red lines represent $\eta'_{k0}s$ as well as the $\eta'_{Nk}s$ and the blue lines stand for the $\eta_{kk'}$. The green line marks the correlation between the starting point and the endpoint, η_{N0}. The latter is the first correlation to be neglected by the evaluation of $A(dt)$ via Equation (5.25). The correlation η_{N0} is dependent on the absolute value of t_N and therefore has to be calculated for each evaluation of Equation (5.17). The evaluation of $A(dt)$ makes $K + 1$ more propagations necessary and connects each of the following time slices to the end point, thus uses η_{Nk}. While comparing these two objects can give valuable information about convergence, often times the t_N investigated is well beyond the memory time τ considered and other convergence measures have to be employed instead.

This differs from the original paper, where ρ_{red} is defined as

$$\rho_{red}(o_f, o'_f,) = A_N(o_f, o'_f, 0, 0, ...0, 0,)\widetilde{I_{k;K}}(o_f, o'_f, 0, ..., 0) \ . \tag{5.26}$$

The error created by this original evaluation of the A tensor is rather small, Michael Thorwart used this original QUAPI scheme to calculate the displaced dissipative harmonic oscillator and compared it with analytical results and found very good agreements [119]. Differences between the two evaluation methods become smaller with longer simulation times since, the number of correct $\eta_{kk'}$ used increases accordingly. Additional errors can only occur in non-diagonal matrix elements for ρ_{red} written in the eigenbasis O and therefore the trace is not affected at all. More interesting are cases, where the full evaluation of the path integral for the first K time steps creates a significant difference to the first result of the iterative scheme, which will be discussed in more detail later on in chapter 7. This difference showcases the effect of the approximation of finite memory times and thus of the neglect of $\eta_{kk'}$ for $k - k' > \tau$ and most importantly of η_{N0}, which can create a discontinuity between the evaluation of ρ at time t_K and t_{K+1}, during the research of this thesis, this typically became apparent during the transition from the strongly damped regime of the TLS to the overdamped regime and also for unconverged results, giving an additional indication if convergence is reached.

5.2.1 Converged parameters

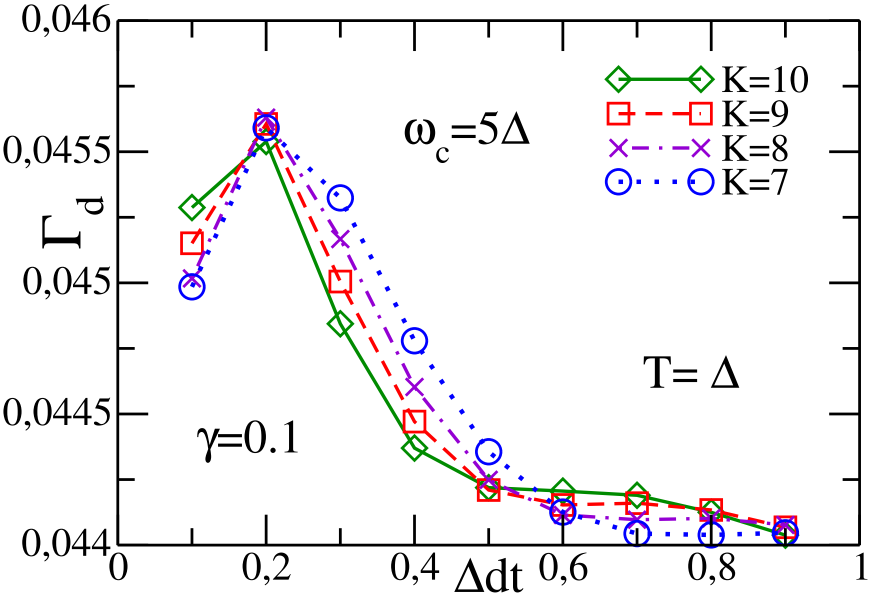

Figure 5.3: This figure shows a comparison of the decoherence rates for different QUAPI parameters K and dt. The results are obtained from fitting the form of the small coupling result to the time evolution of the expectation value of σ_z for a symmetric TLS $H_S = \frac{\Delta}{2}\sigma_x$ with a single bath coupled via σ_z with $\gamma = 0.1$, $T = \Delta$ and $\omega_c = 5\Delta$. Four cases of memory lengths K, $K = 7$ to $K = 10$, and nine different dt's, $dt = 0.1\Delta^{-1}$ to $dt = 0.9\Delta^{-1}$, are considered.

An important feature of these simulations is the interplay of two competing errors. With the first one resulting from the Trotter splitting, which increases as dt increases. As well as a second one resulting from the memory cut off, which increases for a constant K as dt decreases. Additionally with too large dt sampling problems become evident, limiting the dt to a maximum of half the oscillation time of the system. These errors will be showcased with the model used throughout this thesis: the symmetric two level system, see chapter 3. The system Hamiltonian for the symmetric two level system is defined there as: $H_S = \frac{\Delta}{2}\sigma_x$. For small system-bath coupling one finds $\langle\sigma_z(t)\rangle \approx \cos(\Delta t)\exp[-\Gamma_d t]$, see chapter 4, with a system oscillation time of $T_S \approx 2\pi\Delta^{-1}$ therefore the limitation is $dt \leq \pi\Delta^{-1}$. In Figure 5.3 a comparison for different time slices dt and memory lengths K is shown. While overall the rates obtained for this specific case only vary between $\Gamma_d = 0.0457$ and $\Gamma_d = 0.0442$, thus with a percentage difference of only $\approx 3.3\%$. While all these QUAPI results are acceptable to give a qualitative statement about the decoherence rate, the general considerations to obtain converged results can be illustrated. At first the differences are considered large, with the Γ_d reaching a maximum at $dt = 0.2$. These differences remain large until a plateau is reached. In this plateau the memory time τ is large enough, that a further increase of the memory does not improve the results significantly. For the maximum memory steps considered here, $K = 10$ represented by the green line, the plateau is reached between $dt = 0.4\Delta^{-1}$ and $dt = 0.5\Delta^{-1}$, taking the average one could assume that at $dt = 0.45\Delta^{-1}$ the plateau is reached implying a memory of $\tau = 4.5\Delta^{-1}$ is necessary. This is confirmed by the red line, representing $K = 9$ and $dt = 5$, which implies $\tau = 4.5\Delta^{-1}$ as well, also by the purple line, which stands for $K = 8$ and $dt = 0.6$ implying $\tau = 4.8\Delta^{-1}$ and the blue line, representing $K = 7$, and $dt = 0.7$ implying $\tau = 4.9\Delta^{-1}$. The length of this plateau is limited by the dt error from the Trotter splitting of Equation (5.14). This error is quadratic in dt, as explained before, and a linear increase starting at the end of the plateau between $dt = 0.8\Delta^{-1}$ and $dt = 0.9\Delta^{-1}$ shows this. As an additional measurement for convergence one can look at the actual function of dt and search for a discontinuity between $\rho(Kdt)$ and $\rho((K+1)dt)$. Thereby comparing the last evaluation of the full path integral to the first evaluation of the A tensor. Even though this only appears to be useful, if one is far off the actual plateau.

5.3 Hybrid-QUAPI: combination with a master equation

A possible and numerically cheap way to include multiple bath fluctuation in the QUAPI scheme is the combination of the original scheme with a master equation approach as introduced in chapter 2.2. For the following derivation a PDB will be phenomenologically included in the system propagation, with the same Lindblad equation employed in chapter 4.4. A standard SBM will be included via a bath with system-bath coupling operator $o = \frac{\sigma_z}{2}$. The regular QUAPI approach employs a time discretization to split the quantum mechanical time evolution operator $U(t) = \exp(-iHt)$ and further separates system and bath contributions via a symmetric Trotter splitting as detailed above. Since a quantum mechanical time evolution operator can only be formulated for hermitian dynamics, here instead a time evolution superoperator must be used, as introduced in Chapter 3.1.

$$U(t) = e^{\mathcal{L}t} \quad \text{and} \quad W(t) = \mathcal{U}(t)W(0) \ . \tag{5.27}$$

Thereby $\mathcal{L} = \mathcal{L}_S + \mathcal{L}_{SB}$, $\mathcal{L}_{SB} = -\frac{i}{\hbar}[H_{SB}, .]$ and $\mathcal{L}_S = -\frac{i}{\hbar}[H_S, .] + \Gamma_L$ including the Lindblad superoperator Γ_L. As in the case of normal operators the time discretization is straightforward: $\mathcal{U}(t) = \prod_{i=1,N} \mathcal{U}(dt)$ for $t = Ndt$. The full superoperator $\mathbb{1}$ is defined by :

$$\mathbb{1} = \int_{-\infty}^{\infty} d\sigma_z^+ \int_{-\infty}^{\infty} d\sigma_z^- \int_{-\infty}^{\infty} d\mathbf{x}^+ \int_{-\infty}^{\infty} d\mathbf{x}^- |\sigma_z^\pm, \mathbf{x}^\pm)(\sigma_z^\pm, \mathbf{x}^\pm| \ , \tag{5.28}$$

with superstates $|\sigma_z^\pm, \mathbf{x}^\pm) = |\sigma_z^+, \mathbf{x}^+\rangle\langle\sigma_z^-, \mathbf{x}^-|$ and scalar product $(A|B) = Tr\{A^+B\}$ for operators A,B acting on the Hilbert space. Inserting the superoperator $\mathbb{1}$ in between the discretized time evolution superoperator $\mathcal{U}(dt)$ at a time $t_j = j * dt$ gives elements of the form:

$$(\sigma_{z,j}^\pm, \mathbf{x}_j^\pm | e^{\mathcal{L}\delta t} | \sigma_{z,j+1}^\pm, \mathbf{x}_{j+1}^\pm) = \mathrm{Tr}\{|\sigma_{z,j}^-, \mathbf{x}_j^-\rangle\langle\sigma_{z,j}^+, \mathbf{x}_j^+| e^{\mathcal{L}\delta t}[|\sigma_{z,j+1}^+, \mathbf{x}_{j+1}^+\rangle\langle\sigma_{z,j+1}^-, \mathbf{x}_{j+1}^-|]\} \ , \tag{5.29}$$

here [.] is being used to highlight on which operator the superoperator $\mathcal{L}$ is acting. As in the regular scheme a symmetrical Trotter splitting is employed to separate the system and bath dynamics:

$$\mathcal{U}(dt) \simeq e^{-i\mathcal{L}_{SB}\frac{\delta t}{2}} e^{-i\mathcal{L}_{SB}\delta t} e^{-i\mathcal{L}_{SB}\frac{\delta t}{2}} + \mathcal{O}(\delta t^3) \ , \tag{5.30}$$

using the fundamental relation $e^{\mathcal{L}_\alpha \delta t}A = e^{-iH_\alpha \delta t} A e^{iH_\alpha \delta t}$, the Hermitian dynamics can be recovered for the bath:

$$\begin{aligned}
&(\sigma_{z,j}^\pm, \mathbf{x}_j^\pm | e^{\mathcal{L}\delta t} | \sigma_{z,j+1}^\pm, \mathbf{x}_{j+1}^\pm) \\
&= (\sigma_{z,j}^\pm | e^{\mathcal{L}_S \delta t} | \sigma_{z,j+1}^\pm) \langle \mathbf{x}_{j+1}^+ | e^{-iH_{SB}(\sigma_{z,j}^+)\frac{\delta t}{2}} e^{-iH_{SB}(\sigma_{z,j+1}^+)\frac{\delta t}{2}} | \mathbf{x}_j^+ \rangle \langle \mathbf{x}_j^- | e^{iH_{SB}(\sigma_{z,j}^-)\frac{\delta t}{2}} e^{iH_{SB}(\sigma_{z,j+1}^-)\frac{\delta t}{2}} | \mathbf{x}_{j+1}^- \rangle \ .
\end{aligned} \tag{5.31}$$

Thus the Feynman-Vernon-influence functional of the regular QUAPI scheme is recovered. Assuming a factorized initial condition $W(0) = \rho_S(0) \otimes \rho_{SB}(0)$, with the bath being in thermal equilibrium initially, the components of the statistical operator can be obtained:

$$\begin{aligned}
&\langle \sigma_{z,N}^+ | \rho_{eff}(t = t_N) | \sigma_{z,N}^- \rangle \\
&= \prod_{j=0,N-1} \int_{-\infty}^{\infty} d\sigma_{z,j}^+ \int_{-\infty}^{\infty} d\sigma_{z,j}^- (\sigma_{z,j+1}^\pm | e^{\mathcal{L}_S \delta t} | \sigma_{z,j}^\pm) \langle \sigma_{z,0}^+ | \rho_S(0) | \sigma_{z,0}^- \rangle I_{FV}(\sigma_0^\pm, ..., \sigma_N^\pm) \ .
\end{aligned} \tag{5.32}$$

Completely analogously to Chapter 5.2 a memory time $\tau = K * \delta t$ is defined and the tensors A and Λ are defined, yielding an iterative scheme that is only slightly modified:

$$A(\sigma^{\pm}_{z,j+1}, ..., \sigma^{\pm}_{z,j+1+K}) = \int_{-\infty}^{\infty} d\sigma^{+}_{z,j} \int_{-\infty}^{\infty} d\sigma^{-}_{z,j} (\sigma^{\pm}_{z,j+1}| e^{\mathcal{L}_S \delta t} |\sigma^{\pm}_{z,j}) A(\sigma^{\pm}_{z,j}, ..., \sigma^{\pm}_{z,j+K}) \Lambda(\sigma^{\pm}_{z,j}, ..., \sigma^{\pm}_{z,j+K+1}) \ . \tag{5.33}$$

Numerically this is not any more expensive than the original Quapi program since only the system dynamics are affected and the superoperator $\mathcal{U}_S$ only has to be determined once.

5.4 QUAPI for multiple baths with commuting system-bath coupling operators

The generalization of the generic system-bath Hamiltonian for multiple baths is straightforward, one only has to add the additional Hamiltonians. This is done by the introduction of an additional index e, which sums over all the baths one wishes to consider. The Hamiltonian therefore reads:

$$H_{gen,multi} = H_S + \sum_e \sum_j \frac{p_{j,e}^2}{2m_{j,e}} + \frac{1}{2} m_{j,e} \omega_{j,e}^2 \left(x_{j,e} - \frac{c_{j,e} O_e}{m_{j,e} \omega_{j,e}^2} \right)^2 \quad . \tag{5.34}$$

Note the different system-bath coupling operators O_e, corresponding to $H_{B,e} + H_{SB,e}$, are general in this equation and the additional baths are all uncorrelated, thus $[x_{a,e}, p_{c,e'}] = i\hbar\delta_{ac}\delta_{ee'}$. Under the condition $[O_e, O_{e'}] = 0$, hence commuting system-bath coupling operators, extending the QUAPI scheme is straightforward. Fundamental is that it is possible to chose the same eigenbasis $|\psi_j\rangle$ with different eigenvalues $o_{k,e,j}$, for a $j-$ dimensional Hilbert space. One great example where this method was employed is the FMO-complex [96, 120, 121]. Here the exciton transport through a protein complex is described with a model Hamiltonian of a seven-state system. With each site representing the exciton sitting on one of the proteins involved. Now one can take the vibration modes, essentially representing the stretching and twisting of the molecules in question, as an example of a bath that acts on the exciton, if it is localized on the respective protein. A natural way to describe such a system-bath interaction, is to let the baths couple to only one of the sites of the system. For the seven baths considered this way, the system-bath coupling operators would therefore be $|j\rangle\langle j|$, with $j \in [1, 7]$. For simplicity the following outline is for the case of only two different baths and will be generalized later on. The applied Trotter splitting for the complete propagator U in Equation (5.14) yields the same form, if one substitutes H_{env} with $H_{env_1} + H_{env_2}$. Furthermore the separation of the two bath dynamics poses no problem and does not give an additional error, since the bath Hamiltonians commute as per construction. The traces over the degrees of freedom for both baths are independent of each other and therefore can be written as $\mathrm{Tr}_{bath}\left\{\exp[iH_{env_1}/\hbar]\exp[iH_{env_2}/\hbar]\right\} = \mathrm{Tr}_{bath_1}\left\{\exp[iH_{env_1}/\hbar]\right\}\mathrm{Tr}_{bath_2}\left\{\exp[iH_{env_2}/\hbar]\right\}$. This allows to write the complete influence functional as a product of all influence functionals, each of the same form as in Equation (5.20) and with the same definition of $\eta's$: $F_{FV,commuting} = \prod_e F_{FV,e}$. While the eigenvalues may differ since the eigenbasis is shared the resulting form is the same as in the single bath:

$$\mathrm{F}_{FV,commuting} = \exp\left[-\frac{1}{\hbar} \sum_e \sum_{k=0}^{N} \sum_{k'=0}^{k} (o_{k,e} - o'_{k,e})(\eta_{kk',e} o_{k',e} - \eta^*_{kk',e} o'_{k',e}) \right] \quad . \tag{5.35}$$

Herein already lies a fundamental advantage of QUAPI compared to other numerical methods. The increase in numerical cost is negligible for the calculation of the η_s. The Λ introduced in Equation (5.23) only has to be calculated once, though each of the K factors in $\widetilde{I}_{k;K}(o_k, ..., o_{k+K})$ now has larger sums in the exponent to calculate, also not numerically expensive. The original iterative scheme for A_k, as defined by Equation (5.22), has exactly the same numerical cost in terms of calculations to be done and storage needed. The only difference is, that one has to choose one of the eigenvalues o_e as o_k, where $o_{e,k}$ is effectively only counting which eigenstate is considered at time t_k. It is even possible to combine all $\eta's$ into one. First it is necessary to introduce new "dummy" eigenvalues defined by $Z|\psi_j\rangle = z_j|\psi_j\rangle$, where the absolute value of z_j has to be non zero. Then one can write

$$o_{k,e,j}\eta_{kk',e}o_{k',e,j'} = z_{k,j}\widetilde{\eta}_{kk',e,j,j'}z_{k',j'} \quad , \tag{5.36}$$

where $\widetilde{\eta}_{kk',e,j,j'} = \eta_{kk',e}\frac{o_{k,e,j}}{z_{k,j}}\frac{o_{k',e,j'}}{z_{k',j'}}$. This definition can be used to combine all bath influentials into one $\eta_{kk',jj'} = \sum_e \widetilde{\eta}_{kk',e,j,j'}$ and rewrite the influence functional as:

$$\mathrm{F}_{FV,commuting} = \exp\left[-\frac{1}{\hbar}\sum_{k=0}^{N}\sum_{k'=0}^{k}(z_k - z'_k)(\eta_{kk',jj'}z_{k'} - \eta^*_{kk',jj'}z'_{k'})\right] \quad . \tag{5.37}$$

Now the only increase in numerical cost lies in the calculation of the $\eta_{kk',e}$ and the calculation of Equation (5.36), which are both negligible. The new type of η is a (2,2)-tensor instead of a (1,1)-tensor, which also evaluates the value of z_k and z_j instead of just the times t_k and $t_{k'}$. All the entries in $\eta_{kk',jj'}$ only have to be calculated once and afterwards the numerical cost is exactly the same.

Herein lies one of the advantages of QUAPI over other numerical methods, such as HEOM [84, 85, 122] or HOPS [123]. If one wishes to increase the number of baths in these methods, the number of differential equation grows rapidly. Surely there are ways to incorporate multiple baths while restricting some of the properties the hierarchy, for example one can reduce the number of bath modes. A few examples for employed restrictions are given and tested in [124].

While in this approach many more interesting cases than just the one described above can be studied, some other very interesting cases are beyond it. As soon as one tries to include system-bath coupling operators that do not commute, this simple approach does not work any more. To investigate these questions the QUAPI method has to be extended to handle these non-commuting baths as well.

5.5 QUAPI for two baths with non-commuting system-bath coupling operators

As mentioned in Chapter 1 there a multiple interesting scenarios, in which one wishes to include non-commuting baths. For simplicity we focus on two non-commuting baths at first, though the line of thought can be employed to two sets of baths, where each set shares the same eigenbasis. To achieve an extension for QUAPI one can follow the derivation of the original QUAPI scheme up to the Trotter splitting. The form of equation (5.14) is still valid for $H_{env} = H_{env,1} + H_{env,2}$.

$$U = \exp[-iH_{env}dt/(2\hbar)]\left(\prod_{j=1}^{N}\exp[-iH_S dt/\hbar]\exp[-iH_{env}dt/\hbar]\right)\exp[iH_{env}dt/(2\hbar)] \ . \tag{5.38}$$

Now a second non-trivial Trotter splitting has to be applied, since $[O_1, O_2] \neq 0$. Again a symmetric Trotter splitting is used to keep the therein resulting overall error of order $O(dt^3)$. Applied this gives:

$$\begin{aligned} U = &\exp[-iH_{env,1}dt/(4\hbar)]\exp[-iH_{env,2}dt/(2\hbar)]\exp[-iH_{env,1}dt/(4\hbar)] \\ &\times\left(\prod_{j=1}^{N-1}\exp[-iH_S dt/\hbar]\exp[iH_{env_1}dt/(2\hbar)]\exp[-iH_{env_2}dt/\hbar]\exp[iH_{env_1}dt/(2\hbar)]\right) \\ &\times\exp[-iH_S dt/\hbar]\exp[-iH_{env,1}dt/(4\hbar)]\exp[-iH_{env,2}dt/(2\hbar)]\exp[-iH_{env,1}dt/(4\hbar)] \ . \end{aligned} \tag{5.39}$$

According to the previous train of thought it becomes necessary for each time step to insert two additional completeness relations, one with O_2 and two with O_1, which will be denoted by an additional index a and b, as the basis for system dynamics and thus with o_2 and o_1 eigenvalues respectively:

$$\mathbb{I}_{1/2} = \int do_{1/2}|o_{1/2}\rangle\langle o_{1/2}| \prod_{l,e=1,2}\int dx_{l,e}|x_{l,e}\rangle\langle x_{l,e}| \ . \tag{5.40}$$

Application for a propagation over one time step, $U(dt)$, therefore gives:

$$\mathbb{I}_{1_b,k}\exp[-iH_S dt/\hbar]\exp[-iH_{env_1}dt/2\hbar]\mathbb{I}_{1_a,k-1}\exp[-iH_{env_2}dt/\hbar]\mathbb{I}_{2,k-1}\exp[-iH_{env_1}dt/2\hbar]\mathbb{I}_{1_b,k-1} \tag{5.41}$$

$$\begin{aligned}
&= \int do_{1_b,k} \int do_{1_a,k-1} \int do_{2,k-1} \prod_l \int do_{1_b,k-1} \prod_{e=1,2} \int dx^3_{l,e,k} \prod_{j=1,2,3} \prod_{l_j} \int dx^j_{l,e,k-1} \\
&\times \langle o_{1_b,k}|\exp[-iH_S dt/\hbar]|o_{1_a,k-1}\rangle\langle x^3_{l,1,k}|\exp[-iH_{env_1}(o_{1_a,k-1})dt/2\hbar]|x^1_{l,1,k-1}\rangle \\
&\times \langle x^1_{l,2,k}|\exp[-iH_{env_2}(o_{2,k-1})dt/\hbar]|x^2_{l,2,k-1}\rangle\langle x^2_{l,1,k-1}|\exp[-iH_{env_1}(o_{1_b,k-1})dt/2\hbar]|x^3_{l,1,k-1}\rangle \\
&\times \langle o_{1_a,k-1}|o_{2,k-1}\rangle\langle o_{2,k-1}|o_{1_b,k-1}\rangle\langle x^1_{l,1,k-1}|x^2_{l,1,k-1}\rangle\langle x^3_{l,2,k}|x^1_{l,2,k-1}\rangle\langle x^2_{l,2,k-1}|x^3_{l,2,k-1}\rangle \\
&\times |o_{1_b,k}\rangle\langle o_{1_b,k-1}| \otimes |x^3_{l,1,k}\rangle\langle x^3_{l,1,k-1}| \otimes |x^3_{l,2,k}\rangle\langle x^3_{l,2,k-1}| \ .
\end{aligned}$$

Here, the index j is according to the order in which each $\mathbb{I}$ have been inserted, counting from left to right. Note that $\prod_{l_j}$ is the product over all degrees of freedom for the j.-th $\mathbb{I}$, for the bath states the convention $|x^j_{l_j,e,k}\rangle \equiv |x^j_{l,e,k}\rangle$ is used, with k the time step and e the two different sets of eigenbases o_e. Furthermore $\langle x^\lambda_{l,e,k}|x^j_{l,e,k}\rangle = \delta(x^\lambda_{l,e,k} - x^j_{l,e,k})$, thus reducing the number of integrals per time slice to one for bath 2 and to two for bath 1. In the following the convention $x^2_{l,2,k} = x_{l,2,k}$ and $x^1_{l,1,k} = x^a_{l,1,k}$,$x^3_{l,1,k} = x^b_{l,1,k}$ will be used.

According to this Equation (5.17) becomes:

$$\begin{aligned}
\rho_{red}(o_{1,a,N}, o'_{1,a,N}, t) &= \oint do_{1,a} \oint do_{1,b} \oint do_2\, \overline{U_S(o_{1,a}, o_{1,b})}\, \Phi(\{o_{1,a}\}, \{o_{1,b}\}, \{o_2\})\, \rangle\langle o_{1_b,0}|\rho_S(0)|o'_{1_b,0}\rangle \\
&\times \oint dx_{1,a} \oint dx_{1,b} \oint dx_2 \widetilde{B}_1\, \widetilde{B}_2\, \langle x^b_{l,1,0}|\rho_{bath,1}(0)|x'^b_{l,1,0}\rangle\langle x_{l,2,0}|\rho_{bath,2}(0)|x'_{l,2,0}\rangle \ .
\end{aligned} \tag{5.42}$$

We have introduced the following definitions:

$$\oint da \equiv \int da_N ... \int da_0 \int da'_N ... \int da'_0 \ . \tag{5.43}$$

Note that $\oint$ does not represent a pathintegral in the conventional sense, but a discretized one. Moreover,

$$\begin{aligned}
\overline{U_S(o_{1,a}, o_{1,b})} &\equiv \langle o_{1_b,N}|\exp[-iH_S dt/\hbar]|o_{1_a,N-1}\rangle....\langle o_{1_b,1}|\exp[-iH_S dt/\hbar]|o_{1_a,0}\rangle \\
&\times \langle o_{1_a,0}|\exp[iH_S dt/\hbar]|o_{1_b,1}\rangle....\langle o_{1_a,N-1}|\exp[iH_S dt/\hbar]|o_{1_b,N}\rangle \ ,
\end{aligned} \tag{5.44}$$

$$\Phi(\{o_{1,a}\},\{o_{1,b}\},\{o_2\}) \equiv \langle o_{1_a,N}|o_{2,N}\rangle\langle o_{2,N}|o_{1_b,N}\rangle....\langle o_{1_a,0}|o_{2,0}\rangle\langle o_{2,0}|o_{1_b,0}\rangle \\ \times \langle o'_{1_a,0}|o'_{2,0}\rangle\langle o'_{2,0}|o'_{1_b,0}\rangle....\langle o'_{1_a,N}|o'_{2,N}\rangle\langle o'_{2,N}|o'_{1_b,N}\rangle \ . \tag{5.45}$$

The $\widetilde{B}_1$ and the $\widetilde{B}_2$ are compromised of the respective bath propagators evaluated according to the inserted $\mathbb{I}'s$ and the delta function that is created by the evaluation of the trace of the bath:

$$\widetilde{B}_2 \equiv \langle x_{l,2,N}|\exp[-iH_{env_2}(o_{2,N})dt/2\hbar]|x_{l,2,N-1}\rangle\langle x_{l,2,N-1}|\exp[-iH_{env_2}(o_{2,N-1})dt/\hbar]|x_{l,2,N-2}\rangle \\ \times ....\langle x_{l,2,1}|\exp[-iH_{env_2}(o_{2,0})dt/2\hbar]|x_{l,2,0}\rangle\langle x'_{l,2,0}|\exp[iH_{env_2}(o'_{2,0})dt/2\hbar]|x'_{l,2,1}\rangle.... \\ \times \langle x'_{l,2,N-2}|\exp[iH_{env_2}(o_{2,N})dt/\hbar]|x'_{l,2,N-1}\rangle\langle x'_{l,2,N-1}|\exp[-iH_{env_2}(o_{2,N})dt/2\hbar]|x'_{l,2,N}\rangle \\ \times \delta(x_{l,2,N} - x'_{l,2,N}) \ . \tag{5.46}$$

Note that Equation (5.46) has the same form as the bath propagators in Equation (5.17). Moreover, we have

$$\widetilde{B}_1 \equiv \langle x^a_{l,1,N}|\exp[-iH_{env_1}(o_{1_a,N})dt/4\hbar]|x^b_{l,1,N}\rangle\langle x^b_{l,1,N}|\exp[-iH_{env_2}(o_{1_b,N-1})dt/4\hbar]|x^a_{l,1,N-1}\rangle \\ \times \langle x^a_{l,1,N-1}|\exp[-iH_{env_1}(o_{1_a,N-1})dt/2\hbar]|x^b_{l,1,N-1}\rangle\langle x^b_{l,1,N-1}|\exp[-iH_{env_2}(o_{1_b,N-1})dt/2\hbar]|x^a_{l,1,N-2}\rangle \\ \times ....\langle x^b_{l,1,1}|\exp[-iH_{env_1}(o_{1_a,0})dt/4\hbar]|x^a_{l,1,0}\rangle\langle x^a_{l,1,0}|\exp[-iH_{env_2}(o_{1_b,0})dt/4\hbar]|x^b_{l,1,0}\rangle \\ \times \langle x'^b_{l,1,0}|\exp[iH_{env_1}(o'_{1_a,0})dt/4\hbar]|x'^a_{l,1,0}\rangle\langle x'^a_{l,1,0}|\exp[iH_{env_2}(o'_{1_b,0})dt/4\hbar]|x'^b_{l,1,1}\rangle.... \\ \times \langle x'^a_{l,1,N-1}|\exp[iH_{env_1}(o_{1_a,N})dt/4\hbar]|x'^b_{l,1,N}\rangle\langle x'^b_{l,1,N}|\exp[-iH_{env_2}(o'_{1_b,N-1})dt/4\hbar]|x'^a_{l,1,N}\rangle \\ \times \delta(x^a_{l,1,N} - x'^a_{l,1,N}) \ . \tag{5.47}$$

In the case of the bath described by B_2 everything is analogous to the original QUAPI scheme, thus Equation (5.21) is the form of the influence functional for this bath. For B_1 a few different steps are necessary. First another path distribution has to be used, the first bath effectively has half or a quarter time slices dt in which the eigenvalues are constant before they change via a unitary basis transformation. To achieve the form of Equation (5.18) the following definition can be used :

$$\widetilde{o_1} = o_{1_b,0}(1 - \Theta[t - dt/4]) + o_{1_a,0}(\Theta[t - dt/4] - \Theta[t - dt/2]) \\ + \sum_{m=1}^{N-1}\{o_{1_b,m}(\Theta[t-(m+1/2)dt] - \Theta[t - mdt]) + o_{1_a,m}(\Theta[t - mdt] - \Theta[t-(m-1/2)dt]\} \\ + o_{1_b,N}(\Theta[t-(N-1/2)dt] - \Theta[t-(N-1/4)dt]) + o_{1_a,N}\Theta[t-(N-1/4)dt] \ . \tag{5.48}$$

After some algebra a similar form to equation (5.20) can be achieved:

$$F^1_{FV,dis} = \exp\left[-\frac{1}{\hbar}\sum_{s=a,b}\sum_{r=a,b}\sum_{k=0}^{N}\sum_{k'=0}^{k}(o_{1_s,k} - o'_{1_s,k})(\eta_{k,s;k',r}o'_{1_r,k'} - \eta^*_{k,s;k',r}o'_{1_r,k'})\right] \ , \tag{5.49}$$

with slightly more complex $\eta_{k,s;k',r}$ compared to the original scheme. Now it is possible to apply the finite memory approximation and derive a modified version of Equation (5.21). Of course it is important to stay consistent with the memory approximation $\tau = Kdt$. The cut off imposes additional conditions for the cases, with non local correlations in time between o_a's and o_b's. For the simple case of $dt = \tau$ this becomes obvious, $\eta_{k+1,a;k,b}$ couples two operators with a time difference of $1.5dt$ and thus would be zero even though in this convention $k - k' = 1$. With this in mind the modified version of the influence functional with non zero exponentials becomes:

$$\begin{aligned} F^1_{FV,\tau} = \exp&\left[-\frac{1}{\hbar}\sum_{s=a,b}\sum_{k'=0}^{N}\sum_{k=k'}^{\min\{N,k'+K\}}(o_{1_s,k} - o'_{1_s,k})(\eta_{k,s;k',s}o'_{1_s,k'} - \eta^*_{k,s;k',s}o'_{1_s,k'})\right] \\ \times \exp&\left[-\frac{1}{\hbar}\sum_{k'=0}^{N}\sum_{k=k'}^{\min\{N,k'+K-1\}}(o_{1_a,k} - o'_{1_a,k})(\eta_{k,a;k',b}o'_{1_b,k'} - \eta^*_{k,a;k',b}o'_{1_b,k'})\right] \\ \times \exp&\left[-\frac{1}{\hbar}\sum_{k'=0}^{N}\sum_{k=k'}^{\min\{N,k'+K\}}(o_{1_b,k} - o'_{1_b,k})(\eta_{k,b;k',a}o'_{1_a,k'} - \eta^*_{k,b;k',a}o'_{1_a,k'})\right] \ . \end{aligned} \tag{5.50}$$

For convenience in notation the zero exponential for $s = a, r = b$ and $k - k' = K$ is included as a factor 1, similar to before, if $k' + k > N$ then $o_{k+k'} = o'_{k+k'}$:

$$\begin{aligned} &= \prod_{k'=0}^{N}\prod_{s,r=a,b}\prod_{k=k'}^{\min\{N,k'+K\}} \exp\left[-\frac{1}{\hbar}(o_{1_s,k} - o'_{1_s,k})(\eta_{k,s;k',r}o'_{1_r,k'} - \eta^*_{k,s;k',r}o'_{1_r,k'})\right] \\ &= \prod_{k'=0}^{N} \bar{I}^1_{k';K}(o_{1_a,k'}, o_{1_b,k'}, \ldots, o_{1_a,k'+K}, o_{1_b,k'+K}) \ . \end{aligned} \tag{5.51}$$

With the condition that for $k = \widetilde{k} + k' > N$ the differences $o_{1_a,k} + o'_{1_a,k}$ and $o_{1_b,k} + o'_{1_b,k}$ are set to zero. This form of the influence functionals has different η's as the original QUAPI scheme, again with special start and end correlations. For the correlations in between the endings, e.g. $k, k' \neq 0, N$, the η's are however similar to the η's of the original scheme with $(k - k' + 1/2)dt$ instead of $(k - k')\Delta$, for $s \neq r$ and equal time arguments for $s = r$. The new iterative scheme becomes:

$$\begin{aligned} &A^{n.c.}_{k+1}(o_{1_a,k+1}, o_{1_b,k+1}, o_{2,k+1}, o'_{1_a,k+1}, ..., o_{2,k+K}, o'_{1_a,k+K}, o'_{1_b,k+K}, o'_{2,k+K}) \\ &\quad = \int do_{1_a,k} \int do_{1_b,k} \int do_{2,k} \int do'_{1_a,k} \int do'_{1_b,k} \int do'_{2,k} \Lambda^{n.c.}_k A^{n.c.}_k(o_{1_a,k}, ..., o'_{2,k+K-1}) \ , \end{aligned} \tag{5.52}$$

with initial condition:

$$A^{n.c.}_0(o_{1_a,0}, ..., o'_{2,K-1}) = |o_{1_b,0}\rangle\langle o_{1_b,0}|\rho_S(0)|o'_{1_b,0}\rangle\langle o'_{1_b,0}| \ . \tag{5.53}$$

The definition of $\Lambda^{n.c.}_k$ is:

$$\begin{aligned} \Lambda^{n.c.}_k &= \Lambda^{n.c.}_k(o_{1_a,k}, o_{1_b,k}, o_{2,k}, o'_{1_a,k'}, ..., o_{2,k+K}, o'_{1_a,k'+K}, o'_{1_b,k'+K}, o'_{2,k'+K}) \\ &= \bar{I}^2_{k;K}(o_{2,k}, .., o_{2,k+K})\bar{I}^1_{k;K}(o_{1_a,k}, o_{1_b,k}, ..., o_{1_a,k'+K}, o_{1_b,k'+K}) \\ &\times \langle o_{1_b,k+1}|\exp[-iH_S dt/\hbar]|o_{1_a,k}\rangle\langle o'_{1_a,k'}|\exp[iH_S dt/\hbar]|o'_{1_b,k'}\rangle \\ &\times \langle o_{1_a,k}|o_{2,k}\rangle\langle o_{2,k}|o_{1_b,k}\rangle\langle o'_{1_b,k'}|o'_{2,k'}\rangle\langle o'_{2,k'}|o'_{1_a,k'}\rangle \ . \end{aligned} \tag{5.54}$$

Again to calculate the reduced density matrix for the first K time slices the whole path integral as in Equation (5.42) has to be evaluated. For times beyond $t = Kdt$ the $A^{n.c.}$ tensor has to be evaluated in the following way. Here the end time of the simulation is given by $t_N = t_k + Kdt$ and accordingly $o_f = o_{1_a,N}$,$o'_f = o'_{1_a,N}$:

$$\begin{aligned} &\rho_{red}(o_{1_a,N}, o'_{1_a,N}, t_N) = \\ &\int do_{1_a,k} \int do_{1_b,k} \int do_{2,k} .... \int do_{1_b,k} \int do_{2,N} \langle o_{1_a,k}|o_{2,k}\rangle\langle o_{2,k}|o_{1_b,k}\rangle ... \langle o_{1_a,N}|o_{2,N}\rangle\langle o_{2,N}|o_{1_b,N}\rangle \\ &\times \int do'_{1_a,k} \int do'_{1_b,k} \int do'_{2,k} .... \int do'_{1_b,N} \int do'_{2,N} \langle o'_{1_a,k}|o'_{2,k}\rangle\langle o'_{2,k}|o'_{1_b,k}\rangle ... \langle o_{1_a,N}|o'_{2,N}\rangle\langle o'_{2,N}|o'_{1_b,N}\rangle \\ &\times \langle o_{1_b,N}|\exp[-iH_S dt/\hbar]|o_{1_a,N-1}\rangle ... \langle o_{1_b,k+1}|\exp[-iH_S dt/\hbar]|o_{1_a,k}\rangle A^{n.c.}_k(o_{1_a,k}, ..., o'_{2,N-1}) \\ &\times \langle o'_{1_b,k+1}|\exp[iH_S dt/\hbar]|o'_{1_a,k}\rangle ... \langle o'_{1_b,N-1}|\exp[iH_S dt/\hbar]|o'_{1_a,N}\rangle \bar{I}^1_{k;K}(o_{1_a,k}, ..., o_{1_b,N})\bar{I}^2(o_{2,k}, ..., o'_{2,N}) \\ &\times \bar{I}^1_{k;K}(o_{1_a,k+1}, ..., o_{1_b,N}, 0, 0, 0, 0) ... \bar{I}^2(o_{2,N}, o'_{2,N}, 0, ..., 0) \ . \end{aligned} \tag{5.55}$$

While this scheme is generic for two sets of system-bath coupling operators that do not commute, it also holds some disadvantages. The dimension of the original QUAPI tensors A_k and Λ_k are $\dim(A) = \dim(H_S)^{2K}$ and $\dim(\Lambda_k) = \dim(H_S)^{2K+2}$ corresponding to the $2K$ and $2K + 2$ sets of eigenvalues they depend on respectively . The new schemes tensors $A^{n.c.}_k$ and $\Lambda^{n.c.}_k$ depend on $6K$ and $6K + 6$ sets of eigenvalues respectively, thus $\dim(A^{n.c.}_k) = \dim(A_k)^3$. This is a major problem with this scheme. The numerical cost to achieve a converged simulation such that dt is sufficient small while τ is still large enough, is in most cases out of reach. A solution to this problem is a loss of generality, which keeps the non-commuting property of the sets of system-bath coupling operators, but imposes the condition, that one of the sets must share the same eigenbasis with the Hamiltonian, e.g. one of the sets consists of pure dephasing baths. This will be derived in the following chapter and is the two bath code used throughout this thesis.

5.6 QUAPI for multiple baths with non-commuting system-bath coupling operators with pure dephasing bath

A solution of the problem of numerical cost can be achieved through the reduction of the size of the tensors by imposing the condition:

$$[H_S, H_{env,1}] = 0 \ . \tag{5.56}$$

Then the Trotter splitting is exact: $e^{-i(H_S+H_{env,1})dt/\hbar} = e^{-iH_S dt/\hbar}e^{-iH_{env,1}dt/\hbar}$. Now the dynamics can be split two times. First the non-commuting Hamiltonian $H_{env,2}$ is separated:

$$U = \exp[-iH_{env_2}dt/(2\hbar)]\left(\prod_{j=1}^{N}\exp[-i(H_S + H_{env_1})dt/\hbar]\exp[-iH_{env_2}dt/\hbar]\right)\exp[iH_{env_2}dt/(2\hbar)] \ . \tag{5.57}$$

Now the separation of the commuting Hamiltonian $H_{env,1}$ follows:

$$\begin{aligned} &= \exp[-iH_{env_2}dt/(2\hbar)]\left(\prod_{j=1}^{N}\exp[-iH_S dt/\hbar]\exp[-iH_{env_1}dt/\hbar]\exp[-iH_{env_2}dt/\hbar]\right) \\ &\times \exp[iH_{env_2}dt/(2\hbar)] \ . \end{aligned} \tag{5.58}$$

The insertion of the completeness relations $\mathbb{I}_{1/2}$ for the baths in each time step, for details see Equation (5.40)to Equation (5.41) , thus gives :

$$
\begin{aligned}
&\exp[-iH_S dt/\hbar]\exp[-iH_{env_1}dt/\hbar]\mathbb{I}_{1,k}\exp[-iH_{env_2}dt/\hbar]\mathbb{I}_{2,k} \\
&\quad = \int do_{1_b,k}\int do_{2,k}\prod_{e=1,2}\prod_{j=1,2}\int dx^j_{l,e,k} \\
&\quad \times \exp[-iH_S(o_{1,k})dt/\hbar]\langle x^1_{l,1,k}|\exp[-iH_{env_1}(o_{1,k})dt/\hbar]|x^2_{l,1,k}\rangle \\
&\quad \times \langle x^1_{l,2,k}|\exp[-iH_{env_2}(o_{2,k})dt/\hbar]|x^2_{l,2,k}\rangle\langle o_{1,k}|o_{2,k}\rangle \\
&\quad \times |o_{1,k}\rangle\langle o_{2,k}|\otimes|x^1_{l,1,k}\rangle\langle x^2_{l,1,k}|\otimes|x^1_{l,2,k}\rangle\langle x^2_{l,2,k}| \enspace .
\end{aligned}
\tag{5.59}
$$

Now only a dependence on two eigenvalues for the bath propagation in a time step is necessary instead of three as in the general case. This translates into the reduced density matrix, the A tensor and the Λ tensor. For the second bath the $\eta' s$ resulting from this are the same as in the original QUAPI scheme, with special $\eta' s$ for the beginning and end points, see appendix B.1.1. While the first bath only contains two different $\eta' s$: η_{kk} and $\eta_{kk'}$, since there are no accentuated points in the propagation. The iterative scheme becomes:

$$
A^{s.c.}_0(o_{2,0}, o_{1,1}, ..., o'_{2,K-1}, o'_{1,K}) = |o_{2,0}\rangle\langle o_{2,0}|\rho_S(0)|o'_{2,0}\rangle\langle o'_{2,0}| \tag{5.60}
$$

$$
. \tag{5.61}
$$

The Λ tensor becomes:

$$
\begin{aligned}
\Lambda^{s.c.}_k &= \Lambda^{s.c.}_k(o_{2,k}, o_{1,k+1}, ..., o'_{2,k+K}, o'_{1,k+K+1}) \\
&= \bar{I}^2_{k;K}(o_{2,k}, o'_{2,k'}, .., o_{2,k+K})\bar{I}^1_{k;K}(o_{1,k+1}, o'_{1,k'+1}, ..., o'_{1,k'+K+1}) \\
&\times \exp[-iH_S(o_{1,k+1})dt/\hbar]\exp[iH_S(o'_{1,k'+1})dt/\hbar] \\
&\times \langle o_{2,k+1}|o_{1,k+1}\rangle\langle o_{1,k+1}|o_{2,k}\rangle\langle o'_{2,k'}|o'_{1,k+1}\rangle\langle o'_{1,k+1}|o'_{2,k+1}\rangle \enspace ,
\end{aligned}
\tag{5.62}
$$

yielding a slightly modified iteration scheme:

$$
\begin{aligned}
&A^{n.c.}_{k+1}(o_{2,k+1}, o_{2,k+2}, ..., o_{2,k+K}, o'_{1,k+K+1}) \\
&\quad = \int do_{1,k+1}\int do_{2,k}\int do'_{1,k+1}\int do'_{2,k}\Lambda^{n.c.}_k A^{n.c.}_k(o_{2,k}, o_{2,k+1}, ..., o'_{2,k'+K-1}, o'_{1,k+K}) \enspace ,
\end{aligned}
\tag{5.63}
$$

and an accordingly modified evaluation scheme:

$$
\begin{aligned}
&\rho_{red}(o_{2,N}, o'_{2,N}, t_N) = \\
&\int do_{1,k+1} \int do_{2,k} .... \int do_{1,N} \int do_{2,N} \langle o_{2,k} | o_{1,k+1} \rangle \langle o_{1,k+1} | o_{2,k+1} \rangle ... \langle o_{2,N-1} | o_{1,N} \rangle \langle o_{1,N} | o_{2,N} \rangle \\
&\times \int do'_{1,k+1} \int do'_{2,k} .... \int do'_{1,N} \int do'_{2,N} \langle o'_{2,k} | o'_{1,k+1} \rangle \langle o'_{1,k+1} | o'_{2,k+1} \rangle ... \langle o'_{2,N-1} | o'_{1,N} \rangle \langle o'_{1,N} | o'_{2,N} \rangle \\
&\times \langle o_{1_b,N} | \exp[-iH_S dt/\hbar] | o_{1_a,N-1} \rangle ... \langle o_{1_b,k+1} | \exp[-iH_S dt/\hbar] | o_{1_a,k} \rangle A_k^{n.c.}(o_{1_a,k}, ..., o'_{2,N-1}) \\
&\times \langle o'_{1,k'+1} | \exp[iH_S dt/\hbar] | o'_{1_a,k} \rangle ... \langle o'_{1_b,N-1} | \exp[iH_S dt/\hbar] | o'_{1_a,N} \rangle \bar{I}^1_{k;K}(o_{1_a,k}, ..., o_{1_b,N}) \bar{I}^2(o_{2,k}, ..., o'_{2,N}) \\
&\times \bar{I}^1_{k;K}(o_{1,N}, o'_{1,N}, 0, ..., 0) \bar{I}^2(o_{2,N}, o'_{2,N}, 0, ..., 0) \ .
\end{aligned}
\tag{5.64}
$$

With this iteration scheme it is now possible to achieve $K = 6$ for convergence investigations. Though $K = 7$ is possible to be run as a code, it is impractical to be used for convergence investigations due to the long calculation times needed. After all to get a valid simulation of the density matrix for one set of parameters over reasonably long times t multiple dt's and K's have to be used. To get a feeling for this, note a typical convergence investigation had dt's ranging between $0.1\Delta^{-1} - 0.9\Delta^{-1}$ and $K = 4, 5, 6$, thus needing on average 27 simulations for a single usable one. Simulation times above a day where therefore unacceptable for the problems we wished to examine in this project. This method is published in [97].

Chapter 6

Non-pertubative environmental influence on decoherence

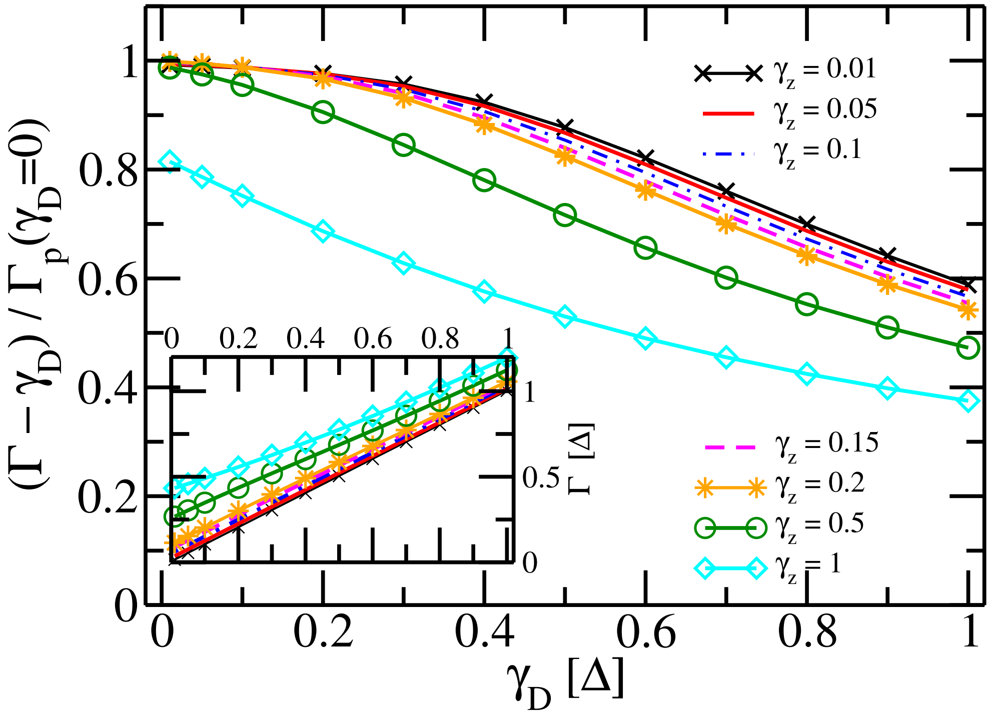

Figure 6.1: The difference of decoherence rate and γ_D normalized by the standard RESPET result $\Gamma_p(\gamma_d = 0)$ is plotted against γ_D. Various system-bath couplings γ_z have been investigated at temperature $T = \Delta/k_\mathrm{B}$ for $\omega_c = 5\Delta$. The inset shows the monotonical increase of the overall decoherence rate Γ

The first question investigated as part of this project was an already dissipative quantum system which is exposed to environmental fluctuations. This was studied by employing the technically easiest approach to include dissipation independently of fluctuations with the derived Hybrid methods, for which the details have been shown in chapter 4.4 for the perturbative method RESPET and in chapter 5.3 for the numerically exact simulation QUAPI. In both cases an already dissipative quantum system is exposed to environmental fluctuations. A dissipative quantum system is created by modifying the von-Neumann equation with Lindblad operators such that the system only experiences dephasing. The strength of these Lindblad rates is given by γ_D. The investigated Hamiltonian is a SBM as given in Equation 4.1. For simplicity an Ohmic spectral function $J(\omega) = \gamma_z \omega f_c(\omega, \omega_c)$ is used, with a cut off function of Debye form $f_c(\omega, \omega_c) = \frac{\omega_c^2}{\omega_c^2+\omega^2}$. The decoherence rate Γ of the TLS is then determined by fitting $f(t) = \cos(\Delta t)e^{-\Gamma t}$ to the expectation value $\langle \sigma_z(t) \rangle$ to the numerical results of the Hybrid-Quapi scheme. The inset of figure 6.1 shows the decoherence rate Γ versus the dephasing rate γ_D at $T = \Delta/k_B$ with $\omega_c = 5\Delta$. For all studied system-bath couplings γ_z the rate Γ increases monotonically with γ_D, which is qualitatively in agreement with equation 4.39.

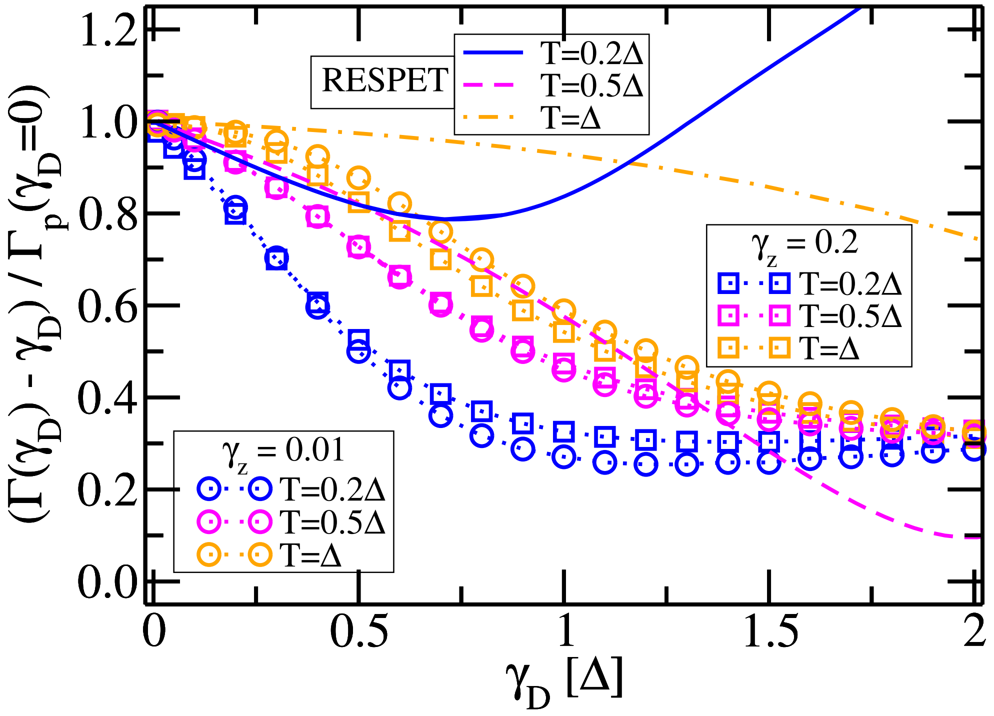

Figure 6.2: The ratio Γ_{rat} is plotted for various temperatures and two system-bath couplings $\gamma_z = 0.01$ and $\gamma_z = 0.2$ obtained from the Hybrid-QUAPI simulation. The ratio Γ_{rat} was also calculated for the Hybrid-RESPET result for three different temperature $T = 0.2\Delta/k_B, 0.5\Delta/k_B, \Delta/k_B$. For visibility $k_B = 1$ is used here.

In order to separate out the contribution of the system-bath coupling γ_z in figure 6.1 the difference between the decoherence rate and the dephasing rate is plotted and normalized by the perturbative result Γ_p, given in Equation (4.39), for $\gamma_D = 0$, thus a non-modified von-Neumann equation. In the following this ratio will be called $\Gamma_{rat} = (\Gamma(\gamma_D) - \gamma_D)/\Gamma_P(\gamma_D = 0)$. For $\gamma_D = 0$ the normalized rate is different from 1 only if the system-bath coupling γ_z is large, e.g. $\gamma_z = 1$. Here, in contrast to QUAPI, RESPET fails to accurately describe a SBM, even without the inclusion of the Lindblad rate. Therefore we focus on system-bath couplings $\gamma_z \leq 0.2$ here after. Nonetheless for small γ_D and small γ_z the decoherence rate is the sum of the dephasing rate γ_D and the weak coupling result for the SBM. Surprisingly for all γ_z the ratio decreases for a larger dephasing rate γ_D. This means the inclusion of a phenomenological dephasing rate suppresses the decohering effect of the fluctuations in the SBM. In contrast the relaxation rate remains unaffected within the numerical accuracy of the hybrid QUAPI scheme. The relaxation rate is determined by fitting to the expectation value $\langle\sigma_x\rangle$.

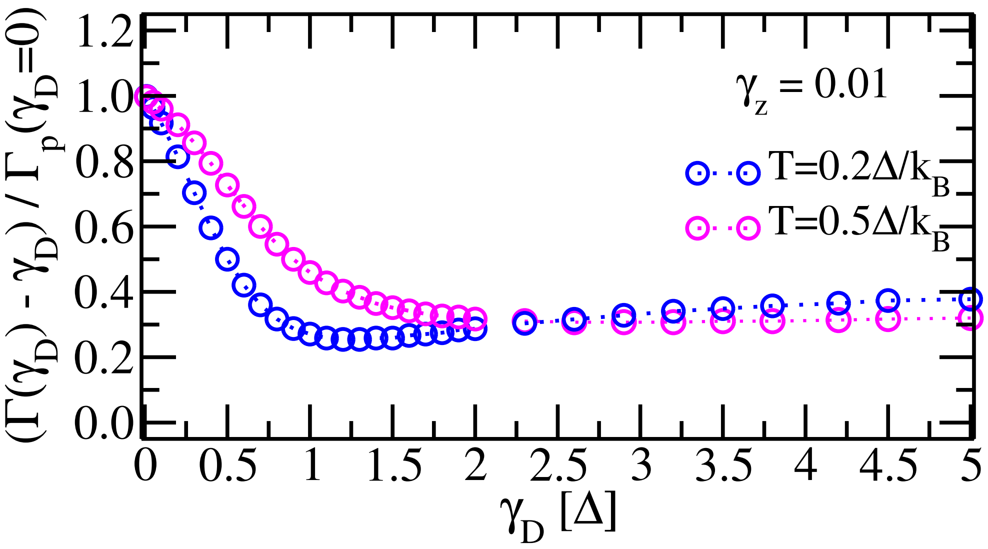

Figure 6.3: The ratio Γ_{rat} for the Hybrid-QUAPI results is investigated at weak system-bath coupling $\gamma_z = 0.01$ for two temperatures $T = 0.2\Delta/k_B$ and $T = 0.5\Delta/k_B$ for a larger range of γ_D.

To further study suppressing of the decoherence in figure 6.2 Γ_{rat} is investigated in the case of a rather strong coupling with $\gamma_z = 0.2$ as well in the case of weak coupling with $\gamma_z = 0.01$ at five temperatures, e.g. $T = 0.01\Delta/k_B, 0.05\Delta/k_B, 0.2\Delta/k_B, 0.5\Delta/k_B, \Delta/k_B$, and three temperatures, e.g. $T = 0.2\Delta, 0.5\Delta, \Delta$. In case of $T = 0.01\Delta/k_B, 0.05\Delta/k_B$ the data coincides thus representing the low-temperature limit. For the perturbative results the ratio Γ_{rat} is independent of γ_z, since $\Gamma_p - \gamma_D$ is proportional to γ_z according to Equation (4.39), though this only holds for lowest order perturbation.

Surprisingly there are cases in which small coupling numerically exact results results differ not only strongly from the perturbative rate, they even differ more then the strong coupling results. The simulation data shows small deviations between $\gamma_z = 0.01$ and $\gamma_z = 0.2$ for $T = 0.2\Delta/k_B$ and

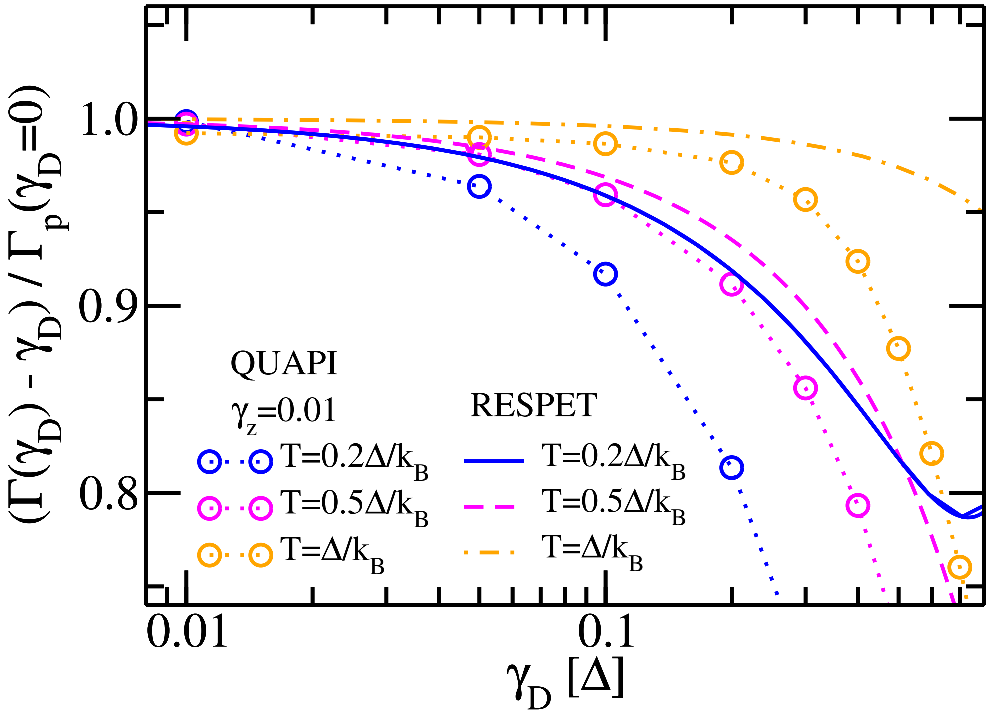

Figure 6.4: The ratio Γ_{rat} for the Hybrid-QUAPI result and the Hybrid-RESPET result are compared for small γ_D. the temperatures investigated are $T = 0.2\Delta/k_\mathrm{B}$,$T = 0.5\Delta/k_\mathrm{B}$ and $T = \Delta/k_\mathrm{B}$ and the Hybrid-QUAPI result was calculated for weak coupling $\gamma_z = 0.01$.

$T = \Delta/k_\mathrm{B}$ but not for $T = 0.5\Delta/k_\mathrm{B}$. This lack of γ_z dependence points towards a lowest-order effect in the system-bath coupling as determined by the perturbation rate. Surprisingly, however, numerical results differ substantially from perturbative results except for very small dephasing γ_D. Furthermore, pertubation shows with increasing γ_D first a suppression of decoherence and then an increase. The minimum shifts towards larger γ_D with increasing temperature and, thus, is only visible for $T = 0.2\Delta/k_\mathrm{B}$ in figure 6.2. In contrast, the correct behaviour, as determined by QUAPI, shows at first a decrease of decoherence which seems to level off for larger γ_D. To investigate this further figure 6.3 plots the data for $\gamma_z = 0.01$ and $T = 0.2\Delta/k_\mathrm{B}$ and $T = 0.5\Delta/k_\mathrm{B}$ for an extended range of γ_D. Therein, the γ_D dependence is very weak for $\gamma_D \ll 2\Delta$. The $T = 0.2\Delta/k_\mathrm{B}$ data exhibit a shallow minimum while the $T = 0.5\Delta/k_\mathrm{B}$ simply levels off. In total, we find that a perturbative approach, which is standard to treat weak system-bath coupling successfully, fails when the system dynamics is not Hamiltonian but follows a Liouvillian dynamics.

One might argue heuristically that a large dephasing rate γ_D is the result of strong environmental noise and further that such a strongly coupled environment even invalidates a perturbative treatment of an additional independent noise source even when this noise is weak, i.e., its system-bath coupling is small, i.e., $\gamma_z = 0.01$. Then, discrepancy between QUAPI and RESPET should occur only for large γ_D . Figure 6.4 plots the data for $\gamma_z = 0.01$ and $T = 0.2\Delta/k_\mathrm{B}, 0.5\Delta/k_\mathrm{B}$, with a focus on small dephasing rate γ_D . As expected RESPET and QUAPI results agree for vanishing phenomenological dephasing. Sizeable differences, however, already occur for $\gamma_D \geq 0.1$ with stronger deviations at lower temperatures.

6.1 Conclusion

In both Hybrid-QUAPI and Hybrid-RESPET a suppression of the contribution from the environment to the decoherence rate with increasing dephasing is observed. Thus, dephasing suppresses the effects of additional environmental fluctuations. By including a phenomenological dephasing rate in two well established methods and comparing the results the reliability of a simple inclusion of a master equation in these methods becomes questionable. Surprisingly, strong quantitative and qualitative deviations are found between the perturbative and the numerically exact results, even for system-bath couplings that are considered to justify a perturbative treatment, for example $\gamma_z = 0.1$. This however, has to be taken in the context of model. Absorbing one bath in the system dynamics introduces correlation between the baths in lowest order, while treating both baths equally results in no correlation in lowest order, as was shown for RESPET in chapter 4.3. To truly treat both baths equally the extension of QUAPI, as done in chapter 5.6, can be employed. Sadly RESPET in next higher order is already not solvable any more and can only be used to interpret results qualitatively. These findings have been published in reference [98].

Chapter 7

The Two Level System: Dynamics under the influence of two non-commuting fluctuations

We wish to investigate two types of noise in non-commuting operators: fully correlated and uncorrelated fluctuations. These types of fluctuations are important to understand how the underlaying noise sources in multiple different, important systems, such as the ones used in molecular dynamics [17], in quantum wells [70] and in the multiple realisations of qubits, as discussed in the introduction of this thesis. We focus on the two level system (TLS) and compare both fluctuations in terms of dissipative properties.

A rigorous study of the dynamics of a TLS under the influence of two uncorrelated, non-commuting fluctuations demands a method which goes beyond the hybrid methods employed in the previous chapter. The extended QUAPI method for two non-commuting baths with the additional condition $[H_S, H_{SB,1}] = 0$ as derived in chapter 5.6 is employed throughout this chapter. The additional condition treats dephasing fluctuations which do cause relaxation. We call this the two bath model (TBM), as introduced in chapter 4.3. Furthermore, the standard QUAPI scheme is employed to model two fully correlated fluctuations in non-commuting system-bath operators via the rotated bath model (RBM), which was introduced in Chapter 4.2. We compare our findings to the effect of classical fluctuations, which are additive in nature. Thus, we simply add the rates resulting from single fluctuations in the same system-bath operators, corresponding to the Spin-Boson model and the independent boson model, the latter being an example for a pure dephasing bath.

As shown in the calculations of Chapter 4.3 in 1-loop approximation the integral kernel M for the TBM coincides with the sum of the kernel M_{σ_x} for a single bath coupled via σ_x, called the pure dephasing bath (PDB), and the kernel M_{σ_z} of the relaxational bath coupled via σ_z. The interpretation as a pure dephasing bath, which fulfills $[H_S, H_{SB,1}] = 0$, is in fact only true in absence of second bath. While for vanishing system-bath coupling the dephasing rates resulting from the uncorrelated, the correlated and the additive fluctuations should coincide, under the condition that the bath consists of the same kind of harmonic oscillators described by the same spectral densities, with increasing system-bath coupling this is not to be expected. First, differences between the fully correlated fluctuations and the other two models should emerge and second, for further increased system-bath coupling, differences between the uncorrelated fluctuations and the additive fluctuations should arise. This is apparent if one looks at the Taylor expansion $\mathcal{U}_{eff}(z) = \mathcal{U}_S(z)\sum_{m=0}^{\infty}(-1)^m\alpha^m(z)$. For small system-bath coupling γ it is sufficient to employ the expansion only up to the first order $m = 1$, this allows to find rates independently for (back transformed) $\alpha^1_{\sigma_z}(t)$ and $\alpha^1_{\sigma_x}(t)$, where the overall rate would be given by the sum of these rates. Thus, additive fluctuations describe uncorrelated, non-commuting fluctuations accurately for weak system-bath coupling. The rotated bath model, on the other hand, already has differences in the first order, as shown by the additional terms in the 1-loop kernel M proportional to the coefficients of σ_x as well as to the coefficients of σ_z. These terms are called M_{mix} in Chapter 4.1. As a model the symmetric two-level system (TLS) is studied, $H_S = \frac{\Delta}{2}\sigma_x$, coupled to two baths, one, described by $H_{SB,z}$, causing relaxational fluctuations due to its coupling via σ_z to the TLS and the other, described by $H_{SB,x}$, coupled via σ_x, causing pure dephasing fluctuations. This leads to a total Hamiltonian

$$H = H_S + H_{SB,z} + H_{SB,x} \ , \tag{7.1}$$

with

$$H_{SB,\nu} = \sum_j \frac{p_{j,\nu}^2}{2m_{j,\nu}} + \tfrac{1}{2} m_{j,\nu}\omega_{j,\nu}^2 \left(x_{j,\nu} - \frac{c_{j,\nu} a_\nu \sigma_\nu}{m_{j,\nu}\omega_{j,\nu}^2} \right)^2 \ , \tag{7.2}$$

for the TBM. The σ_ν are the corresponding Pauli matrices of the TLS algebra in which the corresponding baths cause fluctuations. For fully correlated fluctuations the Hamiltonian is given for only one bath with $\nu = RBM$ and $a_{RBM} = \sqrt{a_x^2 + a_z^2}$ and an asymmetric TLS. Additionally, σ_{RBM} is a Pauli matrix in a different basis, such that a basis transformation leads to the same system Hamiltonian $H_S = \frac{\Delta}{2}\sigma_x$ and $a_{RBM}\sigma_{RBM} = a_x\sigma_x + a_z\sigma_z$. The corresponding basis transformation is $V = \exp[i\frac{\arctan(a_z/a_x)}{2}]$, see Equation (4.15).

The spectral densities are:

$$J_\nu(\omega) = \frac{\pi}{2}\sum_{k=1}^{M} \frac{\lambda_{k,\nu}^2 \delta(\omega - \omega_{k,\nu})}{2m_{k,\nu}\omega_{k,\nu}} =: \widetilde{\gamma}_\nu \omega e^{-\omega/\omega_c} \ , \tag{7.3}$$

with $\nu = x$,$\nu = z$ or $\nu = RBM$. Here, $J(\omega)$ is chosen as an Ohmic spectral density with an exponential cut-off function. The bath cut-off frequency is chosen to be $\omega_c = 5\Delta$ for both baths. The coupling strength is now redefined as $\gamma_\nu = a_\nu^2 \widetilde{\gamma_\nu}$ for the ν fluctuations to the quantum system. Note the system-bath coupling strength γ_{RBM} of the rotated bath model (RBM), as defined by Equation (4.16), can be expressed in terms of γ_x and γ_z as well. To compare our models we chose $\Omega = \Delta$. Then $a_{RBM}^2 = a_x^2 + a_z^2$ and thus $\gamma_{RBM} = a_{RBM}^2 \widetilde{\gamma}_{RBM} = (a_x^2 + a_z^2)\widetilde{\gamma}_{RBM}$. Thus, by fixing $\widetilde{\gamma_\nu} \equiv 1$, we find $\gamma_{RBM} = \gamma_x + \gamma_z$.

7.1 Dephasing and Relaxation

In this section the bulk of the numerical efforts invested into this thesis is presented in the form of an extensive study of the dissipative properties of the models we have proposed. Both the RBM and the TBM simplify to the standard spin-boson model (SBM) for $a_x = 0$ or alternatively to an independent boson model or pure dephasing bath (PDB) for $a_z = 0$. The third model, additive fluctuations, uses the simple approximation, that two non-commuting fluctuations yield the same relaxation and dephasing rates as the sum of independent fluctuations. Thus, the rate for additive fluctuations is given by: $\Gamma^{\Sigma}_{r/d}(\gamma_x, \gamma_z) = \Gamma^{\mathrm{PDB}}_{r/d}(\gamma_x) + \Gamma^{\mathrm{SBM}}_{r/d}(\gamma_z)$.

We explicitly study the time evolution of $P_z(t) = \langle\sigma_z\rangle(t)$ with initially $P_z(0) = 1$ to investigate dephasing and $P_x(t) = \langle\sigma_x\rangle(t)$ with initially $P_x(0) = 1$ to study relaxation. We employ a fitting function

$$P_z^{\mathrm{fit}}(t) = P_z^{\mathrm{stat}} + [x_1 + x_3 * \sin(\widetilde{\Delta}(t) * t) + x_2 * \cos(\widetilde{\Delta}(t) * t)] * e^{x_7 * t} \tag{7.4}$$

with $\widetilde{\Delta}(t) = (x_4 + x_5 * e^{x_6 * t})$ and $P_z^{\mathrm{stat}} = 1 - x_1 - x_2$ and with the x_i the fit parameters to describe the numerical data. As expected from weak coupling analytical results we observe $|P_z^{\mathrm{stat}}| \ll 1$ and $\widetilde{\Delta}(t) \simeq \Delta$ and $x_1, x_3 \ll x_2$ for all studied cases, i.e. $\gamma_x \leq 0.5$, $\gamma_z \leq 0.5$ and temperatures $0.1\Delta \leq k_{\mathrm{B}}T \leq 2\Delta$. The dephasing rates extracted are $x_7 = \Gamma_d^{RBM}$ for fully correlated fluctuations in the rotated bath model or $x_7 = \Gamma_d^{TBM}$ for uncorrelated fluctuations in the two bath model. The relaxation rate Γ_r^{RBM} and Γ_r^{TBM} are extracted similarly by fitting $P_x^{\mathrm{fit}}(t) = P_x^{\mathrm{stat}} + (1 - P_x^{\mathrm{stat}}) * e^{x_8 * t}$ to the data. These dephasing and relaxation rates are functions of both coupling strength γ_x and γ_z. Note that by fixing $\widetilde{\gamma_\nu} \equiv 1$ and choosing a_x and a_z identical for fully correlated or uncorrelated fluctuations, it is ensured that in lowest order of the coupling to the bath the dephasing and relaxation rates for the quantum two state system are identical for fully correlated and uncorrelated fluctuations. All differences result from higher order corrections due to strong system-bath coupling of at least one of the fluctuation sources.

7.1.1 Dephasing at $T = 0.2\Delta/k_B$

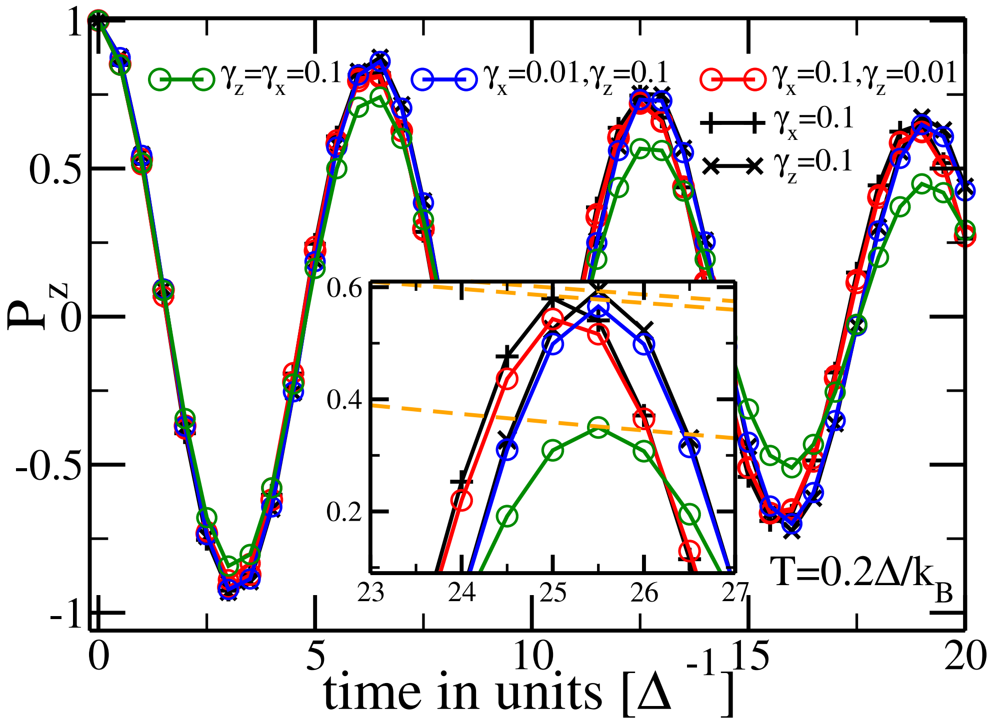

Figure 7.1: In this figure P(z)= $\langle\sigma_z\rangle(t)$ is plotted for the SBM (crosses), the PDB (plusses) and the TBM (circles) at $T = 0.2\Delta/k_B$. For PDB and SBM the respective system-bath couplings are $\gamma_x = 0.1$ and $\gamma_z = 0.1$. For the TBM three different set ups are plotted $\gamma_x = 0.01, \gamma_z = 0.1$, $\gamma_x = 0.1, \gamma_z = 0.01$ and $\gamma_x = \gamma_z = 0.1$.The orange lines represent the envelop $\exp[-\Gamma_d^i]$

.

At first we investigate the dephasing for a temperature $T = 0.2\Delta/k_B$. In Figure 7.1 the function $P_z(t)$ is plotted for five different cases. The TBM result (circles) is given for the three cases $\gamma_x = 0.1; \gamma_z = 0.01$,$\gamma_x = 0.01; \gamma_z = 0.1$ and $\gamma_x = 0.1; \gamma_z = 0.1$. Additionally we show the PDB result (pluses) for $\gamma_x = 0.1$ and the SBM (crosses) for $\gamma_z = 0.1$. As to be expected for $\gamma_z = 0.01$ or $\gamma_x = 0.01$ the TBM deviates negligibly from the PDB with $\gamma_x = 0.1$ and the SBM with $\gamma_z = 0.1$. The inset shows a maximum of $P(z)$ for later times to compare the damping of the different models. The orange lines represent the envelops $\exp[-\Gamma_d^i t]$. We find $\Gamma_d^{PDB}(\gamma_x = 0.1) = 0.021858$, $\Gamma_d^{SBM}(\gamma_z = 0.1) = 0.019326$ and $\Gamma_d^{TBM}(\gamma_x = 0.1, \gamma_z = 0.1) = 0.0415311$. Thus $\Gamma_d^{\Sigma}(\gamma_x = 0.1, \gamma_z = 0.1) = \Gamma_d^{PDB}(\gamma_x = 0.1) + \Gamma_d^{SBM}(\gamma_z = 0.1)$, then $\Gamma_d^{\Sigma}(\gamma_x = 0.1, \gamma_z = 0.1) = 0.041184$. Such that $\Gamma_d^{PDB}(\gamma_x = 0.1) + \Gamma_d^{SBM}(\gamma_z = 0.1) = \Gamma_d^{TBM}(\gamma_x = 0.1, \gamma_z = 0.1) + O(\Gamma_d^{\Sigma}/100)$, a deviation about twice as large as the error resulting from the QUAPI error, which is $< 0.5\%$ for the calculations shown

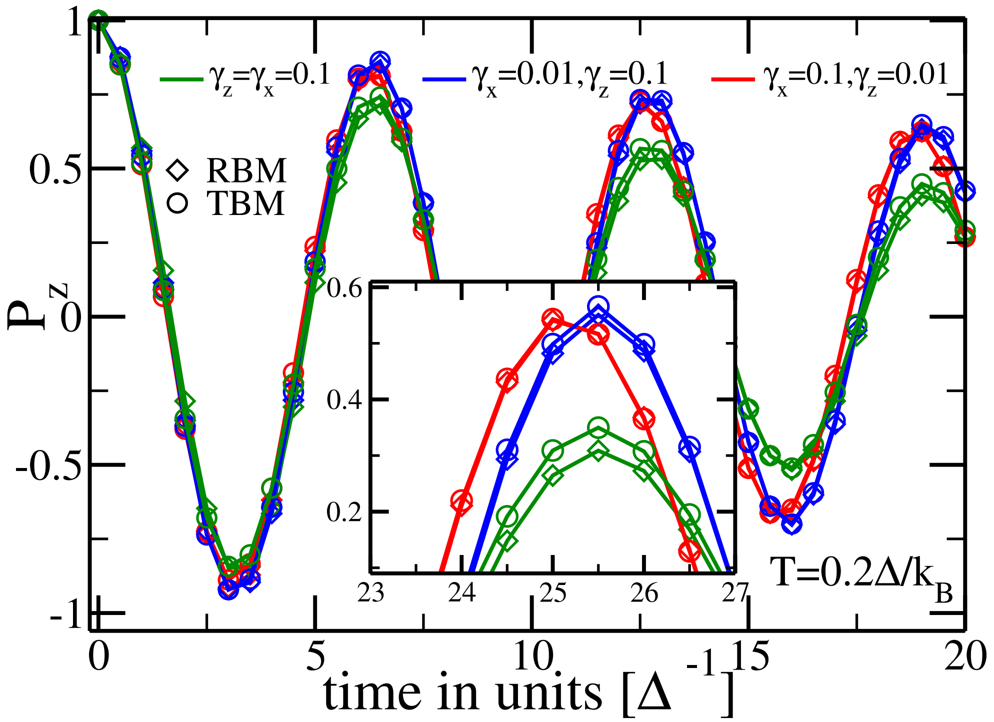

Figure 7.2: Here P(z) is compared for the TBM (circles) and the RBM (diamonds) at $T = 0.2\Delta/k_B$ for three different scenarios: $\gamma_x = 0.1; \gamma_z = 0.01$,$\gamma_x = 0.01; \gamma_z = 0.1$ and $\gamma_x = 0.1; \gamma_z = 0.1$.

here. Thus, additive fluctuations are a reasonable approximation for uncorrelated, non-commuting fluctuations in this regime.

In Figure 7.2 the RBM results (diamonds) and the TBM results (circles) for $P_z(t)$ are compared for the same three combinations of relaxational and dephasing couplings: $\gamma_x = 0.1; \gamma_z = 0.01$,$\gamma_x = 0.01; \gamma_z = 0.1$ and $\gamma_x = 0.1; \gamma_z = 0.1$. We find again agreement between the TBM and the RBM if either of the two coupling is small. For $\gamma_x = 0.1$ and $\gamma_z = 0.1$ the rates are $\Gamma_d^{TBM} = 0.0415311$ and $\Gamma_d^{RBM} = 0.043582$. The relative difference between them is $(\Gamma_d^{TBM} - \Gamma_d^{RBM})/\Gamma_d^{RBM} = -4.7058\%$, while the relative difference between the RBM rate and the sum of both rates is $(\Gamma_d^{RBM} - \Gamma_d^{\Sigma})/\Gamma_d^{\Sigma} = 5.8229\%$ and for the TBM rate it is: $(\Gamma_d^{TBM} - \Gamma_d^{\Sigma})/\Gamma_d^{\Sigma} = 0.8428\%$. The QUAPI error in this region is less then 0.5%. While the deviations are not large, they still show a trend: The rates resulting from non-commuting uncorrelated fluctuations are about the same as the rates for additive fluctuations, which are thus a good approximation, whereas the rates caused by fully correlated non-commuting fluctuations are larger then the other two, thus additive fluctuations are not as accurate of an description in this case. Furthermore fully correlated fluctuations enhance the dephasing rate compared to uncorrelated fluctuations in this set-up. To further investigate this behaviour we focus on the relative rates as defined by $\frac{\Gamma_d^{TBM}-\Gamma_d^{\Sigma}}{\Gamma_d^{\Sigma}}$, $\frac{\Gamma_d^{RBM}-\Gamma_d^{\Sigma})}{\Gamma_d^{\Sigma}}$ and $\frac{\Gamma_d^{TBM}-\Gamma_d^{RBM}}{\Gamma_d^{RBM}}$.

In Figure 7.3 these three relative rates are presented in a plot against γ_z for six different values of γ_x: $\gamma_x = 0.01, 0.2, 0.25, 0.3, 0.4, 0.5$. The error of the QUAPI simulation grows for larger system-bath couplings γ_x up to 3%. Strong dephasing poses a problem due to larger memory requirements [125]. Still, the differences between the set-ups are large enough to not only make qualitative but also quantitative statements. While the uncorrelated and additive fluctuations agree well for $\gamma_x = 0.01$ and $\gamma_z = 0.5$, fully correlated fluctuations show a difference of 4%. Thus, if one of the fully correlated fluctuations is large, another small fluctuation can already enhance the dephasing rate. For $\gamma_x = \gamma_z = 0.5$ the deviations are the largest between uncorrelated fluctuations and additive fluctuations. Overall the deviations between them grow with both γ_x and γ_z.

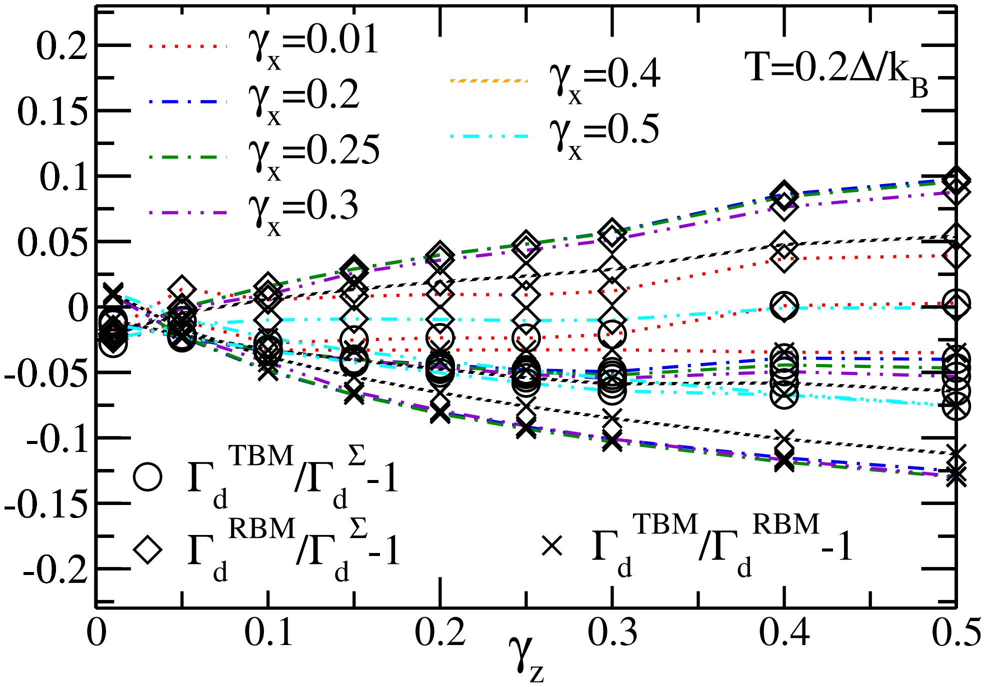

Figure 7.3: In this figure relative rates are plotted at $T = 0.2\Delta/k_B$ against γ_z. The circles represent the differences between the Γ_d^{TBM} and Γ_d^{Σ}, the diamonds the ones between Γ_d^{RBM} and Γ_d^{Σ} and the crosses the ones between Γ_d^{TBM} and Γ_d^{RBM}. The relative rates are given for six fixed values of γ_x: $\gamma_x = 0.01, 0.2, 0.25, 0.3, 0.4, 0.5$.

The same can not be said for fully correlated fluctuation. While the differences to additive fluctuations grow with γ_z, they do not show the same behaviour for increasing γ_x. Instead they reach a maximum in the region $\gamma_x = 0.2 - 0.3$, where all three curves agree well with each other, and then start to decrease again, so much that they agree better with additive fluctuations for $\gamma_x = 0.5$ then for $\gamma_x = 0.01$. This behaviour of the fully correlated fluctuations results in an decrease of the deviations between them and the uncorrelated fluctuations as well.

Since the behaviour for γ_z is consistently an increase, we now focus on only three fixed value of γ_z:

$\gamma_z = 0.01, 0.2$ and 0.5. In Figure 7.4 the three relative rates are plotted against γ_x. The deviations between the three rates are almost constant and relatively small for $\gamma_z = 0.01$, they are of the order of the numerical error, the largest deviation is at $\gamma_x = 0.05$ with $\frac{\Gamma_d^{RBM}-\Gamma_d^{\Sigma}}{\Gamma_d^{\Sigma}} = 0.02487917$, which is slightly larger then the sum of the relative errors of the three simulations. Still even there the agreement is acceptable enough to claim additive fluctuations are a good approximation. For the fully correlated model with $\gamma_z = 0.2$ and $\gamma_z = 0.5$ we observe that a maximum plateau of the deviations emerges in the region of $\gamma_x = 0.1 - 0.3$. The increase of the deviations between fully correlated and additive fluctuations increase with γ_x, with a larger gradient for larger γ_z.

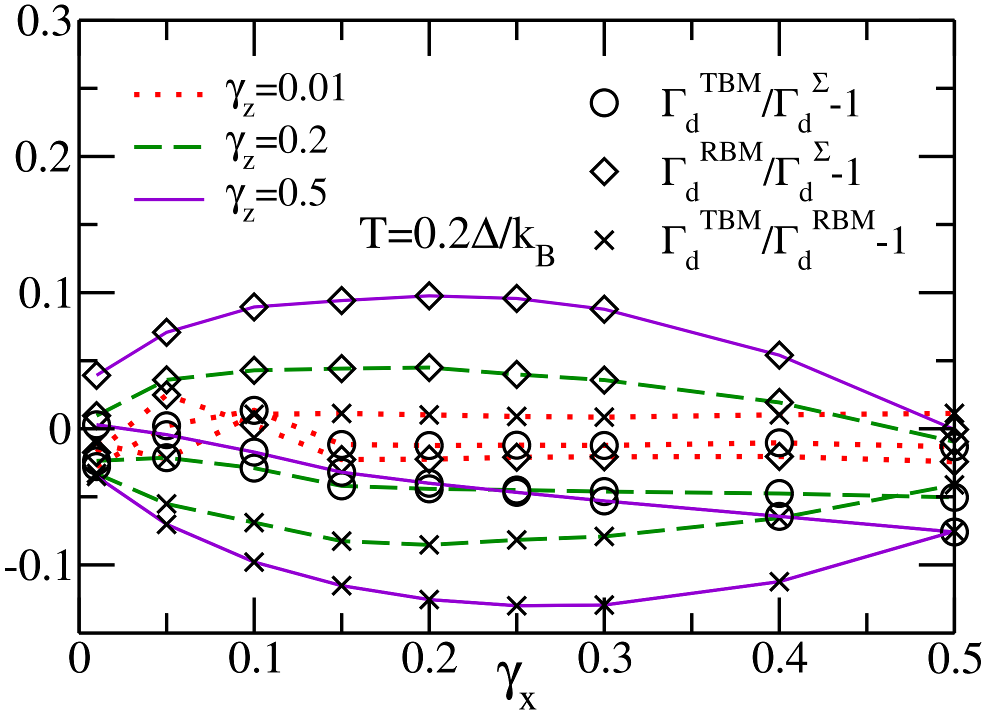

Figure 7.4: In this figure relative rates are plotted at $T = 0.2\Delta/k_B$ against γ_x for three fixed values of γ_z:$\gamma_z = 0.01, 0.2, 0.5$. The circles represent the differences between the Γ_d^{TBM} and Γ_d^{Σ}, the diamonds the ones between Γ_d^{RBM} and Γ_d^{Σ} and the crosses the ones between Γ_d^{TBM} and Γ_d^{RBM}.

Overall the results indicate, that additive fluctuations are an acceptable approximation for uncorrelated fluctuations at this temperature for moderate system-bath couplings, with all deviations being less then 8%. We observe a maximum relative deviation between the rates of uncorrelated and additive fluctuations of 7.5%. The dephasing is consistently weaker than the one caused by additive fluctuation, allowing the statement that uncorrelated fluctuations reduce the decoherence rate in this region. Fully correlated fluctuations, on the other hand tend, to cause stronger dephasing compared to additive ones, with a maximum difference of approximately 10% for $\gamma_z = 0.5$ in the region of the plateau. It is to be expected, that a further increase of γ_z yields even stronger deviations. The same can not be said for γ_x, we find a more complex connection between γ_x and the dephasing rate induced by fully correlated fluctuations. Moderate system-bath couplings γ_x of dephasing fluctuations enhance the dephasing rate, while stronger couplings destroy this enhancement again. Fully correlated and uncorrelated fluctuations show a relative difference of more then 12% in the region of the plateau. For a further investigation we will look into different temperature regimes. Larger temperatures result in stronger dephasing for weaker system-bath couplings, thus we hope an additional temperature investigation will allow us to gain further insight on the γ_x dependency of fully correlated fluctuations.

7.2 Dephasing at Temperatures: $0.1\Delta/k_B \leq T \leq 2\Delta/k_B$

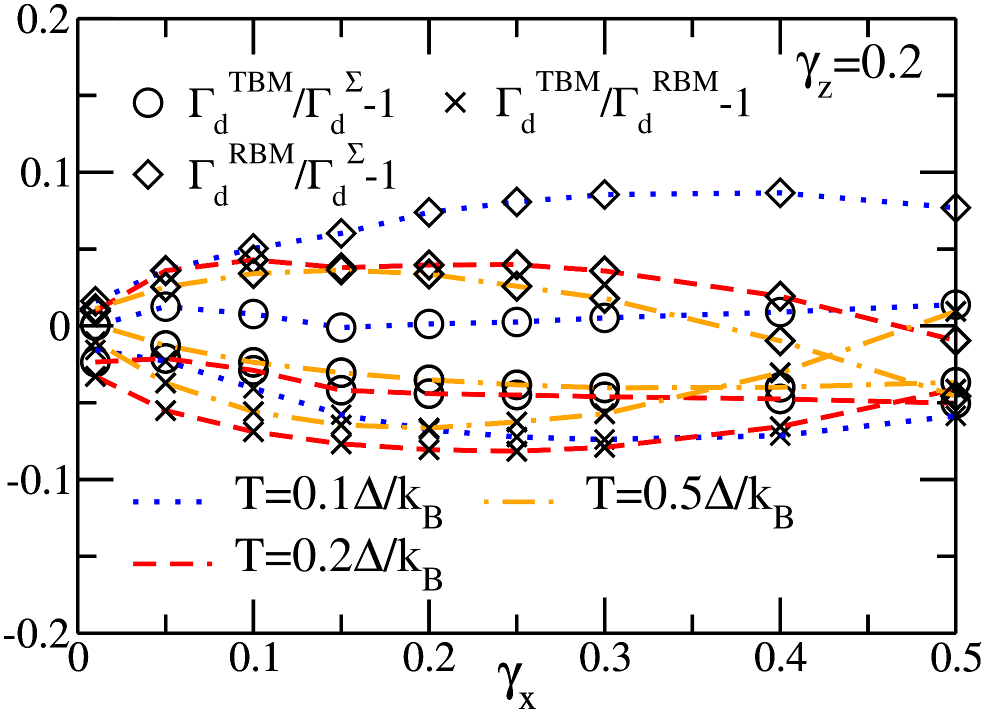

Figure 7.5: In this figure relative rates are plotted for $\gamma_z = 0.2$ against γ_x for three fixed values of T:$T = 0.1\Delta/k_B, 0.2\Delta/k_B, 0.5\Delta/k_B$. The circles represent the differences between the Γ_d^{TBM} and Γ_d^{Σ}, the diamonds the ones between Γ_d^{RBM} and Γ_d^{Σ} and the crosses the ones between Γ_d^{TBM} and Γ_d^{RBM}.

In Figure 7.5 we investigate a range of low temperatures for a fixed $\gamma_z = 0.2$. The blue dots represent $T = 0.1\Delta/k_B$, the dashed red line $T = 0.2\Delta/k_B$ and the dashed-dotted orange line $T = 0.5\Delta/k_B$. For uncorrelated fluctuations at $T = 0.1\Delta/k_B$ we find almost perfect agreement with additive fluctuations for any given coupling γ_x. While not shown here, even an increase of the system-bath coupling to $\gamma_z = 0.5$ only yields a maximum difference of $\frac{\Gamma_s^{TBM}-\Gamma_s^{\Sigma}}{\Gamma_d^{\Sigma}} = -0.045407$. Thus, the lower the temperature the better the approximation as additive fluctuations for uncorrelated fluctuations. For larger temperatures $T = 0.2\Delta$ and $T = 0.5\Delta$ we find almost the same relative deviation for uncorrelated fluctuations up to 5% and 4% respectively. Since 1% is of the order of the numerical error they should be viewed as equal. The deviation of uncorrelated fluctuations increases as temperature decreases, again for $T = 0.2\Delta/k_B$ and $T = 0.5\Delta/k_B$ the maxima are about the same height, while the maximum increases substantially for $T = 0.1\Delta/k_B$. The relative differences between uncorrelated and additive fluctuations grow up to 10%, which is as much as the maximum deviation at $T = 0.2\Delta/k_B$ for a large relaxational system-bath coupling $\gamma_z = 0.5$. Overall we find a strong temperature dependence of the maximum and the width of the plateau. While the decrease of the plateau is only partly visible from $\gamma_z = 0.4$ to $\gamma_z = 0.5$ for $T = 0.1\Delta/k_B$, we can further observe the decrease for $T = 0.5\Delta/k_B$. Here the rate of fully correlated fluctuations decreases so much, that it is less then the rate caused by additive fluctuations for $\gamma_z = 0.4$ and even becomes about equal to the rate caused by uncorrelated fluctuations at $\gamma_z = 0.5$. The concave form of the relative rate between fully correlated and additive fluctuations lead to the expectation, that it will decrease even further when increasing γ_x. Our results show that a bad composition of γ_x and γ_z is possible for the for fully correlated fluctuations, where the dephasing rate is enhanced compared to the other two models.

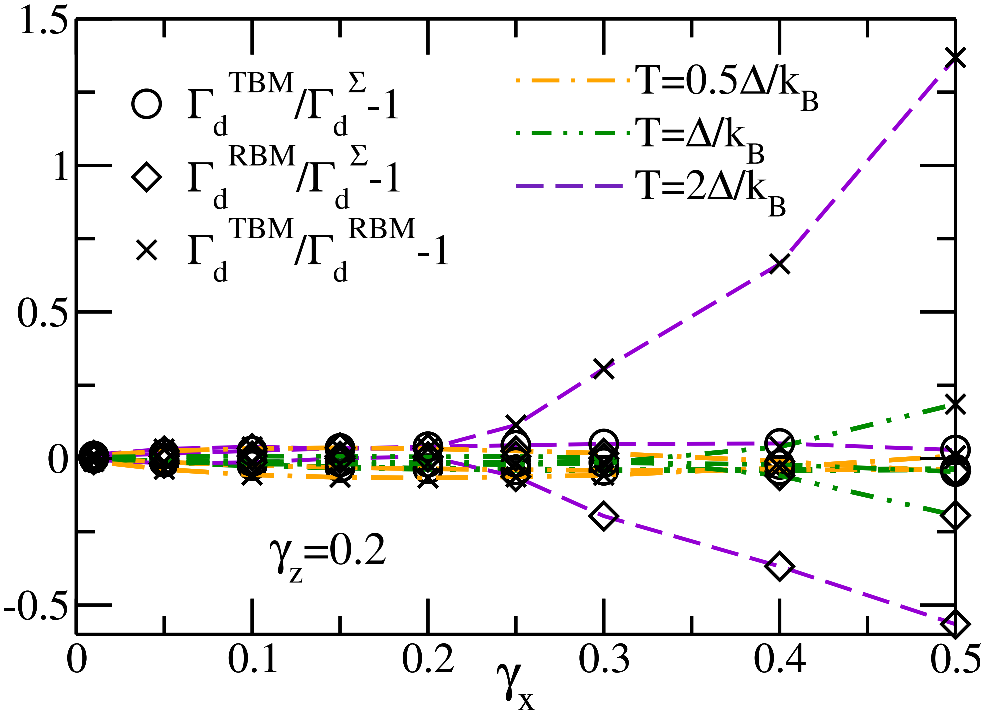

Figure 7.6: In this figure relative rates are plotted for $\gamma_z = 0.2$ against γ_x for three fixed values of T:$T = 0.5\Delta/k_B, \Delta/k_B, 2\Delta/k_B$. The circles represent the differences between the Γ_d^{TBM} and Γ_d^{Σ}, the diamonds the ones between Γ_d^{RBM} and Γ_d^{Σ} and the crosses the ones between Γ_d^{TBM} and Γ_d^{RBM}.

In Figure 7.6 the relative rates are plotted for $\gamma_z = 0.2$ and three temperature $T = 0.5\Delta/k_B, \Delta/k_B$ and $2\Delta/k_B$. The behaviour that emerged for large γ_x at $T = 0.5\Delta/k_B$ is further amplified. At $T = \Delta/k_B$ and $T = 2\Delta/k_B$ the differences between all three models can be neglected until the rate caused by fully correlated fluctuations starts to deviate strongly. In this region of comparably small deviations, the ones for $T = 0.5\Delta/k_B$ are the largest. Interestingly, the deviations between uncorrelated and additive fluctuations become smaller at larger temperatures, even though they still grow with γ_x, they only reach a maximum difference of about 5% for $T = \Delta$ and 3% at $T = 2\Delta/k_B$. Before the fully correlated fluctuations start their extreme behaviour, they reach a maximum difference at $\gamma_x = 0.1$ with $\frac{\Gamma_d^{RBM}-\Gamma_d^{\Sigma}}{\Gamma_d^{\Sigma}} = 0.84\%$ for $T = \Delta/k_B$ and at $\gamma_x = 0.05$ with $\frac{\Gamma_d^{RBM}-\Gamma_d^{\Sigma}}{\Gamma_d^{\Sigma}} = 1.65\%$ for $T = 2\Delta/k_B$, which are both of the order of the QUAPI error and thus these differences are negligible. Thus, we do not find a plateau for these two temperatures. The fundamentally different behaviour of the RBM remains to be investigated in more detail. To achieve this, we will investigate dephasing at $T = 2\Delta/k_B$, where the effect is most prominent.

7.3 Dephasing at $T = 2\Delta/k_B$

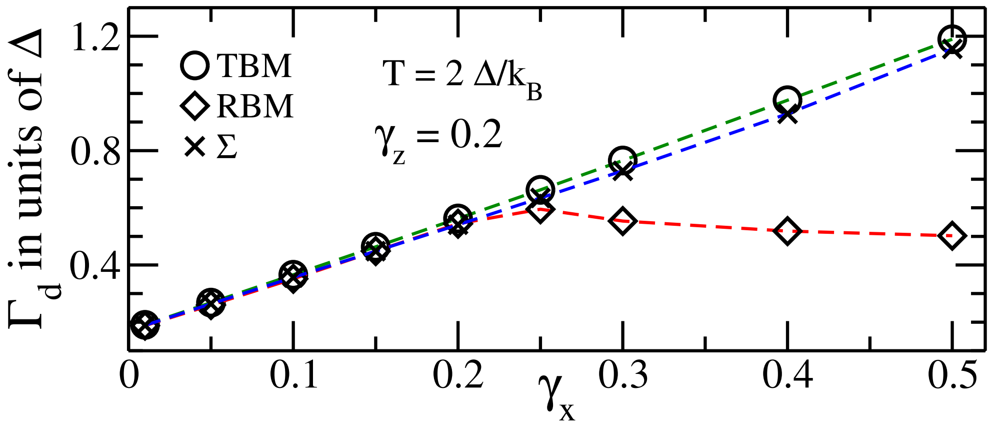

Figure 7.7: The dephasing rates Γ_d^{RBM} for the RBM, diamonds, and Γ_d^{TBM}, circles, for the TBM and Γ_d^{Σ} , plus symbols, for the sum of the dephasing rate of the SBM and the PDB, are plotted versus the coupling strength for the dephasing fluctuations γ_x for a fixed $\gamma_z = 0.2$ and a high temperature $T = 2\Delta/k_\mathrm{B}$.

In Figure 7.7 the dephasing rate is plotted at $T = 2\Delta/k_B$ for a coupling strength $\gamma_z = 0.2$ against γ_x. The dephasing rates of the additive fluctuations and the uncorrelated ones grow linear. The rate of uncorrelated fluctuations grows to be larger the rate of additive fluctuations around $\gamma_x = 0.2$, the maximum difference is at $\gamma_x = 0.4$ with $\frac{\Gamma_d^{TBM} - \Gamma_d^{\Sigma}}{\Gamma_d^{\Sigma}} = \frac{0.976423 - 0.928821}{0.928821} = 5.1\%$ and then decreases to $\frac{\Gamma_d^{TBM} - \Gamma_d^{\Sigma}}{\Gamma_d^{\Sigma}} = \frac{1.1896 - 1.155942}{1.155942} = 2.9\%$ at $\gamma_x = 0.5$. Fully correlated fluctuations show very different behaviour, while the dephasing rate increases linearly up to $\gamma_x = 0.2$, it reaches a maximum at $\gamma_x = 0.25$ and then decreases afterwards to a constant rate of about $\Gamma_d^{RBM} = 0.5$. This indicates, that the TLS undergoes a transition to the overdamped regime. It is to be mentioned, that it was not possible to fit to the evaluation of the QUAPI tensor in this region, but only to the solution of the full path integral, for details see appendix C .

In Figure 7.8 the dephasing rate Γ_d is shown for a pure dephasing coupling strength $\gamma_x = 0.5$. Fully correlated fluctuations cause the TLS to undergo the transition to the overdamped regime already for $\gamma_z = 0.05$ and it reaches the overdamped region around $\gamma_z = 0.3$. Here, uncorrelated fluctuations cause the TLS to start its transition to the overdamped regime at $\gamma_z = 0.4$ as well, reaching a maximum of Γ_d^{TBM} there. Before the transition, it diverges notably from dephasing rate cause by additive fluctuations. Neither the SBM nor the PDB reach the transition to the overdamped region in the investigated regime, with maximum coupling strengths $\gamma_\nu = 0.5$, therefore this feature can not be reproduced by additive fluctuations. This is consistent with fully correlated fluctuations, which do cause a transition to the overdamped regime for $\gamma_{RBM} = 0.51$ for $\gamma_x = 0.5$ and $\gamma_z = 0.01$ and vice versa. Interestingly, we find transitions for compositions with $\gamma_{RBM} = 0.5$, as shown in Figure 7.7 one such composition is $\gamma_x = 0.3$ and $\gamma_z = 0.2$. Thus, two fully correlated fluctuations enhance the dissipative effect of both fluctuation beyond a simple additive effect and show transitions to the overdamped regime for weaker system-bath couplings than uncorrelated fluctuations. Uncorrelated fluctuations not only show a transition to the overdamped regime as well, they also diverge strongly from additive fluctuations and show an enhancement of the dephasing rate for large temperatures and medium system-bath couplings.

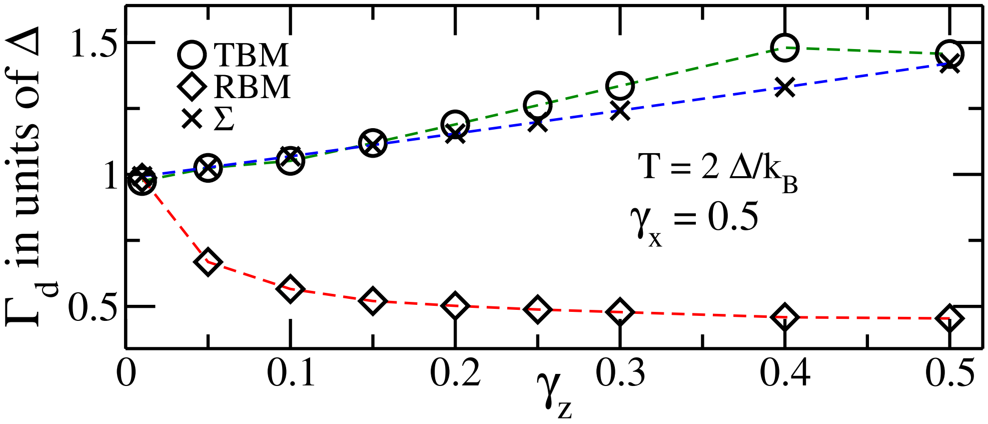

Figure 7.8: The dephasing rates Γ_d^{RBM} for the RBM, diamonds, and Γ_d^{TBM}, circles, for the TBM and Γ_d^{Σ} , crosses, for the sum of the dephasing rate of the SBM and the PDB, are plotted versus the coupling strength for the relaxational fluctuations γ_z for a fixed $\gamma_x = 0.5$ and a high temperature $T = 2\Delta/k_{\mathrm{B}}$.

In Figure 7.9 we take a closer look into the behaviour of $P_z(t)$ for a fixed dephasing coupling strength $\gamma_x = 0.5$ and increasing γ_z. The equilibrium value of the TLS remains unchanged for uncorrelated fluctuations, while fully correlated fluctuations appear to shift it substantially. For a weak relaxational coupling of $\gamma_z = 0.05$ the difference between the TBM and the PDB at $\gamma_x = 0.5$ is small, whereas the RBM result already shows relevant differences. The additional fully correlated relaxational fluctuation gives rise to two competing behaviours even at low coupling strength. The shifted equilibrium value is actually a deception, as shown in the inset, a second, long term behaviour comes into play which has an algebraic characteristic. This is highlighted by seemingly linear behaviour at later times. While looking at the values of $t = 6\Delta^{-1}$, the algebraic behaviour is obvious for $\gamma_z = 0.5$ and the competition between the two behaviour is somewhat visible for $\gamma_z = 0.2$, while for $\gamma_z = 0.05$ it seems to be an exponential decay with a shifted equilibrium value, as observed for lower temperatures and expected by RESPET results. In this regime, especially for strong dephasing coupling γ_x, QUAPI fails to produce a continuous function, but produces a discontinuity between the evaluation of the full path integral at $t = K * dt$ and the evaluation of the QUAPI tensor at $t = (K + 1) * dt$. For this set up the converged results where at

$dt = 0.6\Delta^{-1}$. The discontinuity presents itself as a jump of P_z and it is in all three cases too small to account for the equilibrium shift. In fact, it roughly halves the values. The behaviour afterwards stems from the evaluation of the QUAPI tensor, thus neglects memory that is somewhat important. Therefore the behaviour at later times should rather be seen as a good indication then a numerical exact fact. Some features can still be extracted though.

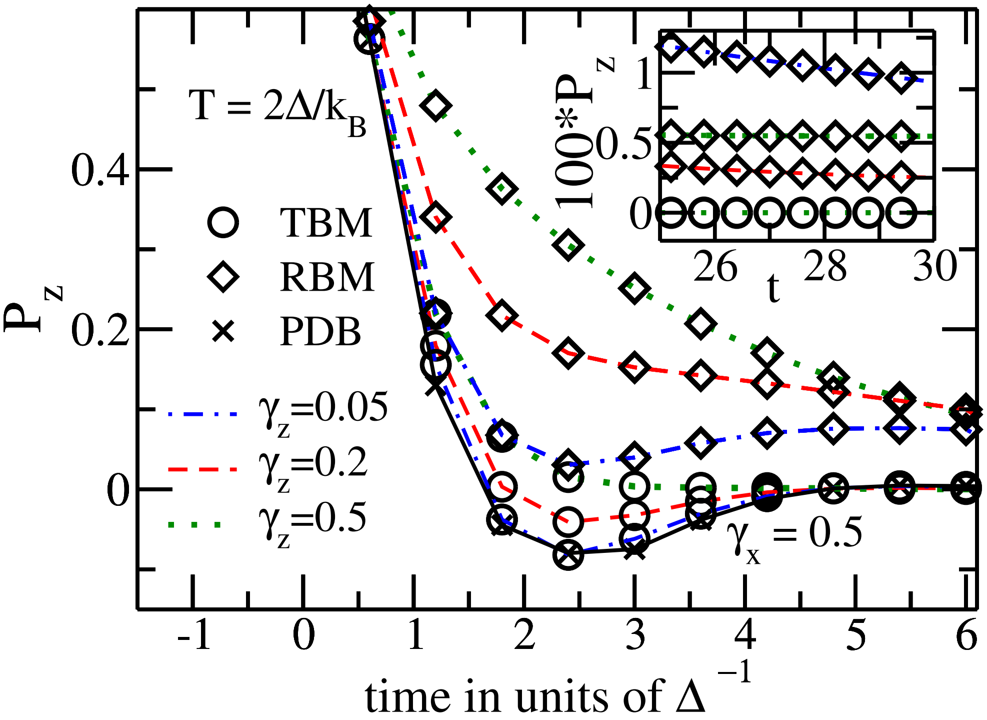

Figure 7.9: $P_z(t)$ versus time is shown for fixed coupling strength $\gamma_x = 0.5$ of pure dephasing fluctuations at temperature $T = 2\Delta/k_B$ and for various coupling strengths γ_z for relaxational fluctuations. The inset shows the behaviour of the RBM at later times, highlighting the competion between the exponential damping behaviour of the damped case and the algrebaic decay of the the overdamped case.

We observe stronger linear behaviour for $\gamma_z = 0.05$ then for the other two cases. For $\gamma_z = 0.2$ linear decay is still observable, while for $\gamma_z = 0.5$ no linear behaviour is observable. Instead, we find non-linear behaviour even for the latest times simulated, though on a smaller scale. The inset is already magnified by a factor 100, to see the non linear behaviour at least a factor 1000 is necessary. Interestingly the discontinuity becomes smaller for more algebraic behaviour. This is also reflected in the non-linear but algebraic behaviour at later times, showing that the QUAPI-tensor seems capable to correctly recover some features of the algebraic behaviour even though the correlation length increases. In all cases $P_z(t)$ goes to zero. For $\gamma_x = 0.5$ and $\gamma_z = 0.5$ fully correlated fluctuations cause the TLS to show a competition between the damped and overdamped regime as well. However, the uncorrelated fluctuations do not exhibit a discontinuity. For the TBM $dt = 0.6$ was chosen as well, but only $K = 6$ was used, thus, if existing, the discontinuity should be visible between $\Delta * t = 3.6$ to 4.2, which it is not. The reason is somewhat technical and related to to the Feynman-Vernon influence functional and it is discussed in appendix C.

7.4 Relaxation at $T = 0.2\Delta/k_B$

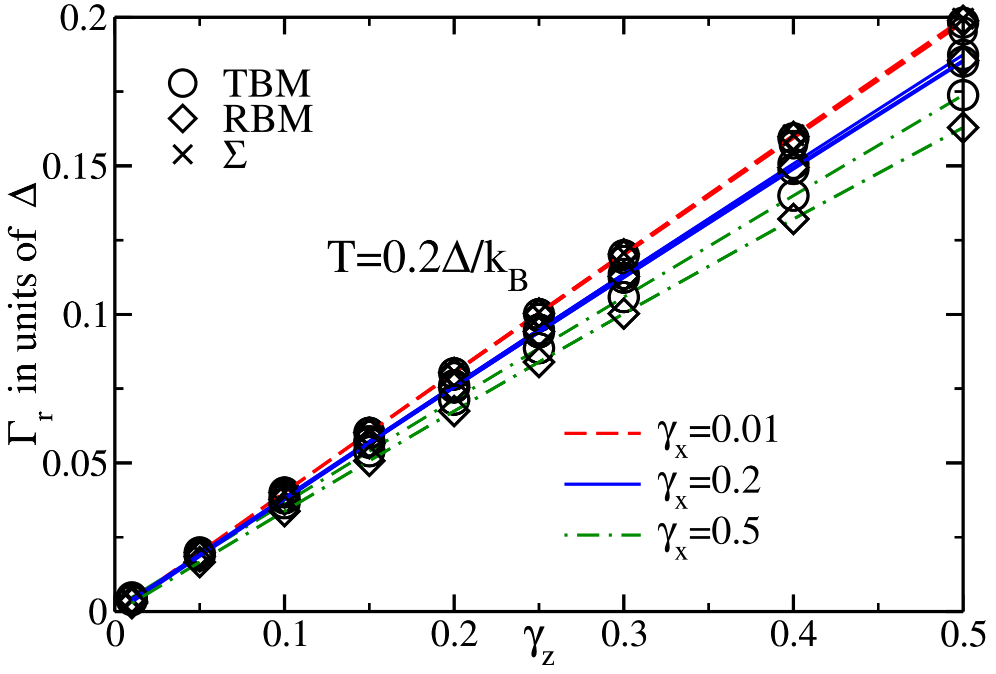

Figure 7.10: Here the Relaxation rate Γ_r, obtained from $P_x(t)$, is shown at $T = 0.2\Delta/k_B$ and plotted against γ_z for three fixed γ_x and the three models.

Now we turn our focus to the relaxation of the excited TLS. In Figure 7.10 the relaxation rate is given for three constant values of γ_x: $\gamma_x = 0.01, 0.2$ and 0.5. and plotted via γ_z at temperature $T = 0.2\Delta/k_B$. We find perfect agreement between all three models for $\gamma_x = 0.01$. For $\gamma_x = 0.2$ the relaxation rates for fully correlated and uncorrelated fluctuations show very small differences, of order of the numerical QUAPI error, that grow with γ_z, but both deviated substantially from the relaxation rate cause by additive fluctuations. For even stronger dephasing fluctuations the differences between the rates caused by fully correlated fluctuations and uncorrelated fluctuations grow. Overall an increase in dephasing fluctuations lowers the relaxation rate. That this effect already starts for a medium coupling of dephasing fluctuations of $\gamma_x = 0.2$ is surprising for the uncorrelated fluctuations, since it is an effect of higher order.

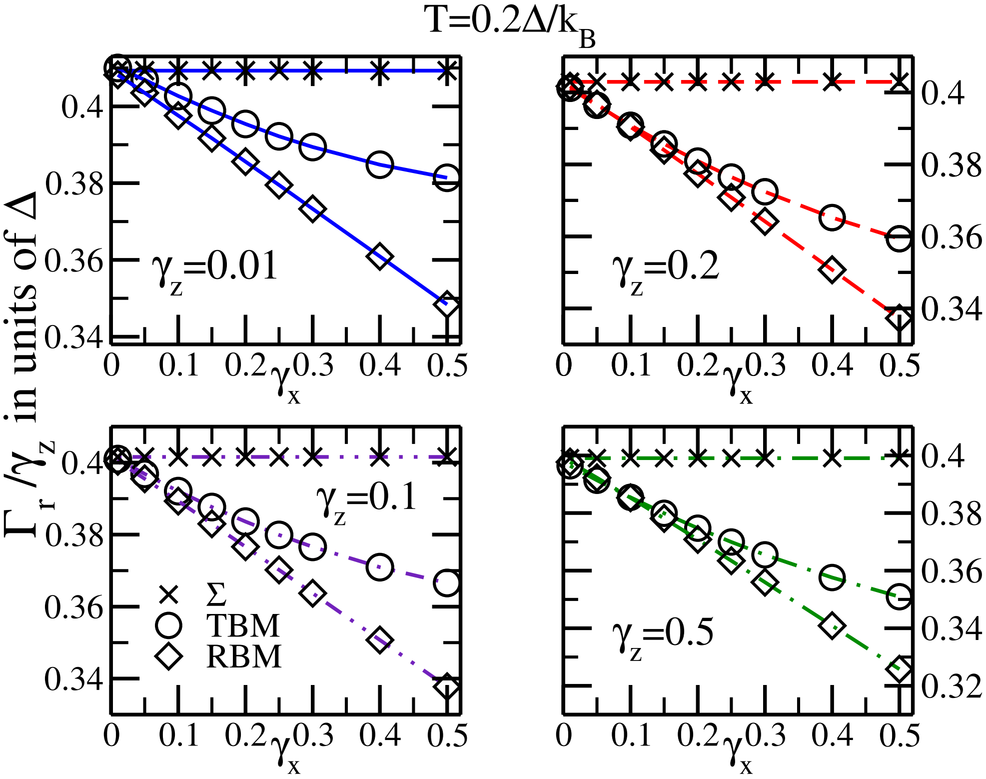

Figure 7.11: In this figure the relaxation rate normalized to the system-bath coupling of the relaxational bath $\frac{\Gamma_r}{\gamma_z}$ is shown for the three models an four different values of γ_z. We investigate the effect of increasing pure dephasing γ_x-depending fluctuation by plotting against γ_x.

To further analyse the deviations between the models, we take a closer look to the relaxation rate at four different $\gamma_z = 0.01, 0.1, 0.2$ and 0.5, as shown in Figure 7.11. To exclude a direct linear effect, since in lowest order $\Gamma_r^{SBM} \propto \gamma_z$, we chose to look at $\frac{\Gamma_r}{\gamma_z}$. While both fully correlated and uncorrelated fluctuations consistently lower the relaxation rate of the SBM for all couplings investigated, a detailed look shows, how differences emerge. The deviations between the fully correlated fluctuations and additive fluctuations grow linearly with γ_x for all couplings γ_z investigated. The uncorrelated fluctuations exhibit a non-linear behaviour, with weaker decrease for lower coupling of the dephasing fluctuations γ_x. This is according to our expectations, since higher order effects are typically non-linear. Interestingly, we observe non-linear behaviour for all γ_x for uncorrelated fluctuations at weak relaxational couplings and linear effects start to emerge with $\gamma_z = 0.1$. All dephasing coupling effects are of higher order but have to be seen as relative to γ_z. In 2-loop RESPET we found contributions that are $\propto \gamma_x \gamma_z$, while the higher order effects of just the relaxational fluctuations are $\propto \gamma_z^2$. Thus, already for $\gamma_z = 0.1$ the higher order effects that stem from a mixing of the baths are only by at most a factor ten smaller then the lowest order effect. The low order is in this case defined by the actual value of the relaxational coupling strength, this is why linear behaviour emerges only for γ_z's which are of $O(\gamma_x)$. It appears as if the relative differences between Γ_r^Σ and γ_r^{TBM} do not increase between $\gamma_z = 0.2$ and $\gamma_z = 0.5$, while the relative differences between Γ_r^Σ and Γ_r^{RBM} do. We will further analyse this by looking at the the relative rates for low to medium relaxational fluctuations and for medium to strong relaxational fluctuations.

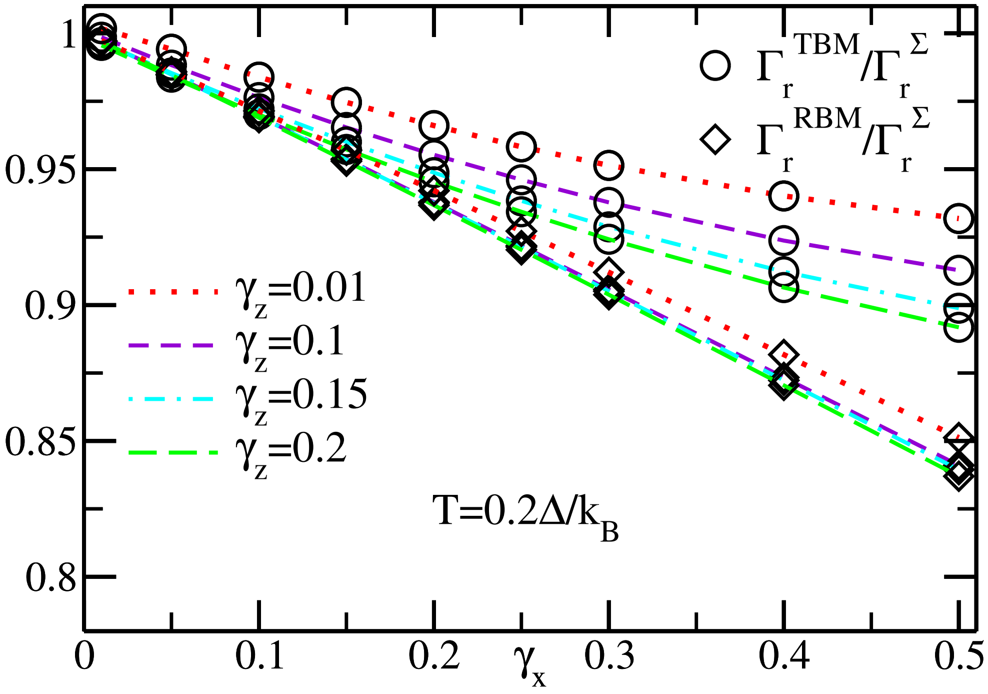

Figure 7.12: The relaxation rates for the TBM (circles) and the RBM (diamonds) normalized to SBM results are shown for low to moderate γ_z at $T = 0.2\Delta/k_B$.

We start with weak to medium relaxational fluctuations and take a look in Figure 7.12 at the relation of the relaxation rate of uncorrelated fluctuations and additive fluctuations $\frac{\Gamma_r^{TBM}}{\Gamma_r^\Sigma}$ and the relation of the rates of fully correlated fluctuations and additive fluctuations $\frac{\Gamma_r^{RBM}}{\Gamma_r^\Sigma}$ for four relaxational couplings between $\gamma_z = 0.01$ and $\gamma_z = 0.2$. We find almost perfect agreement for the relative reduction for fully correlated fluctuations. The only graph deviating is for $\gamma_z = 0.01$, which might be due to the need of longer simulations times and a larger accumulative error. The long simulation times were necessary to achieve meaningful fitting results, since the relaxation was very weak. For uncorrelated fluctuations the region of linear behaviour grows with increased system-bath couplings, resulting in a stronger decrease of the the relaxation rate of additive fluctuations.

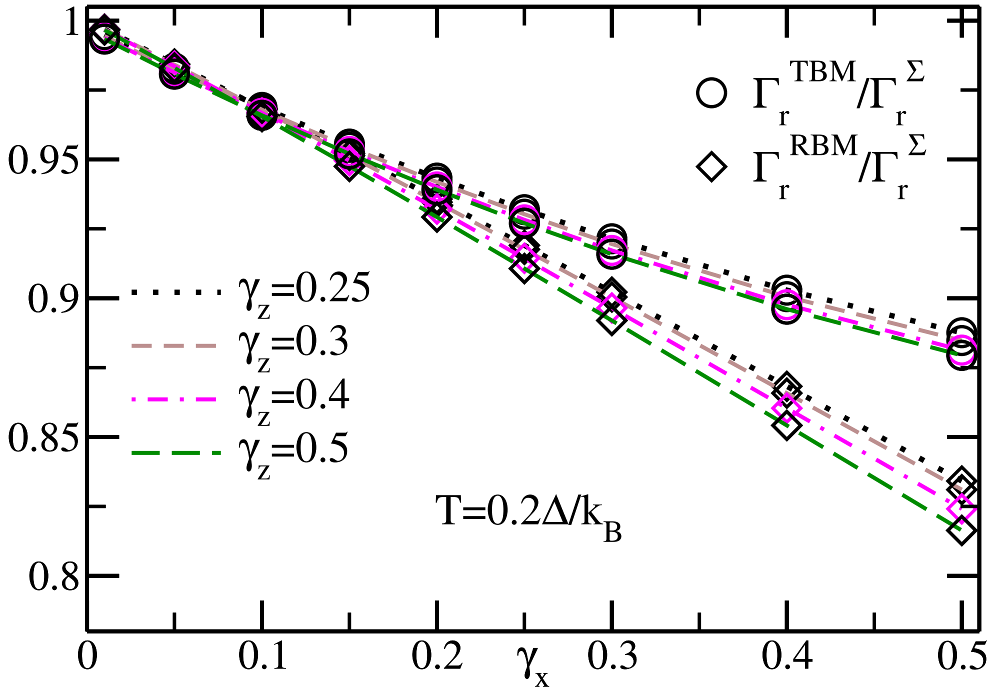

Figure 7.13: The relaxation for the TBM (circles) and the RBM (diamonds) normalized to SBM results is shown for moderate to large γ_z at $T = \Delta/k_B$.

In Figure 7.13 the next region of relaxational coupling, between $\gamma_z = 0.25$ and $\gamma_z = 0.5$, which we investigate is shown. Again we look at the relaxational rates of the uncorrelated and fully correlated fluctuations normalized to the rate of the additive fluctuation. In this region the differences between the relative rates for uncorrelated fluctuations differ only slightly. The region of linear deviations appears to converge between $\gamma_x = 0.1 - 0.15$. The fully correlated fluctuations on the other hand start to show higher order effects now. Both fully correlated and uncorrelated fluctuations agree well in the linear region of the uncorrelated fluctuations, even for large γ_z. We expect the deviations to further grow with larger γ_z and investigate this, through studying higher temperature behaviour. For $T = 0.2\Delta/k_B$ we consistently find a reduction of the relaxation rate resulting from additive fluctuation, thus the assumption of adding rates is a bad description of either fully correlated or uncorrelated fluctuations. The reduction of the relaxation rate at this temperature is stronger than anything we observed for the dephasing rate.

7.5 Relaxation at different temperatures

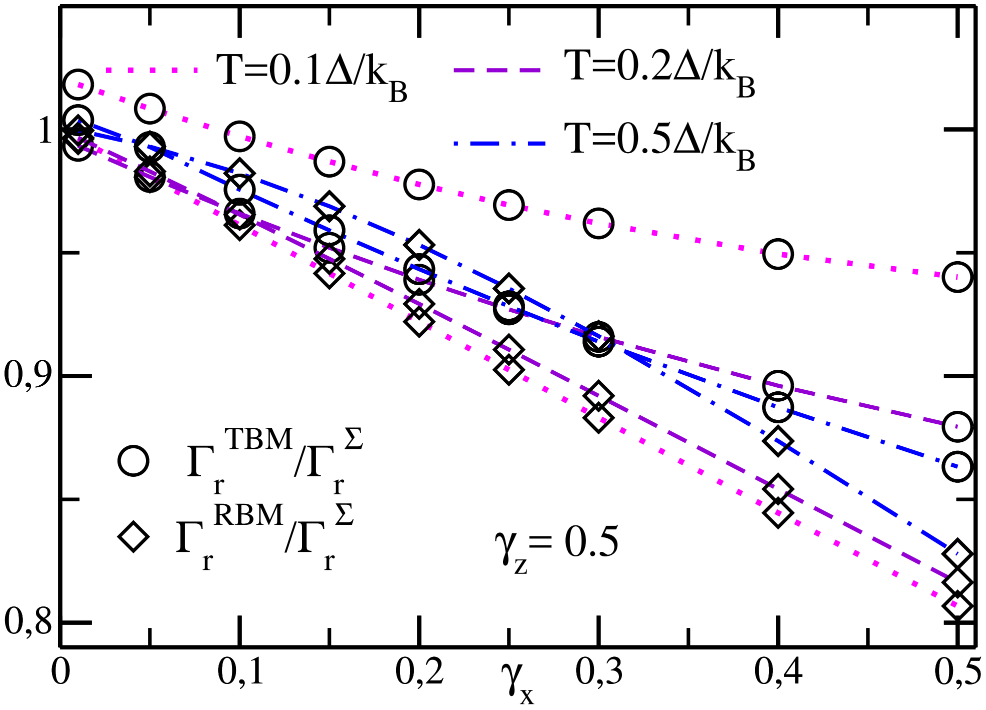

Figure 7.14: The relative relaxation rates for the TBM (circles) and the RBM (diamonds) normalized to SBM results is shown a large $\gamma_z = 0.5$ at temperatures $T = 0.1\Delta/k_B, 0.2\Delta/k_B$ and $0.5\Delta/k_B$.

In Figure 7.14 we look at the behaviour of the relative relaxation rates for three low temperatures $T = 0.1\Delta/k_B, 0.2\Delta/k_B$ and $0.5\Delta/k_B$ for a maximum relaxational coupling $\gamma_z = 0.5$, since the reduction scales with it. The reduction of the relaxation rate is apparent for all these temperatures. Uncorrelated fluctuations cause the lowest reduction for $T = 0.1\Delta/k_B$, with a maximum reduction of about 6%, while the difference for $T = 0.2\Delta/k_B$ and $T = 0.5\Delta/k_B$ is small, with a maximum reduction by about 14% for the latter. Fully correlated fluctuations on the other hand show the largest reduction for $T = 0.1\Delta/k_B$ with about 20%, though the deviations to $T = 0.2\Delta/k_B$ are small for all dephasing couplings γ_x. Interestingly, at $T = 0.5\Delta/k_\mathrm{B}$ uncorrelated and fully correlated fluctuations show non-linear behaviour, the former of concave form and the latter of convex. This leads to a region between $\gamma_x = 0.05$ and $\gamma_x = 0.3$ in which uncorrelated fluctuations reduce the relaxation rate of additive fluctuations stronger than fully correlated ones. The gradiant of the graph for fully correlated fluctuations grows while the gradiant of the graph for uncorrelated fluctuations does not. This leads to a relative reduction of the rate for $\gamma_z = 0.5$ that is almost as low as for the other two temperatures, which suggests a further reduction below them for even larger γ_z. Again to investigate this further we take a closer look to increased temperatures.

In Figure 7.15 we show larger temperature and include $T = 0.5\Delta/k_{\mathrm{B}}$ for comparability. Uncorrelated fluctuations actually cause less of a reduction for larger temperatures and appear to be linear. Larger temperatures somewhat destroy the higher order effects of uncorrelated fluctuations in the relaxation, whereas in the dephasing they enhance it. The higher order effects of fully correlated fluctuations strongly enhance the decrease of the relaxation rate. While for $T = \Delta/k_{\mathrm{B}}$ at first a convex graph is observed it becomes linear in the region $\gamma_x = 0.3$ to $\gamma_x = 0.5$. Fully correlated fluctuations also slightly increase the relaxation rate for additive fluctuations up to $\gamma_x = 0.1$ and are larger then the relaxation rates resulting from the uncorrelated fluctuations up to $\gamma_x = 0.2$. The most interesting behaviour is at $T = 2\Delta/k_{\mathrm{B}}$ for fully correlated fluctuations. At first the relaxation rate is slightly increased compared to the one from the additive fluctuations, but then immediately reduces the relaxation strongly, already being below the relaxation rate of the uncorrelated fluctuations at $\gamma_x = 0.1$. The graph goes from a convex form, to a linear form and finally to a concave form. This coincides with the transition to the overdamped regime apparent in the dephasing rate. The TLS starts it around $\gamma_x = 0.15$ and reaches the overdamped regime around $\gamma_x = 0.3$. At the largest coupling investigated, at $\gamma_z = 0.5$ and $\gamma_x = 0.5$ the reduction of the relaxation rates is 54%.

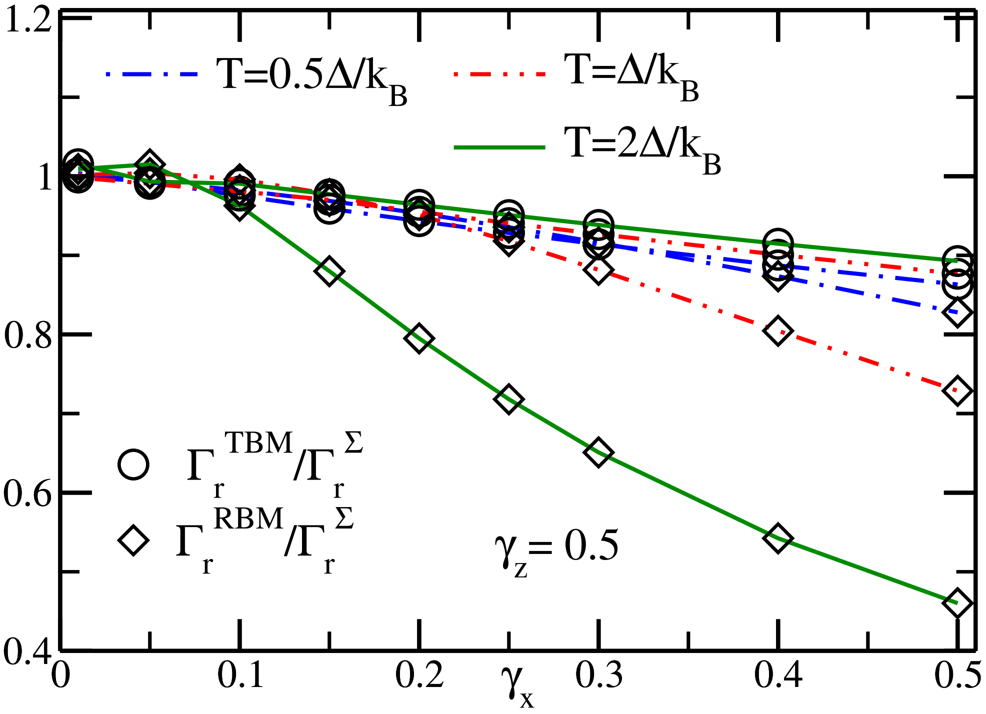

Figure 7.15: The relative relaxation rates for the TBM (circles) and the RBM (diamonds) normalized to SBM results is shown a large $\gamma_z = 0.5$ at temperatures $T = 0.5\Delta/k_B$, Δ/k_B and $2\Delta/k_B$.

7.6 Conclusion

We studied the non equilibrium dynamics of a two level system under the influence of two fully correlated, non-commuting fluctuations and under the influence of two uncorrelated, non-commuting fluctuations. Then, we compare these results to the assumption of simply adding the rates caused by each fluctuation source independently and determine if this would be a decent description. One of the fluctuations commutes with the system Hamiltonian, called dephasing fluctuation, while the other does not commute with the Hamiltonian and is called relaxational fluctuation. For temperatures smaller $T = \Delta/k_B$ we find dephasing rates resulting from uncorrelated fluctuations consistently lower then the additive effect of these fluctuations, these deviations growing with both coupling strengths. For $T = \Delta/k_B$ additive fluctuations and uncorrelated fluctuations do not show any large deviations, but for $T = 2\Delta/k_\mathrm{B}$ they do emerge. A transition to the overdamped regime has been observed at $T = 2\Delta/k_\mathrm{B}$ for a combination of large couplings of both fluctuations. Fully correlated fluctuations show a more complex behaviour. For temperatures less then $T = \Delta$ the dephasing rate consistently grows with the coupling strength to the relaxational fluctuation and is enhanced compared to the additive rate for a regime of the coupling strength for the dephasing fluctuations. Increasing this coupling strength while keeping the relaxational coupling strength constant shows how a plateau is reached, further increasing the dephasing coupling strength yields a decrease on the dephasing rate, even to less then the additive one. Furthermore, the height and width of the plateau grow for decreasing temperature. All the differences to an additive dephasing rate are less than 15% in the coupling strengths investigated. Still, this holds implications for different experimental scenarios, a superconducting charge qubit for instance. The set up of the connected gates and strengths of the voltages applied can lead to faster dephasing, thus one should vary the voltages to find an optimal regime to configure a set up. Our findings suggest instead of using one strongly coupled gate, it is better to use two gates with half the coupling strength, the lower the temperature the larger the effect.

For temperatures $T = \Delta/k_\mathrm{B}$ and $T = 2\Delta/k_B$ the fully correlated fluctuations increase the coupling strength of either fluctuation until a transition to the overdamped regime takes place. Until then the differences to the additive dephasing rate are negligible. The transition to the overdamped regime is more dependent on the dephasing fluctuations then on the relaxational fluctuations. The uncorrelated fluctuations enhance the dephasing rate in this region, compared to the additive rate. Furthermore, the transition to the overdamped rate starts at larger couplings and a completely overdamped regime was not simulated in any of the studied coupling strengths. The transition was only visible at the largest coupling strengths investigated and $T = 2\Delta/k_\mathrm{B}$. All in all additive fluctuations only describe non-commuting fluctuations accurately in certain regions, generally speaking for weak to medium system-bath couplings of either of the fluctuations. They completely fail to describe a transition to the overdamped regime for fully correlated fluctuations, where a transition was observed at an overall coupling strength to the fluctuation source below the coupling strength where either the independent boson model or the Spin-Boson model undergo a transition to the overdamped regime.

We find dephasing fluctuations consistently reduce the relaxation rate compared to the pure Spin-Boson model consistently for either fully correlated or uncorrelated fluctuations. Fully correlated fluctuations decrease the rate for low temperatures $T = 0.1\Delta/k_\mathrm{B}$ to $T = \Delta/k_\mathrm{B}$ very similarly up to a maximum decrease of almost 20% for the maximum coupling strength of dephasing investigated. For larger temperature this effect becomes more extreme, in the overdamped regime the Spin-Boson rate is even reduced by more than 50% for large dephasing fluctuation coupling strengths. Uncorrelated fluctuations reduce the Spin-Boson rate less drastically if temperatures are increased. They exhibit an interesting behaviour at low temperatures, where higher order effects resulting from the dephasing coupling strength are suppressed for increased relaxational coupling strength. These findings indicate a complete failure of additive fluctuations to describe the relaxation of a two level system under the influence of non-commuting fluctuations, either fully correlated or uncorrelated.

All in all we found certain regimes, in which additive fluctuations are an invalid assumption for the determination of the dephasing rate. The reduction of the dephasing rate is, however, not on a scale which would be desirable for qubits, where one wishes to increase the dephasing time by multiples of the ones currently achieved in experimental realisations. The large differences between the dephasing and relaxation times on the other hand are interesting for experimental set ups, allowing for an alternate explanation than simply assuming more dephasing channels. After all we find not just an increase of the dephasing rate by an additional dephasing channel but a reduction of the relaxation rate, thus an additional dephasing channel act oppositely on dephasing and relaxation. Finally, we found that a σ_x bath, as introduced, loses its pure dephasing characteristic in presence of a σ_z bath, which introduces relaxation in the system. Therefore, a similarly by choice of operators constructed pure dephasing bath in larger systems might lose the pure dephasing characteristic as well. This findings have been submitted [99].

Chapter 8

The Two Level System: Under the influence of two polarized, non-commuting baths

In this chapter, we continue to study a symmetric two-level system, this time under the influence of a sub-Ohmic pure dephasing bath and an Ohmic or sub-Ohmic relaxational bath. This describes a typical situation for superconducting phase qubits, while electromagnetic noise exhibit an Ohmic spectrum whereas the defects, normally also modelled as two-level systems, exhibit a 1/f - noise and are thus sub-Ohmic in nature, see chapter 1. We investigate specifically the non-equilibrium dynamics in case that the relaxational or the dephasing bath are polarized, i.e. when they were thermalized with either $\langle\sigma_z\rangle = q_z \neq 0$ or $\langle\sigma_x\rangle = q_x \neq 0$ fixed. The former *polarizes* the relaxational bath and results in an effective asymmetry. We investigate how an additional dephasing bath decreases this effective asymmetry. The decrease can quantitatively be tuned by the dephasing noise spectrum. Thermalizing the baths with $\langle\sigma_x\rangle = q_x \neq 0$ *polarizes* the dephasing bath and generates a shift of the coherent oscillation frequency of the TLS. We study how this frequency shift depends on the spectral function of the dephasing bath and how the relaxational bath influences it.

8.1 Model

The system-bath model is a spin coupled to two uncorrelated fluctuations as introduced in Equation (4.18). The TLS is coupled to two independent baths, one a relaxational bath $H_{SB,z}$ coupled via σ_z and the other a dephasing bath $H_{SB,x}$ coupled via σ_x. We will focus on spectral densities with exponential cut off:

$$J_\nu(\omega) = \sum_{k=1}^{M} \frac{\lambda_{k,\nu}^2 \cdot \delta(\omega - \omega_{k,\nu})}{2m_{k,\nu}\omega_{k,\nu}} =: 2\alpha_\nu \omega_c^{1-s_\nu} \omega^{s_\nu} e^{-\omega/\omega_c} \tag{8.1}$$

with $\nu = x$ or $\nu = z$. The reason for the slightly different definition of the coupling strength is, that it has been used like this in reference [126], which we use to compare our findings. This is related to the γ used before via $\gamma = 2\frac{\alpha}{\pi}$. The bath cut-off frequency is chosen to be $\omega_c = 10\Delta$ for both baths, double the value we chose to use before. α_ν is the dimensionless system-bath coupling strength and s_ν is the spectral exponent. The sub-Ohmic spin-boson problem with a σ_z - bath only shows a localization phase transition at $T = 0$ for coupling strengths $\alpha_c(s_z = 0.25) \simeq 0.022$, $\alpha_c(s_z = 0.5) \simeq 0.1065$ and $\alpha_c(s_z = 0.75) \simeq 0.3$ [127] depending on the spectral exponent s_z. For better comparability of the relaxational and dephasing fluctuations, we discuss the coupling strength ratios

$$\zeta_\nu = \alpha_\nu / \alpha_c(s_z) \tag{8.2}$$

in the following.

8.2 Observables and Bath polarization

We discuss the coherent dynamics of the TLS under the influence of a relaxational as well as a dephasing bath by explicitly investigating the time evolution of $P_z(t) = \langle\sigma_z\rangle(t)$ with initially $P_z(0) = 1$. Without baths, the TLS oscillates around zero with frequency Δ, i.e. $P_z^{(0)}(t) = \cos(\Delta t)$. To include the baths into the consideration we determine the effective time evolution $U_{\text{eff}}(t, t_0)$ of the TLS after tracing out the bath degrees of freedom. Alternatively, we directly determine the reduced density matrix $\rho(t) = U_{\text{eff}}(t, t_0)\rho(t_0)$ of the TLS.

The initial conditions of baths, which are dominated by their low frequency modes, lead to sizable deviations in the TLS dynamics. Typically, for the total initial state, a factorized statistical operator, i.e. $\rho_0 = \rho_S \otimes \rho_B$, with the initial state of the system ρ_S and of the two baths $\rho_B = \rho_{B,z} \otimes \rho_{B,x}$ is assumed. Note that assuming factorized initial conditions neglects possible strong correlation effects relevant for strong system-bath coupling. It nevertheless allows to discuss the much stronger polarization effects of a sub-Ohmic bath which is our focus here.

In thermal equilibrium, a symmetric TLS exhibits $\langle\sigma_z\rangle_{\text{eq}} = 0$. Thus, upon cooling such a TLS with only a relaxational environment at temperature T, the bath can be expected to be in thermal equilibrium with ρ_{Bz0}. Herein, we defined for a polarized bath

$$\rho_{Bvq} = \exp(-H_{SB,\nu}|_{\sigma_\nu=q}/k_\mathrm{B}T)/Z_{B,\nu q} \tag{8.3}$$

with $Z_{B,\nu q} = \mathrm{Tr}\exp(-H_{SB,\nu}|_{\sigma_\nu=q}/T)$. If instead the system plus bath is cooled down while keeping $\langle\sigma_z\rangle(t \leq 0) = 1$, the environment thermalizes to a shifted spin. This results in the shifted or polarized initial condition ρ_{Bz1}. Whereas these two different bath initial states result for an Ohmic bath only to sizeable differences on very short times of the order of $1/\omega_c$ [128], rather strong and long lived deviations are observed for a sub-Ohmic bath [126]. Specifically, the polarized bath creates an effective asymmetry ϵ for the TLS, i.e. an effective term $\epsilon\sigma_z/2$. At preparation time $t = 0$ this effective asymmetry is given by $2qE_R$ with the reorganization energy $E_R = \int_0^\infty d\omega G(\omega)/\omega \simeq 2\alpha_\nu\omega_c/s_\nu$. The effective asymmetry, however, shows a rather strong time-dependence on times scales shorter than Δ^{-1}. On the time scales we are interested in, i.e. between Δ^{-1} and the TLS dephasing time ζ_2^{-1}, the effective asymmetry is roughly time independent [126] but a simple correspondence to the reorganization energy is no longer possible. For an asymmetric TLS one would expect from weak coupling theory damped coherent oscillations with frequency $\Omega = \sqrt{\Delta^2 + \epsilon^2}$ around a long time limit $P_\infty = \epsilon/\Omega$ for a TLS with finite constant asymmetry ϵ. Thus, we determine $P_\infty = \epsilon/\Omega$ (as measure for the generated effective asymmetry) by the long time limit of our data since our longest studied times t_f fulfill $t_f \lesssim 5\zeta_2^{-1}$.

Whereas, the polarization of a relaxational bath is only achieved when cooling the bath while polarizing the spin (by applying external fields), a dephasing bath becomes polarized for any finite temperature since $P_{x.\mathrm{eq}} = \langle\sigma_x\rangle_\mathrm{eq} = -\tanh(\Delta/k_\mathrm{B}T)$. This polarization creates additional effective terms $\delta\Delta\sigma_x/2$ and, thus, shifts the oscillation frequency Ω. On the other hand, keeping $\langle\sigma_z\rangle(t \leq 0) = 1$ while cooling ensures that $P_x(t \leq 0) = 0$ and, thus, an unpolarized dephasing bath. Thus, cooling any real TLS under the influence of the two bath, typically results in a polarization of one of the two bath. In the following, we discuss various polarizations q_x of the dephasing bath and q_z of the relaxational bath which fix the corresponding bath initial states (Eq.(8.3)). For the numerical simulation we employ the QUAPI method as introduced in the previous chapters. An extension for treatment of a single polarized bath [126] was include via modifying the relevant parts of $\eta_{kk'}$, by adding various equal time correlators which can be implemented in a straight forward way.

8.3 Dynamics in polarized sub-Ohmic baths

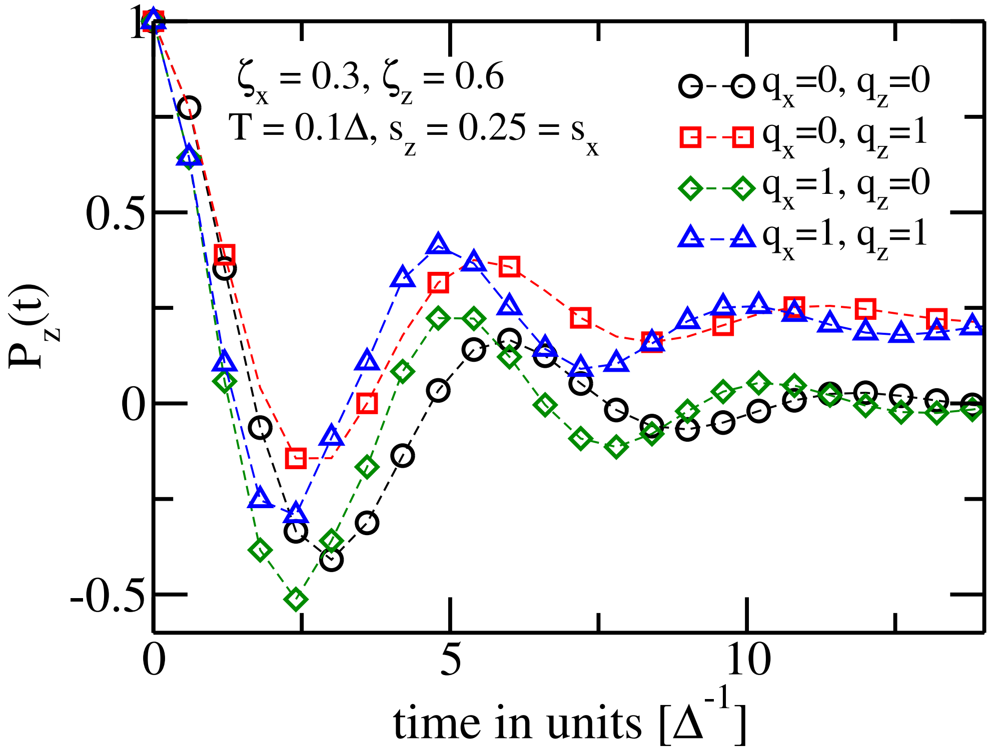

Figure 8.1: $P_z(t)$ versus time is plotted for four different polarization cases.

At first, we choose both baths with a sub-Ohmic spectrum, i.e. $s_x = 0.25$ and $s_z = 0.25$, with coupling strengths $\zeta_x = 0.3$ and $\zeta_z = 0.6$. Both baths are thermalized at a low temperature $T = 0.1\Delta$ since at high temperatures polarizations effects are diminished [126]. Fig. 8.1 plots $P_z(t)$ versus time for four different polarization cases. The black circle symbols reflect data for both baths unpolarized, i.e. $q_z = 0$ and $q_x = 0$. We observe damped coherent oscillations around zero ($P_\infty = 0$) as expected for a symmetric TLS under the influence of environmental fluctuations. A polarized relaxational bath, i.e. $q_z = 1$ and $q_x = 0$, results as expected in damped coherent oscillations around $P_\infty \simeq 0.25$ (red squares) reflecting the generated effective asymmetry. The oscillations frequency is minimally shifted (in line with $\Omega = \sqrt{\Delta^2 + \epsilon^2}$). Polarizing instead the dephasing bath, i.e. $q_z = 0$ and $q_x = 1$, leads to damped coherent oscillations (green diamonds) around zero with an increased oscillation frequency. Polarizing both baths, i.e. $q_z = 1$ and $q_x = 1$, combines both effects. The damped coherent oscillations (blue triangles) are around $P_\infty \simeq 0.25$ with an increased oscillation frequency. In the following, we discuss these effects in more detail. Specifically, we determine how an additional dephasing bath influences the effective asymmetry generated by a polarized sub-Ohmic relaxational bath. Additionally, we investigate the shifted frequency by the dephasing bath and whether and how the relaxational bath influences it.

8.4 Dephasing suppresses the effective asymmetry

A polarized sub-Ohmic relaxational bath creates an effective asymmetry [126] for the TLS. This effect is stronger for smaller s_z, i.e. more dominant slow fluctuations, but gets diminished strongly at temperatures $T \gtrsim \Delta$ [126]. The question arises whether additional fluctuations might suppress the effective asymmetry. Thus, we add to the polarized relaxational bath a second, unpolarized, dephasing bath with various coupling strength and spectral exponents.

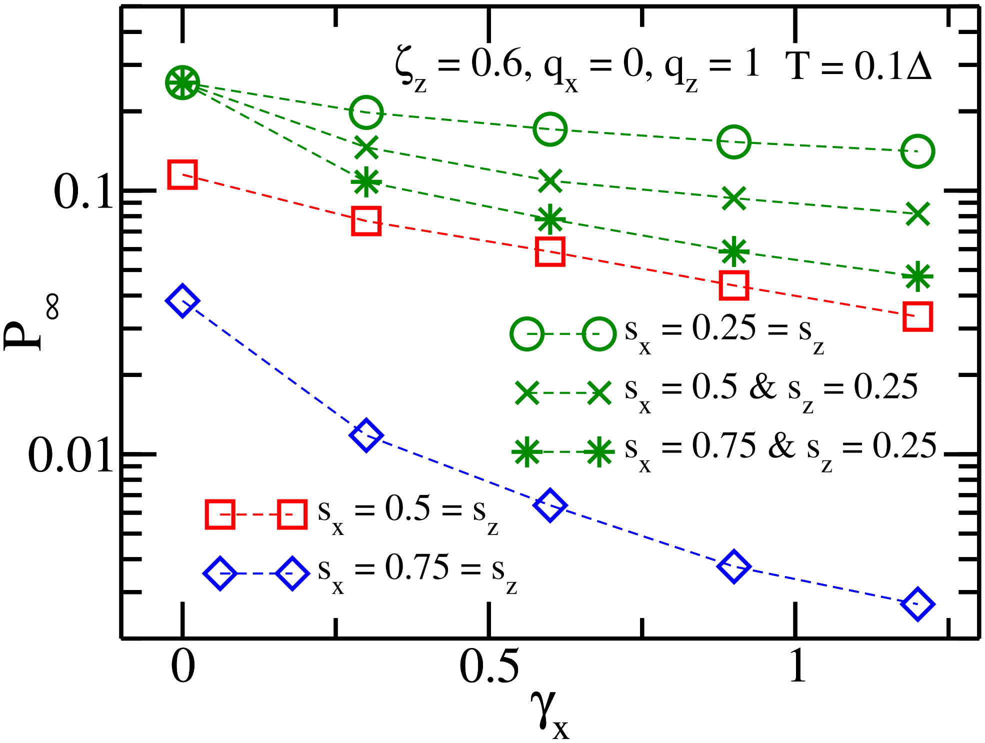

Figure 8.2: P_∞ as measure for the effective asymmetry is plotted versus the coupling strength ζ_x of the dephasing bath for various combinations of spectral exponents for the two baths.

Fig. 8.2 shows P_∞ for both baths with spectral exponents $s_x = 0.25 = s_z$ (green circles), both with $s_x = 0.5 = s_z$ (red squares) and both with $s_x = 0.75 = s_z$ (blue diamonds) plotted versus the coupling strength ζ_x of the dephasing bath. Temperature is $T = 0.1\Delta$ and the coupling strength of the relaxational bath is fixed at $\zeta_z = 0.6$. Fig. 8.2 reveals clearly that (stronger) dephasing fluctuations suppress the effective asymmetry (more). At the same time, *faster* polarized relaxational fluctuations, i.e. with larger spectral exponent s_z have a smaller effective asymmetry which decreases faster with faster dephasing fluctuations, i.e. with increasing spectral exponent s_x. *Faster* dephasing fluctuations decrease the effective asymmetry also more when the effective asymmetry is generated by the same *slow* bath as outlined by the green crosses and green stars in Fig. 8.2. Green circles, crosses and stars show data for a polarized relaxational bath with $s_z = 0.25$. The dephasing bath spectral exponent increases from $s_x = 0.25$ (green circles) over $s_x = 0.5$ (green crosses) to $s_x = 0.75$ (green stars). With increasing spectral exponent of the dephasing bath the effective asymmetry decreases stronger. Thus, *faster* fluctuations create smaller effective asymmetries and are more effective in eradicating such effective asymmetries.

8.5 Shifted Frequency

A polarized dephasing bath creates a shift of the frequency in the coherent oscillations in $P_z(t)$ as shown in Fig. 7.9. We determine $P_z(t)$ for various parameters. To obtain the oscillation frequency Ω we fit the data with $f(t) = \cos(\Omega t)\exp(-\zeta_2 t)$. Note that here no effective asymmetry is generated since the relaxational bath is unpolarized. Figure 8.3 plots the observed oscillation frequency Ω versus the polarization factor q_x of the dephasing bath.

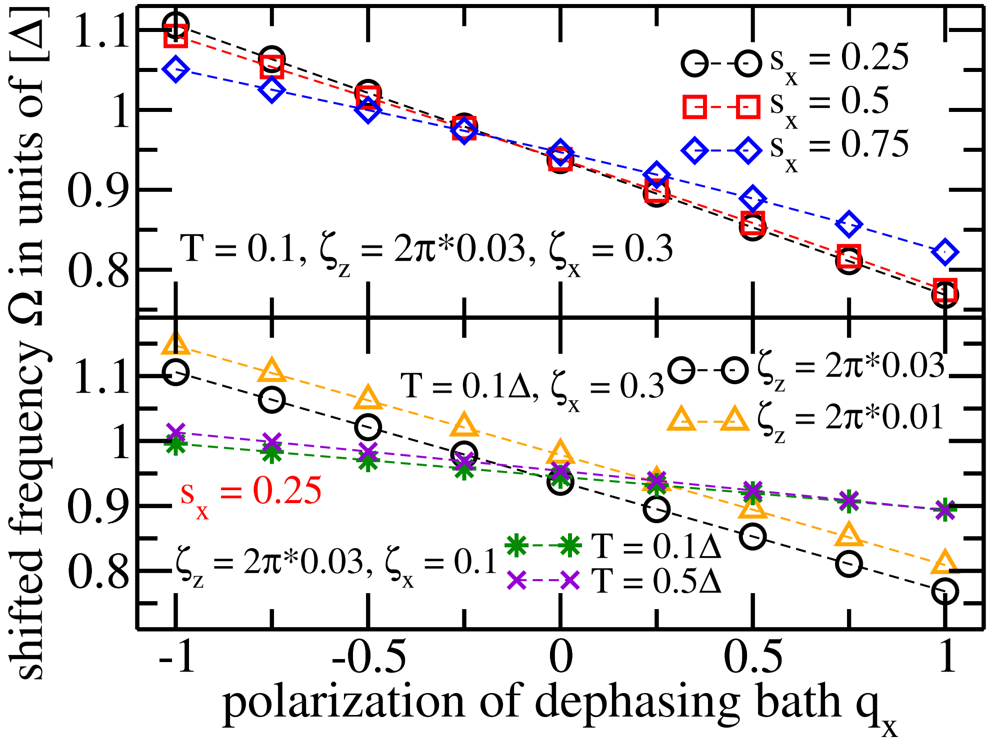

Figure 8.3: Shifted frequency Ω of the damped coherent oscillations of $P_z(t)$ is plotted versus polarization factor q_x of the dephasing bath for various temperatures and coupling strengths and spectral exponents of both baths.

We study an Ohmic relaxational bath and a sub-Ohmic polarized dephasing bath. In the upper graph of Fig. 8.3 we compare Ω versus q_x for three different spectral exponents s_x of the dephasing bath, i.e. $s_x = 0.25$ (black circles), $s_x = 0.5$ (red squares) and $s_x = 0.75$ (blue diamonds). Therein, we employ a coupling strength $\zeta_x = 0.3$ and $\zeta_z = 2\pi \cdot 0.03$ with both baths at temperature $T = 0.1\Delta$. A polarization parameter $q_x = -1$ ($q_x = 1$) reflects the situation of cooling while the TLS is kept in its ground (excited) state. We observe that for $q_x = -1$ the frequency $\Omega > \Delta$ and decreases linearly with increasing q_x. Overall, the change in Ω is roughly 30% for changing $q_x = -1$ to $q_x = 1$ for $s_x = 0.25$. As expected from the effective asymmetry, the frequency shift is smaller for larger spectral exponent s_x. Surprisingly, however, this diminishment is small, i.e. the change in Ω for $s_x = 0.5$ is still 28% and for $s_x = 0.75$ is 22%.

In the lower graph of Fig. 8.3 we compare two different coupling strengths for the relaxational couplings, i.e. $\zeta_z = 2\pi \cdot 0.03$ (black circles) and $\zeta_z = 2\pi \cdot 0.01$ (orange triangles), with $\zeta_x = 0.3$, $s_x = 0.25$ and temperature $T = 0.1\Delta$. Despite an overall shift of the frequency (due to different ζ_z), the dependence on q_x is identical in both cases. As expected a strong deviation is observed for a different coupling strength of the polarized dephasing bath (see $\zeta_x = 0.3$ (black circles) and $\zeta_x = 0.1$ (green stars) in the lower graph of Fig. 8.3 with $\zeta_z = 2\pi \cdot 0.03$, $s_x = 0.25$ and temperature $T = 0.1\Delta$). Increasing the temperature to $T = 0.5\Delta$ does not affect the q_x behaviour as can be seen by data for $T = 0.1\Delta$ (green stars) and $T = 0.5\Delta$ (violet crosses) with $\zeta_z = 2\pi \cdot 0.03$, $s_x = 0.25$ and $\zeta_x = 0.1$. Higher temperatures could not be studied since the dynamics was too strongly damped to accurately determine oscillation frequencies unless the dephasing bath coupling strength was chosen smaller. Then, however, the frequency shift was much smaller which again prevented an accurate investigation.

8.6 Conclusion

We have investigated the non-equilibrium dynamics of a symmetric two-level system (TLS) under the influence of a sub-Ohmic pure dephasing bath and an Ohmic or sub-Ohmic relaxational bath. This model reflects a typical superconducting phase qubit where two-level defects (likely within the dielectrics) exhibit environmental relaxational as well as dephasing noise with sub-Ohmic spectra. Since every cooling protocol of according devices will either polarize the relaxational or the dephasing bath, we studied the coherent dynamics of the two-level system for such polarized bath. A polarized relaxational bath generates an effective asymmetry. Baths with smaller spectral exponent create larger effective asymmetries. Strong additional dephasing fluctuations suppress the asymmetry. This suppression increases with increasing spectral exponent and coupling strength. A polarized dephasing bath generates a shift in the coherent oscillation frequency. We find, thereby, up to 30% changes of the oscillation frequency for the strongest investigated dephasing bath coupling strength. With decreasing dephasing coupling strength the shift decreases. However, the shift seems independent from the coupling strength of the relaxational bath. Thus relaxational fluctuations do not suppress the frequency shift. For temperatures $T \lesssim \Delta/2$ the frequency shift is (almost) temperature independent and it depends only weakly on the spectral exponent of the dephasing bath. These findings haven been published in reference [100].

Chapter 9

Summary and Outlook

In this thesis, non-commuting fluctuations in quantum mechanical systems have been investigated. Typically any single source of such fluctuations is assumed to consist of larger degrees of freedom then the small systems investigated, which are usually quantum mechanically modelled by focusing only on the most relevant states. The experimental set ups for such systems are subject to a multitude of environmental influences and it is difficult to distinguish the effect of a single noise source out of all of them. As a first step for a more profound description I investigated two fundamentally different types of fluctuations: relaxational as well as dephasing ones. These two fluctuations induce different dissipative properties in absence of the other and are typically treated additively in the attempts to analyse noise sources. Achieving a deeper understanding of their interplay is additionally motivated by the differences between the measured relaxation rates and dephasing rates in experimental quantum dot set ups, which are assumed to result from multiple dephasing channels compared to only a few or even only a single relaxational channel. Determining how many gates employed for controlling a quantum dot and with what relative strength to each other, might allow for optimal, therefore minimal dephasing, realisations. As a first step to analyse whether it is preferable to use more or less gates, the cases of fully correlated fluctuations resulting from one bath has been compared to the same type of uncorrelated fluctuations induced by two independent baths. While this toy model is a drastic simplification, after all no quantum dot can be controlled by a single gate or two, it provided remarkable insight.

In the first part of this thesis I extend two well established methods to describe non-commuting fluctuations from independent baths. The perturbative method showed the emergence of contributions in the relaxation rate due to dephasing fluctuations for both fully correlated and uncorrelated fluctuations. The quantitative effect was investigated in later parts of this thesis. In this part the numerical method called Quasi Adiabatic Path Integral has been extended for two non-commuting baths for arbitrary fluctuations, two non-commuting baths in the case of dephasing and relaxational fluctuations and for two sets of baths, where all baths in a set commute but baths from different sets do not commute. The code for arbitrary fluctuations was not numerically feasible at the time of this thesis, but the code for the experimental set up of interest allowed for a simplification which sufficiently reduced the requirements of the calculation.

The second part of this thesis starts with modelling dephasing and relaxational fluctuations by implementing the dephasing fluctuations in the system dynamics and treating the relaxational fluctuations in the system-bath formalism. I compared the perturbative results with the numerical ones and a large difference became apparent. In both cases increasing the dephasing in the system dynamics resulted in an initial reduction of the overall decoherence rate. For the QUAPI results this reduction became constant for large dephasing fluctuations, while the perturbative result reached a minimum and increased thereafter. The second part continues on to show the bulk of the numerical results. I investigated the two level system for multiple temperatures, dephasing system-bath couplings and relaxational system-bath couplings in terms of the decoherence and relaxation properties. For low temperature and uncorrelated fluctuations the decoherence rate is less then additive result while fully correlated fluctuations increase the decoherence rate above the additive result. For larger temperatures drastic effects emerge and fully correlated fluctuations let the two level system undergo the transition to the overdamped regime at moderate system-bath coupling strengths, where single fluctuations are far from causing a transition. Uncorrelated fluctuations enhance the decoherence rate above the additive result at high temperatures, before resulting in a transition to the overdamped regime as well at large system-bath couplings. The relaxation rate is consistently reduced by increasing the dephasing fluctuations for either uncorrelated and fully correlated fluctuations at all temperatures. The effect is larger then the reduction of the decoherence rate. Therefore many multiple dephasing channels are not necessarily the explanation for the difference between the decoherence and relaxation times, instead fewer dephasing channels which additionally reduce the relaxation rate are a possible explanation as well. I observed the emergence of higher order effects for weak relaxational coupling and moderated dephasing couplings for uncorrelated fluctuations. A perturbative weak coupling analysis treating both baths as weak is therefore no longer justified here, even though on their own both baths could be treated in such a way. A simple analysis in terms of weak system-bath coupling can therefore fail, if the dynamics of the observable investigated depend largely on only one of the fluctuations. At the end of the second part I investigated sub ohmic, polarized, non-commuting baths acting on the two level system. A polarized relaxational bath generates an effective asymmetry and smaller spectral exponents create larger effective asymmetries. Strong additional dephasing fluctuations suppress this asymmetry. This suppression increases with increasing spectral exponent and coupling strength. A polarized dephasing bath generates a shift in the coherent oscillation frequency, where decreasing dephasing coupling strength reduce the shift, while relaxational fluctuations do not suppress the frequency shift. For temperatures $T \lesssim \Delta/2$ the frequency shift is (almost) temperature independent and it depends only weakly on the spectral exponent of the dephasing bath.

There are multiple, possible projects which can continue the study of this thesis. Experimentally additional gates in set up schemes can be realised and the effect on the decoherence and relaxation can be investigated. The hierarchical equations of motion can be employed as an alternative numerical simulation and can even include a third fluctuation, not commuting with either of the other two. The extension for two non-commuting sets, a straightforward extension of the extensions derived in this thesis, remains to be employed extensively.

Appendix A

RESPET additonal information

A.1 $\mathcal{U}_{eff}$ for the RBM

The form of $U_{eff}(z)$ for the rotated bath model (RBM) is

$$U_{eff} = \begin{pmatrix} 1 & 0 & 0 & 0 \\ A_1 & \alpha_{11} & \alpha_{12} & \alpha_{13} \\ A_2 & \alpha_{21} & \alpha_{22} & \alpha_{23} \\ A_3 & \alpha_{31} & \alpha_{32} & \alpha_{33} \end{pmatrix} , \tag{A.1}$$

with: $A_1 = z^{-1}q^{-1}(\nu^2\Xi[(\nu^2\chi - z)(\mu^2\Theta + \nu^2\chi - z) - (\nu^2\chi_2 - i\Delta)^2] - (\mu\nu)^2\Sigma[\zeta(\nu^2\chi - z) + \zeta_2(\nu^2\chi_2 - i\Delta)] + (\mu\nu)^2\Phi[\zeta(\nu^2\chi_2 - i\Delta) - \zeta_2(\mu^2\Theta + \nu^2\chi - z)]$ and

$A_2 = z^{-1}q^{-1}(\mu\nu^3\Xi[\zeta(\mu^2\chi - z) - \zeta_2(\nu^2\chi_2 - i\Delta)] - (\mu\nu)\Sigma[(\mu^2\chi - z)(\nu^2\chi - z) - (\mu\nu)^2\zeta_2^2] + \mu\nu\Phi[(\mu^2\chi - z)(\nu^2\chi_2 - i\Delta) - (\mu\nu)^2\zeta\zeta_2]$ and

$A_3 = z^{-1}q^{-1}(\mu\nu^3\Xi[-\zeta(\nu^2\chi_2 - i\Delta) - \zeta_2(\mu^2\Theta + \nu^2\chi - z)] + (\mu\nu)^2\Sigma[(\mu^2\chi - z)(\nu^2\chi_2 - i\Delta) + (\mu\nu)^2\zeta\zeta_2] + (\mu\nu)\Phi[(\mu^2\chi - z)(\mu^2\Theta + \nu^2\chi - z) - (\mu\nu)^2\zeta^2]$ where $q = ((\mu^2\chi - z)(\mu^2\Theta + \nu^2\chi - z)(\nu^2\chi - z) - (\mu\nu)^2\zeta_2^2)(\mu^2\Theta + \nu^2\chi - z) - (\mu\nu)^2\zeta^2(\nu^2\chi - z) + (\nu^2\chi_2 - i\Delta)^2(\mu^2\chi - z))$ with the conventions introduced in the chapter 4.

Furthermore $\alpha_{11} = q^{-1}[(\mu^2\Theta + \nu^2\chi - z)(\nu^2\chi - z) + (\nu^2\chi_2 - i\Delta)^2]$, $\alpha_{12} = q^{-1}\mu\nu[\zeta(\nu^2\chi - z) + \zeta_2(\nu^2\chi_2 - i\Delta)]$, $\alpha_{21} = \alpha_{12} - 2q^{-1}\mu\nu\zeta_2(\nu^2\chi_2 - i\Delta)$. $\alpha_{13} = q^{-1}\mu\nu[\zeta(\nu^2\chi_2 - i\Delta) - \zeta_2(\mu^2\Theta + \nu^2\chi - z)]$, $\alpha_{31} = \alpha_{13} + 2q^{-1}\mu\nu\zeta_2(\mu^2\Theta + \nu^2\chi - z)$. $\alpha_{23} = q^{-1}[(\nu^2\chi_2 - i\Delta)(\mu^2\chi - z) - (\mu\nu)^2\zeta\zeta_2]$, $\alpha_{32} = \alpha_{23} - 2q^{-1}\nu^2\chi_2 - i\Delta)(\mu^2\chi - z)$

A.2 Calculation of $\langle\overline{x}_i\mathcal{U}_B(s-s')\overline{x}_j\mathcal{U}_B(s'-s'')\overline{x}_k\mathcal{U}_B(s''-s''')\overline{x}_l\rangle$

In Chapter 3.3.1. $\langle\overline{x}_i\mathcal{U}_B(s-s')\overline{x}_j\mathcal{U}_B(s'-s'')\overline{x}_k\mathcal{U}_B(s''-s''')\overline{x}_l\rangle$ has to be calculated. Here most of the necessary steps are shown. For reasons of clarity and comprehensibility the following conventions are used: $U_1 = U_B(s-s')$,$U_2 = U_B(s'-s'')$ and $U_3 = U_B(s''-s''')$. The fundamental relations used are $\mathcal{U}_1\rho \equiv U_1\rho U_1^\dagger$ and $\overline{x}_i\mathcal{U}_1\rho = 0.5(x_iU_1\rho U_1^\dagger + U_1\rho U_1^\dagger x_i)$

$$\begin{aligned}
&\langle\overline{x}_i\mathcal{U}_1\overline{x}_j\mathcal{U}_2\overline{x}_k\mathcal{U}_3\overline{x}_l\rangle = \langle x_i\mathcal{U}_1\overline{x}_j\mathcal{U}_2\overline{x}_k\mathcal{U}_3\overline{x}_l\rangle \\
&= \frac{1}{4}Tr\{x_iU_1(x_jU_2(x_kU_3\overline{x}_l\rho U_3^\dagger + U_3\overline{x}_l\rho U_3^\dagger x_k)U_2^\dagger + U_2(x_kU_3\overline{x}_l\rho U_3^\dagger + U_3\overline{x}_l\rho U_3^\dagger x_k)U_2^\dagger x_j)U_1^\dagger\} \\
&= \frac{E+F+G+H}{4}
\end{aligned} \tag{A.2}$$

First, we calculate E:

$$\begin{aligned}
E &= Tr\{x_iU_1x_jU_2x_kU_3\overline{x}_l\rho U_3^\dagger U_2^\dagger U_1^\dagger\} \\
&= Tr\{U_\Sigma x_iU_\Sigma U_3^\dagger U_2^\dagger x_jU_2U_3U_3^\dagger x_kU_3\overline{x}_l\rho\} = \langle x_i(s-s''')x_j(s'-s''')x_k(s''-s''')\overline{x}_l\rangle \ ,
\end{aligned} \tag{A.3}$$

where cyclic permutation of the trace and $\mathbb{1} = U_iU_i^\dagger$ was used. Now performing $\overline{x}_l\rho$ and employing the Wick theorem one can notice:

$$\begin{aligned}
&\langle x_i(s-s''')x_j(s'-s''')x_k(s''-s''')x_l\rangle + \langle x_lx_i(s-s''')x_j(s'-s''')x_k(s''-s''')\rangle \\
&= (\langle x_i(s-s''')x_l\rangle + \langle x_lx_i(s-s''')\rangle)\langle x_j(s'-s''')x_k(s''-s''')\rangle + ... \\
&= \langle x_i(s-s''')\overline{x}_l\rangle\langle x_j(s'-s''')x_k(s''-s''')\rangle + ...
\end{aligned} \tag{A.4}$$

here ... indicates the other four/two terms resulting from the Wick theorem. This results in a slightly modified version of the theorem. Using the convention to not transform $\overline{x}_l\rho$ we find :

$$\begin{aligned}
E = &\langle x_i(s-s''')\overline{x}_l\rangle\langle x_j(s'-s'')x_k\rangle + \langle x_j(s'-s''')\overline{x}_l\rangle\langle x_i(s-s'')x_k\rangle \\
&+ \langle x_k(s''-s''')\overline{x}_l\rangle\langle x_i(s-s')x_j\rangle
\end{aligned} \tag{A.5}$$

The other three terms yield:

$$\begin{aligned}
F &= Tr\{x_i U_1 x_j U_2 U_3 \bar{x}_l \rho U_3^\dagger x_k U_2^\dagger U_1^\dagger\} \\
&= Tr\{U_3^\dagger x_k U_3 U_3^\dagger U_2^\dagger U_1^\dagger x_i U_1 U_2 U_3 U_3^\dagger U_2^\dagger x_j U_2 U_3 \bar{x}_l \rho\} \\
&= \langle x_k(s''-s''') x_i(s-s''') x_j(s'-s''') \bar{x}_l \rangle \\
&= \langle x_k(s''-s''') \bar{x}_l \rangle \langle x_i(s-s') x_j \rangle + \langle x_i(s-s''') \bar{x}_l \rangle \langle x_k(s''-s') x_k \rangle \\
&\quad + \langle x_j(s'-s''') \bar{x}_l \rangle \langle x_k(s''-s) x_i \rangle
\end{aligned} \tag{A.6}$$

$$\begin{aligned}
G &= Tr\{x_i U_1 U_2 x_k U_3 \bar{x}_l \rho U_3^\dagger U_2^\dagger x_j U_1^\dagger\} \\
&= Tr\{U_3^\dagger U_2^\dagger x_j U_2 U_3 U_3^\dagger U_2^\dagger U_1^\dagger x_i U_1 U_2 U_3 U_3^\dagger x_k U_3 \bar{x}_l \rho\} \\
&= \langle x_j(s'-s''') x_i(s-s''') x_k(s''-s''') \bar{x}_l \rangle \\
&= \langle x_j(s'-s''') \bar{x}_l \rangle \langle x_i(s-s'') x_k \rangle + \langle x_i(s-s''') \bar{x}_l \rangle \langle x_j(s'-s'') x_k \rangle \\
&\quad + \langle x_k(s''-s''') \bar{x}_l \rangle \langle x_j(s'-s) x_i \rangle
\end{aligned} \tag{A.7}$$

$$\begin{aligned}
H &= Tr\{U_3^\dagger x_k U_2^\dagger x_j U_1^\dagger x_i U_1 U_2 U_3 \bar{x}_l \rho\} \\
&= Tr\{U_3^\dagger x_k U_3 U_3^\dagger U_2^\dagger x_j U_2 U_3 U_3^\dagger U_2^\dagger U_1^\dagger x_i U_1 U_2 U_3 \bar{x}_l \rho\} \\
&= \langle x_k(s''-s''') x_j(s'-s''') x_i(s-s''') \bar{x}_l \rangle \\
&= \langle x_j(s'-s) x_i \rangle \langle x_k(s''-s''') \bar{x}_l \rangle + \langle x_k(s''-s) x_i \rangle \langle x_j(s'-s''') \bar{x}_l \rangle \\
&\quad + \langle x_k(s''-s') x_j \rangle \langle x_i(s-s''') \bar{x}_l \rangle
\end{aligned} \tag{A.8}$$

Now one can use $\langle x_j(s'-s) x_i \rangle + \langle x_j(s-s') x_i \rangle = 2Re[\langle x_j(s'-s) x_i \rangle] = 2Re[2\langle x_j(s'-s) \bar{x}_i \rangle$ $-i\langle x_j(s'-s) \widetilde{x_i} \rangle] = 4\langle x_j(s'-s) \bar{x}_i \rangle$, sum over all terms and arrive at a Wick theorem for superoperators:

$$\begin{aligned}
&\langle \bar{x}_i U_1 \bar{x}_j U_2 \bar{x}_k U_3 \bar{x}_l \rangle \\
&= \langle \bar{x}_i U_1 \bar{x}_j \rangle \langle \bar{x}_k U_3 \bar{x}_l \rangle + \langle \bar{x}_i U_1 U_2 \bar{x}_k \rangle \langle \bar{x}_j U_2 U_3 \bar{x}_l \rangle + \langle x_i U_1 U_2 U_3 \bar{x}_l \rangle \langle \bar{x}_j U_2 \bar{x}_k \rangle
\end{aligned} \tag{A.9}$$

For the expectation values containing $\widetilde{x_j}$ everything is analogous, only some prefactors and the signs of F, G and H change. For the expectation values appearing in the 2-loop approximation one finds:

$$\langle \overline{x}_i U_1 \overline{x}_j U_2 \overline{x}_k U_3 \widetilde{x_l} \rangle \tag{A.10}$$
$$= 2(\langle \overline{x}_i(s-s')\overline{x}_j\rangle\langle \overline{x}_k(s-s''')\widetilde{x_l}\rangle + \langle \overline{x}(s-s'')\overline{x}_k\rangle\langle \overline{x}_j(s'-s''')\widetilde{x_l}\rangle + \langle x_i(s-s''')\bar{x}_l\rangle\langle \bar{x}_j(s-s'')\widetilde{x_k}\rangle)$$

$$\langle \overline{x}_i U_1 \widetilde{x_j} U_2 \widetilde{x_k} U_3 \overline{x}_l \rangle = 0 \tag{A.11}$$

$$\langle \overline{x}_i U_1 \overline{x}_j U_2 \widetilde{x_k} U_3 \widetilde{x_l} \rangle = -2i(\langle \overline{x_j}(s'-s''')\widetilde{x_l}\rangle\langle \overline{x_i}(s-s'')\widetilde{x_k}\rangle + \langle \overline{x_i}(s-s''')\widetilde{x_l}\rangle\langle \overline{x_j}(s'-s'')\widetilde{x_k}\rangle) \tag{A.12}$$

$$\langle \overline{x}_i U_1 \widetilde{x_j} U_2 \widetilde{x_k} U_3 \widetilde{x_l} \rangle = 0 \tag{A.13}$$

A.3 Additonal two-loop contributions in the TBM

In Chapter 4.3.1 four of the two-loop contribution to the kernel $\mathcal{V}$ were discussed. Again the convention $s_1 = \sin(s-s')$,$s_2 = \sin(s'-s'')$, $s_3 = \sin(s''-s''')$ and $c_i = s_i|\{\sin \rightarrow \cos\}$. The remaining ones are:
For the σ_x-bath only one contribution exists:

$$\widetilde{\sigma}_x U_1 \widetilde{\sigma}_x U_3 \widetilde{\sigma}_x U_3 \widetilde{\sigma}_x \sum_{ijkl} c_{i,1}c_{j,1}c_{k,1}c_{l,1}\langle \overline{x}_{i,1}\mathcal{U}_{B,1}(s-s')\overline{x}_{j,1}\mathcal{U}_{B,1}(s'-s'')\overline{x}_{k,1}\mathcal{U}_{B,1}(s''-s''')\overline{x}_{l,1}\rangle \tag{A.14}$$
$$= 16\begin{pmatrix} 0 & 0 & 0 & 0 \\ 0 & 0 & 0 & 0 \\ 0 & 0 & c_3(c_1c_2 - s_1s_2) + s_3(s_1c_2 + c_1s_2) & c_3(c_1s_2 + c_2s_1) + s_3(c_1c_2 - s_1s_2) \\ 0 & 0 & -c_3(c_1s_2 + c_2s_1) + s_3(c_1c_2 - s_1s_2) & c_3(c_1c_2 - s_1s_2) - s_3(s_1c_2 + c_!s_2) \end{pmatrix}$$
$$\times \sum_{ijkl} c_{i,1}c_{j,1}c_{k,1}c_{l,1}\langle \overline{x}_{i,1}\mathcal{U}_{B,1}(s-s')\overline{x}_{j,1}\mathcal{U}_{B,1}(s'-s'')\overline{x}_{k,1}\mathcal{U}_{B,1}(s''-s''')\overline{x}_{l,1}\rangle$$

For the σ_z-bath, next to the two contributions discussed in Chapter 4.3.1, three additional one exist:

$$\widetilde{\sigma}_z U_1 \widetilde{\sigma}_z U_3 \widetilde{\sigma}_z U_3 \overline{\sigma}_z \sum_{ijkl} c_{i,2} c_{j,2} c_{k,2} c_{l,2} \langle \overline{x}_{i,2} \mathcal{U}_{B,2}(s-s') \overline{x}_{j,2} \mathcal{U}_{B,2}(s'-s'') \overline{x}_{k,2} \mathcal{U}_{B,2}(s''-s''') \widetilde{x}_{l,2} \rangle \tag{A.15}$$

$$= -8 \begin{pmatrix} 0 & 0 & 0 & 0 \\ c_1 s_3 & 0 & 0 & 0 \\ 0 & 0 & 0 & 0 \\ 0 & 0 & 0 & 0 \end{pmatrix} \sum_{ijkl} c_{i,2} c_{j,2} c_{k,2} c_{l,2} \langle \overline{x}_{i,2} \mathcal{U}_{B,2}(s-s') \overline{x}_{j,2} \mathcal{U}_{B,2}(s'-s'') \widetilde{x}_{k,2} \mathcal{U}_{B,2}(s''-s''') \widetilde{x}_{l,2} \rangle$$

$$\widetilde{\sigma}_z U_1 \widetilde{\sigma}_z U_3 \overline{\sigma}_z U_3 \overline{\sigma}_z \sum_{ijkl} c_{i,2} c_{j,2} c_{k,2} c_{l,2} \langle \overline{x}_{i,2} \mathcal{U}_{B,2}(s-s') \overline{x}_{j,1} \mathcal{U}_{B,2}(s'-s'') \widetilde{x}_{k,2} \mathcal{U}_{B,2}(s''-s''') \widetilde{x}_{l,2} \rangle \tag{A.16}$$

$$= -4 \begin{pmatrix} 0 & 0 & 0 & 0 \\ 0 & 0 & 0 & 0 \\ 0 & 0 & 0 & 0 \\ 0 & 0 & s_2 & 0 \end{pmatrix} \sum_{ijkl} c_{i,2} c_{j,2} c_{k,2} c_{l,2} \langle \overline{x}_{i,2} \mathcal{U}_{B,2}(s-s') \overline{x}_{j,1} \mathcal{U}_{B,2}(s'-s'') \widetilde{x}_{k,2} \mathcal{U}_{B,2}(s''-s''') \widetilde{x}_{l,2} \rangle$$

$$\widetilde{\sigma}_z U_1 \overline{\sigma}_z U_3 \overline{\sigma}_z U_3 \overline{\sigma}_z \sum_{ijkl} c_{i,2} c_{j,2} c_{k,2} c_{l,2} \langle \overline{x}_{i,2} \mathcal{U}_{B,2}(s-s') \widetilde{x}_{j,1} \mathcal{U}_{B,2}(s'-s'') \widetilde{x}_{k,2} \mathcal{U}_{B,2}(s''-s''') \widetilde{x}_{l,2} \rangle \tag{A.17}$$

$$= 2 \begin{pmatrix} 0 & 0 & 0 & 0 \\ s_1 c_3 & 0 & 0 & 0 \\ 0 & 0 & 0 & 0 \\ 0 & 0 & 0 & 0 \end{pmatrix} \sum_{ijkl} c_{i,2} c_{j,2} c_{k,2} c_{l,2} \langle \overline{x}_{i,2} \mathcal{U}_{B,2}(s-s') \widetilde{x}_{j,1} \mathcal{U}_{B,2}(s'-s'') \widetilde{x}_{k,2} \mathcal{U}_{B,2}(s''-s''') \widetilde{x}_{l,2} \rangle$$

The additional contributions mixing the σ_z and the σ_x bath correlation and response functions are:

$$\widetilde{\sigma}_x U_1 \widetilde{\sigma}_x U_2 \widetilde{\sigma}_z U_3 \widetilde{\sigma}_z \sum_{k,l} c_{k,1}^2 c_{l,2}^2 C_{qq,k,\sigma_x}(s-s') C_{qq,l,\sigma_z}(s''-s''') \tag{A.18}$$

$$= 16 C_{qq,\sigma_x}(s-s') C_{qq,\sigma_z}(s''-s''') \begin{pmatrix} 0 & 0 & 0 & 0 \\ 0 & 0 & 0 & 0 \\ 0 & 0 & c_1 c_2 - s_1 s_2 & 0 \\ 0 & 0 & -s_1 c_2 - c_1 s_2 & 0 \end{pmatrix}$$

$$\widetilde{\sigma}_x U_1 \widetilde{\sigma}_z U_2 \widetilde{\sigma}_z U_3 \widetilde{\sigma}_x \sum_{k,l} c_{k,1}^2 c_{l,2}^2 C_{qq,k,\sigma_x}(s-s''') C_{qq,l,\sigma_z}(s'-s'') \tag{A.19}$$

$$= 16 C_{qq,\sigma_x}(s-s''') C_{qq,\sigma_z}(s'-s'') \begin{pmatrix} 0 & 0 & 0 & 0 \\ 0 & 0 & 0 & 0 \\ 0 & 0 & -s_1 s_3 & s_1 c_3 \\ 0 & 0 & -c_1 s_3 & c_1 c_3 \end{pmatrix}$$

$$\widetilde{\sigma}_x U_1 \widetilde{\sigma}_z U_2 \widetilde{\sigma}_z U_3 \widetilde{\sigma}_x \sum_{k,l} c_{k,1}^2 c_{l,2}^2 C_{qq,k,\sigma_x}(s-s''') C_{qq,l,\sigma_z}(s'-s'') \tag{A.20}$$

$$= 16 C_{qq,\sigma_x}(s-s''') C_{qq,\sigma_z}(s'-s'') \begin{pmatrix} 0 & 0 & 0 & 0 \\ 0 & 0 & 0 & 0 \\ 0 & 0 & -s_1 s_3 & s_1 c_3 \\ 0 & 0 & -c_1 s_3 & c_1 c_3 \end{pmatrix}$$

$$\widetilde{\sigma}_z U_1 \widetilde{\sigma}_z U_2 \widetilde{\sigma}_x U_3 \widetilde{\sigma}_x \sum_{k,l} c_{k,1}^2 c_{l,2}^2 C_{qq,k,\sigma_x}(s''-s''') C_{qq,l,\sigma_z}(s-s') \tag{A.21}$$

$$= 16 C_{qq,\sigma_x}(s'-s'') C_{qq,\sigma_z}(s-s''') \begin{pmatrix} 0 & 0 & 0 & 0 \\ 0 & 0 & 0 & 0 \\ 0 & 0 & c_2 c_3 - s_2 s_3 & c_2 s_3 + s_2 c_3 \\ 0 & 0 & 0 & 0 \end{pmatrix}$$

$$\widetilde{\sigma}_x U_1 \widetilde{\sigma}_z U_2 \overline{\sigma}_x U_3 \overline{\sigma}_z \sum_{k,l} c_{k,1}^2 c_{l,2}^2 R_{qq,k,\sigma_x}(s-s'') R_{qq,l,\sigma_z}(s'-s''') \tag{A.22}$$

$$= 4 R_{qq,\sigma_x}(s-s'') R_{qq,\sigma_z}(s'-s''') \begin{pmatrix} 0 & 0 & 0 & 0 \\ 0 & 0 & 0 & 0 \\ 0 & 0 & 0 & s_1 \\ 0 & 0 & 0 & c_1 \end{pmatrix}$$

$$\begin{aligned}
&\widetilde{\sigma}_x U_1 \widetilde{\sigma}_z U_2 \widetilde{\sigma}_x U_3 \overline{\sigma}_z \sum_{k,l} c_{k,1}^2 c_{l,2}^2 C_{qq,k,\sigma_x}(s-s'') R_{qq,l,\sigma_z}(s'-s''') \\
&= 8C_{qq,\sigma_x}(s-s'') R_{qq,\sigma_z}(s'-s''') \begin{pmatrix} 0 & 0 & 0 & 0 \\ c_1 s_2 + s_1 c_2 & 0 & 0 & 0 \\ 0 & 0 & 0 & 0 \\ 0 & 0 & 0 & 0 \end{pmatrix}
\end{aligned} \tag{A.23}$$

$$\begin{aligned}
&\widetilde{\sigma}_z U_1 \widetilde{\sigma}_x U_2 \widetilde{\sigma}_x U_3 \overline{\sigma}_z \sum_{k,l} c_{k,1}^2 c_{l,2}^2 C_{qq,k,\sigma_x}(s'-s'') R_{qq,l,\sigma_z}(s-s''') \\
&= 8C_{qq,\sigma_x}(s'-s'') R_{qq,\sigma_z}(s-s''') \begin{pmatrix} 0 & 0 & 0 & 0 \\ (s_1 s_2 - c_1 c_2) s_3 - (s_1 c_2 + c_1 s_2) c_3 & 0 & 0 & 0 \\ 0 & 0 & 0 & 0 \\ 0 & 0 & 0 & 0 \end{pmatrix}
\end{aligned} \tag{A.24}$$

Appendix B

QUAPI: additonal information

B.1 η

B.1.1 η in the original scheme

To calculate the components of η the representation of the path is of utmost importance. After the splitting of the propagator U and the insertion of the completeness relation one arrives at Equation (5.17) from which the definition of the path distribution given in Equation (5.19) followed. With the definition of a "path distribution" $\widetilde{o}$ as:

$$\begin{aligned}\widetilde{o} =& o_0(1-\Theta[t-dt/2]) + \sum_{m=1}^{N-1} o_m(\Theta[t-dt(k-1/2)] - \Theta[t-dt(k+1/2)]) \\ &+ o_N\Theta[t-dt(N-1/2)] \quad .\end{aligned} \tag{B.1}$$

It is convenient to change to the representation of the difference and sum of the coordinates o on the positive time evolution and o' on the negative time evolution, let the difference be $\xi_{i,j} = (p_i - p'_i)$ and the sum $\chi_i = (p_i + p'_i)$. Their time derivatives are:

$$\dot{\xi} = \sum_{i=0}^{N-1}[\xi_{i+1} - \xi_i]\delta(t - idt - dt/2) \quad \text{and} \quad \dot{\chi} = \sum_{i=0}^{N-1}[\chi_{i+1} - \chi_i]\delta(t - idt - dt/2) \tag{B.2}$$

Furthermore, let the second antiderivative of η be $Q(t-t') = Q' + iQ''$, where Q' is the real part and Q'' the imaginary part of Q. The second antiderivative is given by:

$$Q(t) = \frac{1}{\pi}\int_0^{\infty} d\omega \frac{J(\omega)}{\omega^2}\left\{\coth(\frac{\hbar\omega\beta}{2})(1-\cos(\omega t)) + i\sin(\omega t)\right\} \tag{B.3}$$

The conditions imposed on Q are necessary to enable $\Phi_{FV} = 0$ for $t = 0$ and the possible linear term $Q \propto t$ has to be dropped, to ensure $\mathrm{Tr}\{\rho\} = 1$. As explained in the chapter QUAPI, one is able to use the form calculated by Grabert given in Equation (5.12). This equation has to be integrated by parts twice, where $F_{FV} = \exp[-\frac{1}{\hbar}\Phi_{FV}]$. One arrives at:

$$\begin{aligned}\Phi_{FV} = &-\int_0^t dt' \int_0^{t'} dt'' \dot{\xi}(t')\left\{Q(t'-t'')\dot{o}(t'') - Q^*(t'-t'')\dot{o}'(t'')\right\} \\ &+ \xi(t)\int_0^t dt'\left\{Q(t-t')\dot{o}(t') - Q^*(t-t')\dot{o}'(t')\right\} \\ &+ \xi(t)\left\{Q(t)o(0) - Q^*(t)o'(0)\right\} - \int_{t_0}^t dt' \dot{\xi}(t')\left\{Q(t')o(0) - Q^*(t')o'(0)\right\}\end{aligned} \tag{B.4}$$

The evaluation of this integral is straightforward, yielding:

$$= -\xi_N \left\{ -q_0 Q((N-1)dt) + q'_0 Q^*((N-1)dt) + \sum_{j=1}^{N-1} q_j [Q((N-j)dt) - Q((N-1-j))] - q'_j[c.c.] \right\} \tag{B.5}$$

$$\begin{aligned}
&+ \sum_{i=1}^{N-1} \xi_i (q_i Q(dt) - q'_i Q^*(dt) + q_0(Q((i-1)dt) - Q(idt)) - q'_0[c.c.] \\
&+ \sum_{i=2} \xi_i \sum_{j=1}^{i-1} q_j \{Q((i+1-j)dt) - 2Q((i-j)dt) + Q((i-1-j)dt)\}) \\
&+ \xi_N \left\{q_N Q(dt/2) - q'_N Q^*(dt/2) - q_0 Q((N-1/2)dt) + q'_0 Q^*((N-1/2)dt)\right\} \\
&+ \xi_N \sum_{i=1}^{N-1} q_i [Q((N-1+1/2)dt) - Q((N-i-1/2)dt)] - q'_i[c.c.] \\
&+ \xi_N (q_0 Q(Ndt) - q'_0 Q^*(Ndt)) \\
&- q_0 \left\{ \xi_N Q((N-1/2)dt) - \xi_0 Q(dt/2)) + \sum_{i=1}^{N-1} \xi_i [Q((i-1/2)dt) - Q((i+1/2)dt)] \right\} \\
&+ q'_0 \left\{ \xi_N Q^*((N-1/2)dt) - \xi_0 Q^*(dt/2)) + \sum_{i=1}^{N-1} \xi_i [Q^*((i-1/2)dt) - Q^*((i+1/2)dt)] \right\}
\end{aligned}$$

The $\eta_{k,k'}$ can now be found by checking the coefficients, yielding:

$$\eta_{0,0} = \eta_{N,N} = Q(dt/2) \tag{B.6}$$

$$\eta_{N,0} = Q((N-1)dt) + Q(Ndt) - 2Q((N-1/2)dt) \tag{B.7}$$

$$\eta_{k,0} = Q((k-1)dt) - Q(kdt) + Q((k+1/2)dt) - Q((k-1/2)dt) \tag{B.8}$$

$$\eta_{N,k} = Q((N-1-k)dt) - Q((N-k)dt) + Q((N-k+1/2)dt) - Q((N-k-1/2)dt) \tag{B.9}$$

$$\eta_{k,k} = Q(dt) \tag{B.10}$$

$$\eta_{k,k'} = Q((k-k'-1)dt) + Q((k-k'+1)dt) - 2Q((k-k')dt) \tag{B.11}$$

B.1.2 η for two non-commuting baths

The Feynman-Vernon influence functional can be treated as before, the differences are in the paths used. One of the baths reproduces the previous result. This bath will not be discussed any further and the whole focus will be on the other bath, which has to be propagated over two quarter time slices ($dt/4$) in the beginning and the end instead. The path of this bath was given in Equation

(5.48). While the convention $o_{1_a,k}$ and $o_{1_b,k}$ was used in Chapter 5.5 to highlight for which bath this coordinate was used, the distinction between baths is meaningless at this point, since they are completely separated. For convenience here the convention is changed by introducing new indices defined by $(1_a, k) \equiv j = 2k$ and $(1_b, k) \equiv j = 2k + 1$. This allows a very convenient representation of the derivative of the path $\widetilde{o_1}$ as:

$$\dot{\widetilde{o_1}} = (o_1 - o_0)\delta(t - dt/4) + \sum_{l=1}^{2N-1}(o_{l+1} - o_l)\delta(t - l dt/2)) + (o_{2N+1} - o_{2N})\delta(t - Ndt + dt/4) \tag{B.12}$$

Another straightforward evaluation of the integrals to determine Φ_{FV} yields $\eta_{j,j'}$ with:

$$\eta_{0,0} = \eta_{1,1} = \eta_{2N,2N} = \eta_{2N+1,2N+1} = Q\left(dt/4\right) \tag{B.13}$$

$$\eta_{2N+1,2N} = \eta_{1,0} = Q\left(\frac{dt}{2}\right) - 2Q\left(\frac{dt}{4}\right) \tag{B.14}$$

$$\eta_{2N+1,j} = Q\left(\frac{2N+1-i}{2}dt\right) + Q\left(\frac{4N-1-2i}{4}dt\right) - Q\left(\frac{2N-i}{2}dt\right) + Q\left(\frac{4N+1-2i}{4}dt\right) \tag{B.15}$$

$$\eta_{2N+1,1} = Q\left(\frac{4N-3}{4}dt\right) + Q\left(\frac{4N+1}{4}dt\right) - 2Q\left(\frac{2N-1}{2}dt\right) \tag{B.16}$$

$$\eta_{2N+1,0} = Q\left(\frac{2N-1}{2}dt\right) + Q\left(Ndt\right) - 2Q\left(\frac{4N-1}{4}dt\right) \tag{B.17}$$

$$\eta_{2N,j} = Q\left(\frac{4N+1-2j}{4}dt\right) + Q\left(\frac{2N-j-1}{2}dt\right) - Q\left(\frac{4N-1-2j}{4}dt\right) - Q\left(\frac{2N-j}{2}dt\right) \tag{B.18}$$

$$\eta_{2N,1} = Q\left(\frac{4N+1-2j}{4}dt\right) + Q\left(\frac{2N-j-1}{2}dt\right) - Q\left(\frac{4N-1-2j}{4}dt\right) - Q\left(\frac{2N-j}{2}dt\right) \tag{B.19}$$

$$\eta_{2N,0} = Q\left(\frac{4N+3}{4}dt\right) + Q\left(\frac{4N-1}{4}dt\right) - 2Q\left(\frac{2N-1}{2}dt\right) \tag{B.20}$$

$$\eta_{j,0} = Q\left(\frac{2j-3}{4}dt\right) + Q\left(\frac{j}{2}dt\right) - Q\left(\frac{2j-1}{4}dt\right) - Q\left(\frac{j-1}{2}dt\right) \tag{B.21}$$

$$\eta_{j,j} = Q\left(\frac{dt}{2}\right) \tag{B.22}$$

$$\eta_{j,j'} = Q\left(\frac{j+1-j'}{2}dt\right) + Q\left(\frac{j+1-j'}{2}dt\right) - 2Q\left(\frac{j-j'}{2}dt\right) \tag{B.23}$$

$$\eta_{j,1} = Q\left(\frac{2j-1}{4}dt\right) + Q\left(\frac{j-2}{2}dt\right) - Q\left(\frac{j-1}{2}dt\right) - Q\left(\frac{2i-3}{4}dt\right) \tag{B.24}$$

To recover the form $\eta_{k,s;k',r}$ on can simply use the relations: $k = \frac{j-mod_2(j)}{2}$, $s = a|mod_2(j) = 0$ and $s = b|mod_2(j) = 1$. Observing the form of Equation (B.12) one can note, that the sum in the middle is the same as in the original QUAPI scheme, thus one could have already expected, that the $\eta_{j,j'}$ and

$\eta_{j,j}$ have the same form as $\eta_{k,k'}$ with the arguments of Q being halved. The calculation confirms this expectation. This justifies the interpretation of the multibath scheme, as two QUAPI schemes being employed independently, with one with halve the time slice, but the same memory as the other one. This interpretation neglects however the more complex start and endpoints condition, which are of relevance. In principle QUAPI can an extended to an arbitrary number of non-commuting sets of baths, though for each set each "original" time slice dt has to be sliced more. For B baths the necessary time slice for the B.th bath is $dt_B = \frac{dt_1}{2^{B-1}}$, while the memory $\tau_B = \tau_1$ has to stay the same, actually demanding $K_B = 2^{B-1}K_1$. Even For $B = 2$ only $K_1 = 4$ and $K_2 = 8$ were reasonable to be used for convergence investigations and not sufficient to search for convergence meaningfully. With the rise of quantum computing, these versions of QUAPI could become interesting.

Appendix C

P_z^{fit} in the overdamped regime

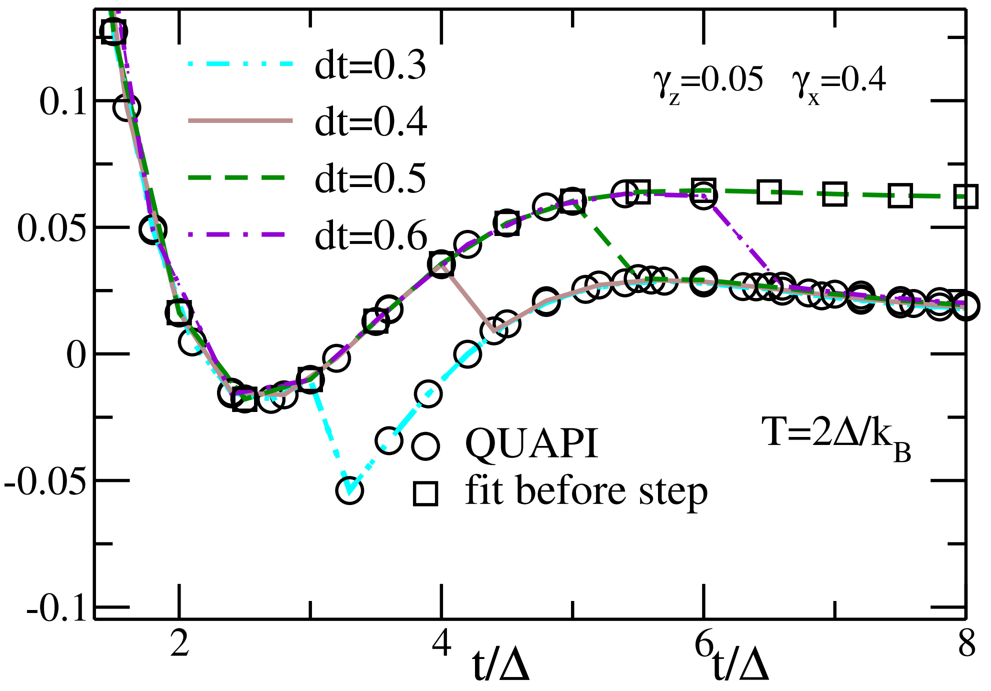

Figure C.1: $P_z(t)$ at $T = 2\Delta/k_B$ with $\gamma_z = 0.05$ and $\gamma_x = 0.4$. The Quapi parameters used are $K = 10$ and $dt = 0.3, 0.4, 0.5, 0.6$. The circles represent the QUAPI results and the squares represent the fit result P_z^{fit} to the full pathintegral before the step happens.

At large temperature and increasing system-bath coupling the system dissipative properties undergo a transition to the overdamped regime. In the overdamped regime two major problems arise. First, the correlation length increases and the neglect of $\eta_{kk'}$ is only valid for $K = k - k'$ outside of our numerical reach. This is highlighted in figure C.1, where at $K = 10$ dt was varied, yet the numerical result of $P_z(t)$ is not continuous, but has a jump visible from $t = K * dt$ to $T = (K+1)dt$, corresponding to the neglect of η_{N0}. For $dt = 0.4$ and $dt = 0.5$ the visible discontinuity becomes minimal, corresponding with the range of dt where the plateau of the convergence is identified. The jump simply magnifies the differences, which otherwise are small in for example the rate extracted or if one compares times of the simulation, which are included in the different time steps, e.g. where the dt splittings share a multiple. This also shows the dependence of the γ_x contribution to the memory, especially the η_{N0} correlation. This problem, however, we were capable to circumvent. For large temperatures most of the dynamics happens before the evaluation of the QUAPI tensor becomes necessary. Thus the $P_z^{fit}(T)$ was only used to fit to $P_z(t)$ for times $t \leq K * dt$. To further highlight the dependence on γ_x in figure C.2 in the same set up additionally $\gamma_x = 0.25$ is shown for otherwise the same parameters. The numeric result is continuous between the evaluation of the full path integral and the evaluation of the QUAPI tensor. Additionally two different fitting approaches are highlighted: The diamonds represent a fit to all data and the squares represent a fit only to the evaluation of the full path integral. While fit over the full simulation is expected to better represent the equilibrium value, it fails to accurately describe dephasing. Therefore the fit to the full path integral was used in the determination of the dephasing rate Γ_d^{RBM}

C.1 TBM vs RBM discontinuity

To understand how the discontinuity emerges, the first memory neglected should be investigated. To do this a closer look to the Feynman-Vernon influence functional is necessary. The first term neglected is given by the term $(q_N - q'_N)(\eta_{N0} q_o + [c.c.])$ in the sum of the exponential. Thus, all elements of ρ with $q_N = q'_N$ are unaffected by the neglect of η_{N0} in the scheme. For the SBM the system-bath coupling does not share the same basis as the system Hamiltonian. In the eigenbasis of σ_z, $|e_z^i\rangle$, the matrix elements $|e_z^i\rangle\langle e_z^i|$ fulfill $(q_N - q'_N) = 0$. These elements can be represented by the eigenvectors of σ_x as $0.5 * (|e_x^1 \pm e_x^2\rangle\langle e_x^1 \pm e_x^2|)$. Therefore the decoherence is not affected by the neglect of η_{N0} but the relaxation is. For the PDB, following the same line of thought, the roles of decoherence and relaxation are reversed, where the relaxation is non-existent anyway. However, the decoherence shows no sign of a discontinuity whatsoever for both the PDB and the SBM (both tested up to $\gamma = 1.8$. Interestingly, for $\gamma_z = 0.05$ an increase of γ_x form 0.25 to 0.4, see Figure C.2 in Appendix C, results in the rise of a discontinuity. This implies, fully correlated fluctuations not only mix the discontinuity of the relaxation, and therefore its stronger memory dependence in the decoherence, they also enhance the dependence. The TBM, by construction, holds the same feature as the SBM, since this is the bath with unique start and endpoints, while the part of the simulation covering the σ_x system-bath coupling does not. Thus it can not show a discontinuity, which stems from a neglect, since no such η is used. In the relaxation we observe a comparable discontinuity to the SBM.

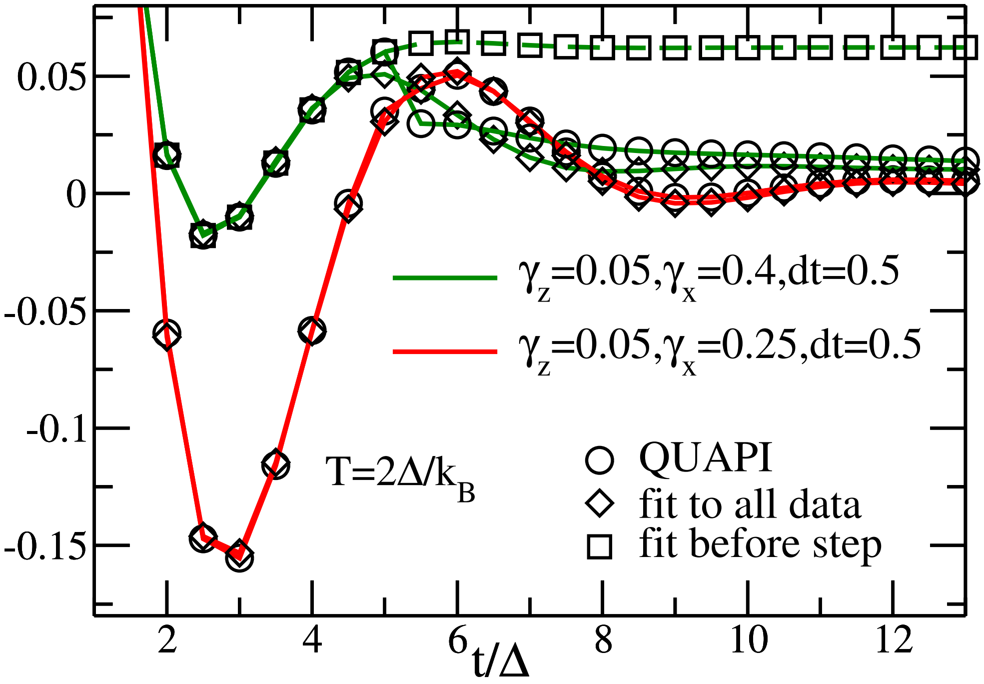

Figure C.2: $P_z(t)$ at $T = 2\Delta/k_B$ with $\gamma_z = 0.05$ and $\gamma_x = 0.4$. The Quapi parameters used are $K = 10$ and $dt = 0.5$. The circles represent the QUAPI results, the squares the fit result P_z^{fit} to the full path integral and the diamonds the fit result to the whole simulation.

Appendix D

Extension of the multibath QUAPI scheme to arbitrary number of baths

The extension is straightforward and simply takes the idea of chapter 5.4 and employs it to the multi-bath codes. Thereby extending η_1 and η_2 to (2,2) tensors, one obtains

$$\eta_{1/2,kk',jj'} = \sum_e \widetilde{\eta}_{1/2,kk',e,j,j'} \quad , \tag{D.1}$$

where $\widetilde{\eta}$ is defined as in Equation (5.36) with dummy coordinates $z_{1/2}$.

The influence functional can then be expressed for each bath as

$$\mathrm{F}_{FV,1/2,commuting} = \exp\left[-\frac{1}{\hbar}\sum_{k=0}^{N}\sum_{k'=0}^{k}(z_k - z_k')(\eta_{1/2,kk',jj'}z_{k'} - \eta^*_{kk',jj'}z_{k'}')\right] \quad . \tag{D.2}$$

This extension remains to be investigated thoroughly, so far only two non-commuting baths have been systematically studied in terms of multiple temperatures and system-bath coupling $\gamma_{x/z}$. An illustration of the usefulness of this extension can be shown by applying it to the quantum well example given in the introduction to this thesis, which was experimentally realized by Allen et al. in reference [70]. In figure 1.1 a) the connection of the top and back voltages to the quantum well are illustrated and in the paper the relationship between the energy difference Δ of the levels in the quantum well and the top Voltage V_t and back voltage V_b is given by $\Delta \propto (\alpha V_t - \beta V_b)$. In the symmetric TLS Hammiltonian this is equivalent to fluctuations in the level splitting as $\delta\Delta \propto (\alpha V_t - \beta V_b)$. As a first step for simplicity it is assumed that the baths representing both voltage gates are identical, except for coupling operators O_b and O_t, which then have the form $O_t = \alpha\sigma_x$ and $O_b = -\beta\sigma_x$. Thus the eigenvalues for each eigenvector of the system-bath coupling operators have opposite signs. The gates responsible for controlling the tunnel barrier, thus the depths of the quantum well, are more in number and do not have such a simple relationship. They will be treated similarly as the level fluctuations under the assumption that there are only two voltages instead of four. Let the barrier controlling voltages be V_c and V_d, then let the tunnel barrier be $\epsilon \propto (\chi V_c - \xi V_d)$. An extensive, numerical study employing this multi-bath code remains to be done, here only one example is be presented. Therein a two bath model is employed, having an ohmic spectral density with $\omega_c = 5\Delta$, a temperature $T = 0.2\Delta/k_\mathrm{B}$ and equal system-bath coupling strengths $\gamma_x = \gamma_z = \gamma = 0.2$ for both baths. Now an additional baths will be investigated, since the energy fluctuations in the symmetric TLS is proportional to σ_x, the two σ_x baths will be denoted with α and β, both coupled via the same γ_z but to different baths, representing an independent voltage source each. Furthermore, an additional σ_z bath will be included in the same way, both σ_z baths will be coupled via the same value of γ_z but to two independent baths. In figure D.1 the black line with stars represents a TBM as introduced in previous chapters, the red line with circles is a model where an additional σ_x-proportional bath with $\beta = 0.8$ is added, the blue lines with squares represent a model where an additional σ_z proportional bath with $\xi = 0.8$ is added and the green line with triangles shows a model with two additional baths, one proportional to σ_x with $\chi = 0.8$ and one proportional to σ_z with $\xi = 0.8$, are included. The dephasing rate increases with additional baths, as to be expected. To compare the effect of additional baths the sum of all system-bath couplings in a model should be similar. A model with parameters chosen in such a way is shown in figure D.2 and in figure D.3. The purple line represents a single bath case with, with $\chi = 1.8$, while the orange line represents a single bath case with $\chi = 1.8$. Absorbing the pre-factor of the system-bath coupling operators into γ, such that the system-bath coupling operators are normalized gives $\gamma_\Sigma = 1.8^2\gamma = 3.24\gamma$. For the model including four baths one finds the sum of all coupling strengths is equal to $\gamma_\Sigma = (2 + 2 * 0.8^2)\gamma = 3.28\gamma$ for the two bath case the pre-factors are chosen to be 1.28 since $2 * 1.28^2 = 3.2768$. Thus the overall coupling the TLS is exposed to is roughly of the same size in all four models. Finally in figure D.4 the four bath model with an overall coupling strength of $\gamma_\Sigma = 3.28$ is compared to a TBM with an overall coupling strength of $\gamma_\Sigma = 2 * 1.28^2 = 3.2768$. Here, the expectation value of σ_z is identical in the error of the simulation. Thus, in a system with two sets of non-commuting baths, where each set consists of two commuting baths coupled to the same operator but with different weights can be instead simulated by one bath. It remains to be investigated how baths coupled to different, but commuting operators, for example $O_1 = \sigma_x$, $O_2 = \mathbb{1} + \sigma_x$ and $O_3 = \mathbb{1} - \sigma_x$, change the results.

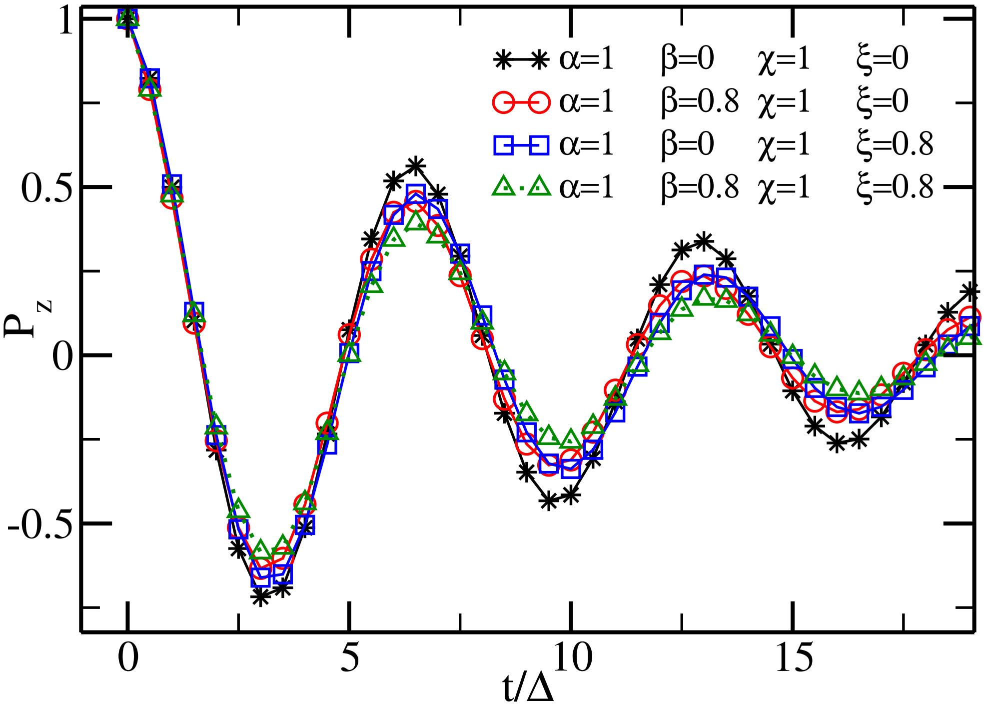

Figure D.1: $P_z(t)$ at $T = 0.2\Delta/k_B$ with $\gamma_z = \gamma_x = 0.2$ for various combinations of α, β, χ, ξ.

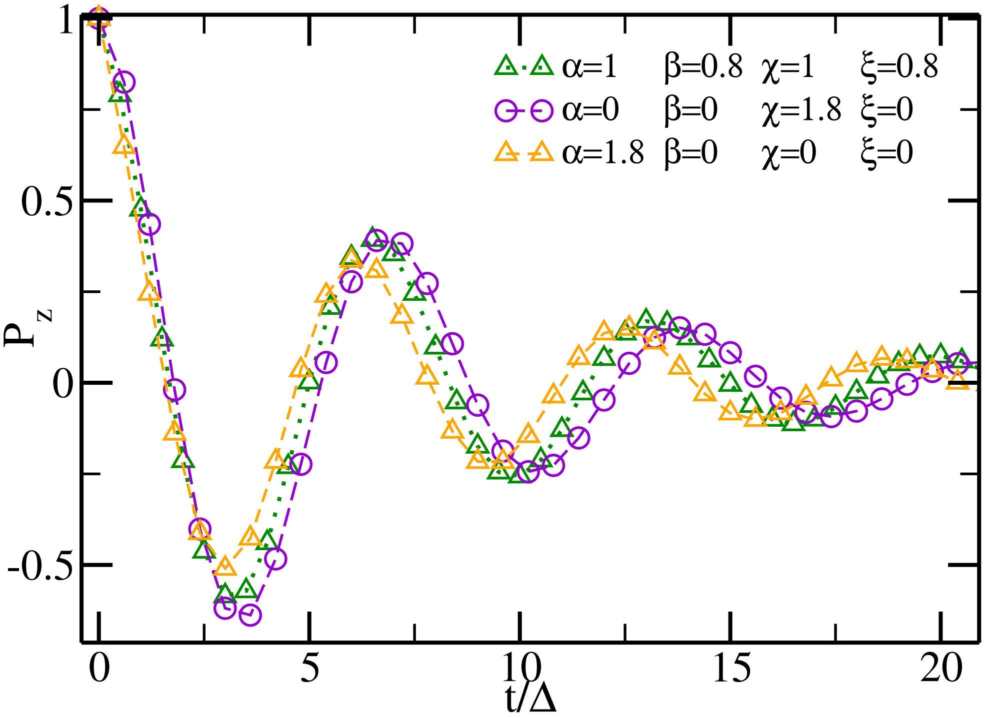

Figure D.2: $P_z(t)$ at $T = 0.2\Delta/k_B$ with $\gamma_z = \gamma_x = 0.2$ for various combinations of α, β, χ, ξ.

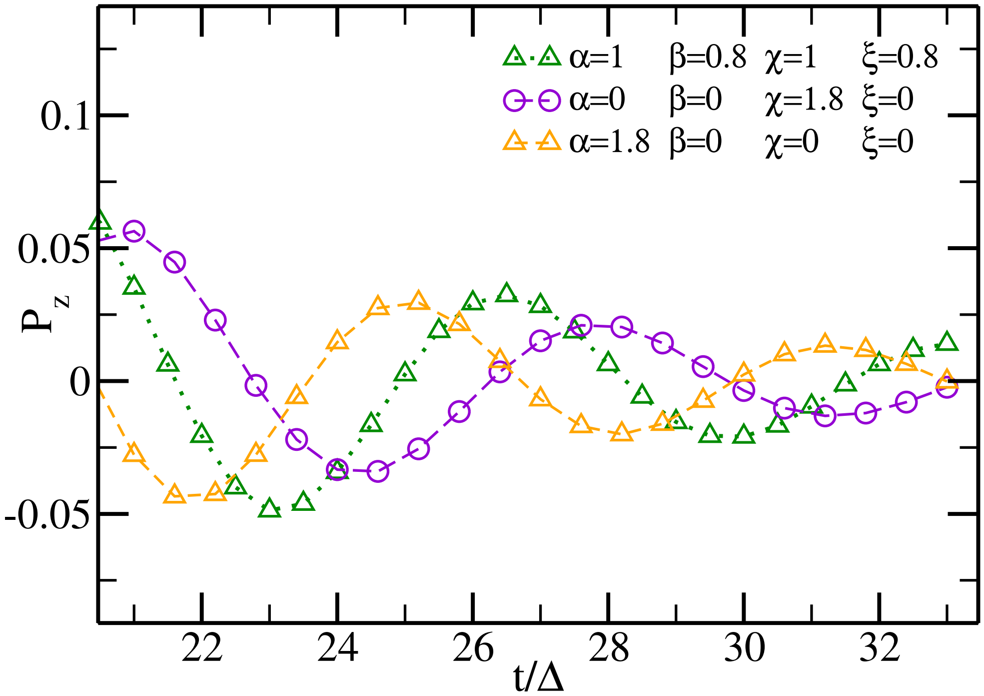

Figure D.3: $P_z(t)$ at $T = 0.2\Delta/k_B$ with $\gamma_z = \gamma_x = 0.2$ for various combinations of α, β, χ, ξ.

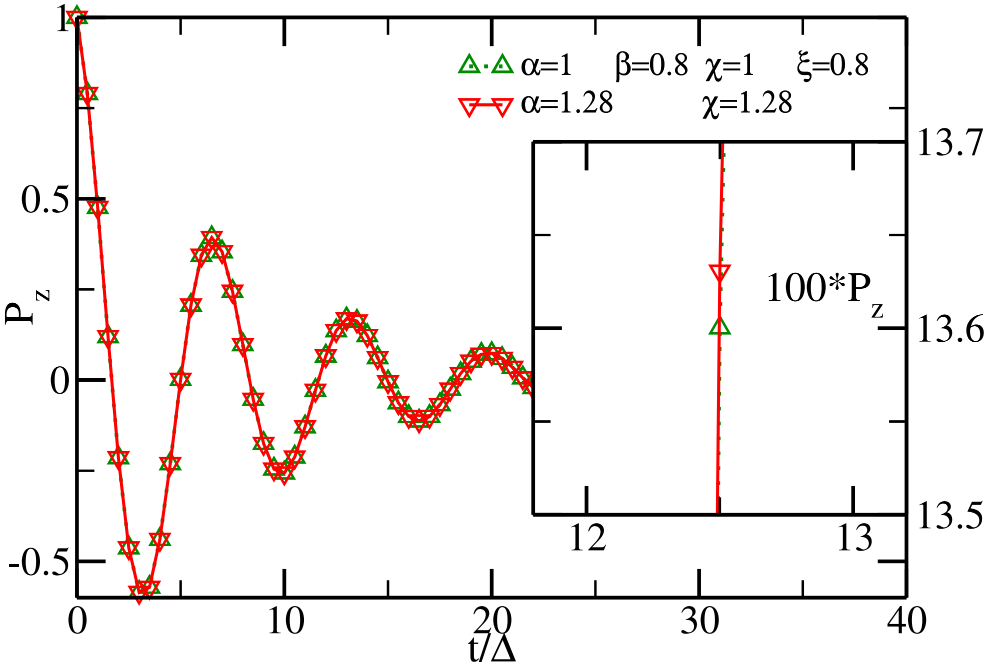

Figure D.4: $P_z(t)$ at $T = 0.2\Delta/k_B$ with $\gamma_z = \gamma_x = 0.2$ for various combinations of α, β, χ, ξ.

Bibliography

[1] L. D. Landau, “Das Dämpfungsproblem in der wellenmechanik,” *Z. Physik*, vol. 45, no. 430, 1927.

[2] J. v. Neumann, “Wahrscheinlichkeitstheoretischer Aufbau der Quantenmechanik,” *Nachrichten von der Gesellschaft der Wissenschaften zu Göttingen, Mathematisch-Physikalische Klasse*, vol. 1927, pp. 245–272, 1927.

[3] P. A. M. Dirac, “The quantum theory of the emission and absorption of radiation,” *Proceedings of the Royal Society A*, vol. 114, no. 767, p. 243265, 1927.

[4] E. Fermi, *Nuclear Physics*. University of Chicago Press, 1950.

[5] A. G. Redfield, “On the theory of relaxation processes,” *IBM Journal of Research and Development*, vol. 1, no. 1, pp. 19–31, 1957.

[6] R. Feynman and F. Vernon, “The theory of a general quantum system interacting with a linear dissipative system,” *Annals of Physics*, vol. 24, pp. 118 – 173, 1963.

[7] A. J. Leggett, S. Chakravarty, A. T. Dorsey, M. P. A. Fisher, A. Garg, and W. Zwerger, “Dynamics of the dissipative two-state system,” *Rev. Mod. Phys.*, vol. 59, pp. 1–85, 1987.

[8] U. Weiss, *Quantum Dissipative Systems*. World Scientific, 2012.

[9] R. C. Ashoori, “Electrons in artificial atoms,” *Nature*, vol. 379, no. 6564, p. 413419, 1996.

[10] M. A. Kastner, “Artificial atoms,” *Physics Today*, vol. 46, no. 1, p. 24, 1993.

[11] J. Tersoff, C. Teichert, and M. G. Lagally, “Self-organization in growth of quantum dot superlattices,” *Phys. Rev. Lett.*, vol. 76, p. 16751678, 1996.

[12] M. Holland, K. Burnett, C. Gardiner, J. I. Cirac, and P. Zoller, “Theory of an atom laser,” *Phys. Rev. A*, vol. 54, pp. R1757–R1760, 1996.

[13] S. A. Haine, J. J. Hope, N. P. Robins, and C. M. Savage, “Stability of continuously pumped atom lasers,” *Phys. Rev. Lett.*, vol. 88, p. 170403, 2002.

[14] H. Steck, M. Naraschewski, and H. Wallis, “Output of a pulsed atom laser,” *Phys. Rev. Lett.*, vol. 80, pp. 1–5, 1998.

[15] V. May and O. Kühn, *Charge and Energy Transfer Dynamics in Molecular Systems*. Wiley, Weinheim, 2004.

[16] S. Leitherer, C. M. Jäger, A. Krause, M. Halik, T. Clark, and M. Thoss, “Simulation of charge transport in organic semiconductors: A time-dependent multiscale method based on nonequilibrium green’s functions,” *Phys. Rev. Materials*, vol. 1, p. 064601, 2017.

[17] H.-G. Duan, P. Nalbach, R. J. D. Miller, and M. Thorwart, “Ultrafast energy transfer in excitonically coupled molecules induced by a nonlocal peierls phonon,” *The Journal of Physical Chemistry Letters*, vol. 10, no. 6, pp. 1206–1211, 2019.

[18] S. Mukamel, “Principles of nonlinear optical spectroscopy,” *Oxford University Press*, 1995.

[19] B. Schumacher, “Quantum coding,” *Phys. Rev. A*, vol. 51, p. 27382747, 1995.

[20] D. P. DiVincenzo, “The physical implementation of Quantum Computation,” *Fortschritte der Physik*, vol. 48, no. 911, p. 771783, 2000.

[21] T. C. Ralph, A. Gilchrist, G. J. Milburn, W. J. Munro, and S. Glancy, “Quantum computation with optical coherent states,” *Phys. Rev. A*, vol. 68, p. 042319, 2003.

[22] S. Glancy, H. M. Vasconcelos, and T. C. Ralph, “Transmission of optical coherent-state qubits,” *Phys. Rev. A*, vol. 70, p. 022317, 2004.

[23] J. S. Neergaard-Nielsen, M. Takeuchi, K. Wakui, H. Takahashi, K. Hayasaka, M. Takeoka, and M. Sasaki, “Optical continuous-variable qubit,” *Phys. Rev. Lett.*, vol. 105, p. 053602, 2010.

[24] A. P. Lund, T. C. Ralph, and H. L. Haselgrove, “Fault-tolerant linear optical quantum computing with small-amplitude coherent states,” *Phys. Rev. Lett.*, vol. 100, p. 030503, 2008.

[25] J. K. Asbóth, P. Adam, M. Koniorczyk, and J. Janszky, “Coherent-state qubits: entanglement and decoherence,” *The European Physical Journal D - Atomic, Molecular, Optical and Plasma Physics*, vol. 30, no. 3, p. 403410, 2004.

[26] W. Harneit, “Fullerene-based electron-spin quantum computer,” *Phys. Rev. A*, vol. 65, p. 032322, 2002.

[27] J. I. Cirac and P. Zoller, “Quantum computations with cold trapped ions,” *Phys. Rev. Lett.*, vol. 74, p. 40914094, 1995.

[28] A. Sørensen and K. Mølmer, “Quantum computation with ions in thermal motion,” *Phys. Rev. Lett.*, vol. 82, p. 19711974, 1999.

[29] T. Monz, K. Kim, A. S. Villar, P. Schindler, M. Chwalla, M. Riebe, C. F. Roos, H. Häffner, W. Hänsel, M. Hennrich, and R. Blatt, “Realization of universal ion-trap quantum computation with decoherence-free qubits,” *Phys. Rev. Lett.*, vol. 103, p. 200503, 2009.

[30] M. B. Plenio and P. L. Knight, “Decoherence limits to quantum computation using trapped ions,” *Proceedings of the Royal Society of London. Series A: Mathematical, Physical and Engineering Sciences*, vol. 453, no. 1965, p. 20172041, 1997.

[31] S. Gulde, M. Riebe, G. P. T. Lancaster, C. Becher, J. Eschner, H. Häffner, F. Schmidt-Kaler, I. L. Chuang, and R. Blatt, “Implementation of the deutsch-jozsa algorithm on an ion-trap quantum computer,” *Nature*, vol. 421, no. 6918, p. 4850, 2003.

[32] C. Monroe and J. Kim, “Scaling the ion trap quantum processor,” *Science*, vol. 339, no. 6124, p. 11641169, 2013.

[33] B. E. Kane, “A silicon-based nuclear spin quantum computer,” *Nature*, vol. 393, no. 6681, pp. 133–137, 1998.

[34] F. Jelezko, T. Gaebel, I. Popa, M. Domhan, A. Gruber, and J. Wrachtrup, “Observation of coherent oscillation of a single nuclear spin and realization of a two-qubit conditional quantum gate,” *Phys. Rev. Lett.*, vol. 93, p. 130501, 2004.

[35] P. Neumann, J. Beck, M. Steiner, F. Rempp, H. Fedder, P. R. Hemmer, J. Wrachtrup, and F. Jelezko, “Single-shot readout of a single nuclear spin,” *Science*, vol. 329, no. 5991, pp. 542–544, 2010.

[36] W. Harneit, “Fullerene-based electron-spin quantum computer,” *Phys. Rev. A*, vol. 65, p. 032322, 2002.

[37] M. Mehring and J. Mende, “Spin-bus concept of spin quantum computing,” *Phys. Rev. A*, vol. 73, p. 052303, 2006.

[38] A. J. Skinner, M. E. Davenport, and B. E. Kane, “Hydrogenic spin quantum computing in silicon: A digital approach,” *Phys. Rev. Lett.*, vol. 90, p. 087901, 2003.

[39] C. Song, K. Xu, W. Liu, C.-p. Yang, S.-B. Zheng, H. Deng, Q. Xie, K. Huang, Q. Guo, L. Zhang, P. Zhang, D. Xu, D. Zheng, X. Zhu, H. Wang, Y.-A. Chen, C.-Y. Lu, S. Han, and J.-W. Pan, "10-qubit entanglement and parallel logic operations with a superconducting circuit," *Phys. Rev. Lett.*, vol. 119, p. 180511, 2017.

[40] L. B. Ioffe, V. B. Geshkenbein, M. V. Feigel'man, A. L. Fauchère, and G. Blatter, "Environmentally decoupled sds -wave Josephson junctions for quantum computing," *Nature*, vol. 398, no. 6729, pp. 679–681, 1999.

[41] L. Tian and P. Zoller, "Quantum computing with atomic Josephson junction arrays," *Phys. Rev. A*, vol. 68, p. 042321, 2003.

[42] G. Wendin and V. S. Shumeiko, "Quantum bits with josephson junctions (review article)," *Low Temperature Physics*, vol. 33, no. 9, p. 724744, 2007.

[43] J. Q. You, J. S. Tsai, and F. Nori, "Scalable quantum computing with josephson charge qubits," *Phys. Rev. Lett.*, vol. 89, p. 197902, 2002.

[44] Z. Zhou, S.-I. Chu, and S. Han, "Quantum computing with superconducting devices: A three-level SQUID qubit," *Phys. Rev. B*, vol. 66, p. 054527, 2002.

[45] V. Mourik, K. Zuo, S. M. Frolov, S. R. Plissard, E. P. A. M. Bakkers, and L. P. Kouwenhoven, "Signatures of majorana fermions in hybrid superconductor-semiconductor nanowire devices," *Science*, vol. 336, no. 6084, p. 10031007, 2012.

[46] D. Litinski and F. von Oppen, "Quantum computing with majorana fermion codes," *Phys. Rev. B*, vol. 97, p. 205404, 2018.

[47] D. Aasen, M. Hell, R. V. Mishmash, A. Higginbotham, J. Danon, M. Leijnse, T. S. Jespersen, J. A. Folk, C. M. Marcus, K. Flensberg, and J. Alicea, "Milestones toward majorana-based quantum computing," *Phys. Rev. X*, vol. 6, p. 031016, 2016.

[48] C. Nayak, S. H. Simon, A. Stern, M. Freedman, and S. Das Sarma, "Non-abelian anyons and topological quantum computation," *Rev. Mod. Phys.*, vol. 80, pp. 1083–1159, 2008.

[49] M. J. L. Michael H. Freedman, Alexei Kitaev and Z. Wang, "Topological quantum computation," *Bull. Amer. Math. Soc.*, vol. 40, p. 3138, 2003.

[50] B. Lian, X.-Q. Sun, A. Vaezi, X.-L. Qi, and S.-C. Zhang, "Topological quantum computation based on chiral majorana fermions," *Proceedings of the National Academy of Sciences*, vol. 115, no. 43, pp. 10938–10942, 2018.

[51] D. Loss and D. P. DiVincenzo, "Quantum computation with quantum dots," *Phys. Rev. A*, vol. 57, p. 120126, 1998.

[52] J. Yoneda, K. Takeda, T. Otsuka, T. Nakajima, M. R. Delbecq, G. Allison, T. Honda, T. Kodera, S. Oda, Y. Hoshi, N. Usami, K. M. Itoh, and S. Tarucha, "A quantum-dot spin qubit with coherence limited by charge noise and fidelity higher than 99.9%," *Nature Nanotechnology*, vol. 13, no. 2, pp. 102–106, 2018.

[53] B. Trauzettel, D. V. Bulaev, D. Loss, and G. Burkard, "Spin qubits in graphene quantum dots," *Nature Physics*, vol. 3, no. 3, pp. 192–196, 2007.

[54] A. Imamoglu, D. D. Awschalom, G. Burkard, D. P. DiVincenzo, D. Loss, M. Sherwin, and A. Small, "Quantum information processing using quantum dot spins and cavity qed," *Phys. Rev. Lett.*, vol. 83, pp. 4204–4207, 1999.

[55] K. Eng, T. D. Ladd, A. Smith, M. G. Borselli, A. A. Kiselev, B. H. Fong, K. S. Holabird, T. M. Hazard, B. Huang, P. W. Deelman, I. Milosavljevic, A. E. Schmitz, R. S. Ross, M. F. Gyure, and A. T. Hunter, "Isotopically enhanced triple-quantum-dot qubit," *Science Advances*, vol. 1, no. 4, 2015.

[56] L. Fedichkin and A. Fedorov, "Error rate of a charge qubit coupled to an acoustic phonon reservoir," *Phys. Rev. A*, vol. 69, p. 032311, 2004.

[57] Y. Hu, H. O. H. Churchill, D. J. Reilly, J. Xiang, C. M. Lieber, and C. M. Marcus, "A Ge/Si heterostructure nanowire-based double quantum dot with integrated charge sensor," *Nature Nanotechnology*, vol. 2, no. 10, pp. 622–625, 2007.

[58] J. Gorman, D. G. Hasko, and D. A. Williams, "Charge-qubit operation of an isolated double quantum dot," *Phys. Rev. Lett.*, vol. 95, p. 090502, 2005.

[59] S.-S. Li, J.-B. Xia, J.-L. Liu, F.-H. Yang, Z.-C. Niu, S.-L. Feng, and H.-Z. Zheng, "Inas/gaas single-electron quantum dot qubit," *Journal of Applied Physics*, vol. 90, no. 12, pp. 6151–6155, 2001.

[60] J. J. L. Morton, A. M. Tyryshkin, R. M. Brown, S. Shankar, B. W. Lovett, A. Ardavan, T. Schenkel, E. E. Haller, J. W. Ager, and S. A. Lyon, "Solid-state quantum memory using the 31p nuclear spin," *Nature*, vol. 455, no. 7216, pp. 1085–1088, 2008.

[61] D. E. Liu and H. U. Baranger, "Detecting a Majorana-fermion zero mode using a quantum dot," *Phys. Rev. B*, vol. 84, p. 201308, 2011.

[62] M. Leijnse and K. Flensberg, “Scheme to measure Majorana fermion lifetimes using a quantum dot,” *Phys. Rev. B*, vol. 84, p. 140501, 2011.

[63] T. Karzig, C. Knapp, R. M. Lutchyn, P. Bonderson, M. B. Hastings, C. Nayak, J. Alicea, K. Flensberg, S. Plugge, Y. Oreg, C. M. Marcus, and M. H. Freedman, “Scalable designs for quasiparticle-poisoning-protected topological quantum computation with Majorana zero modes,” *Phys. Rev. B*, vol. 95, p. 235305, 2017.

[64] D. Bimberg, N. Kirstaedter, N. N. Ledentsov, Z. I. Alferov, P. S. Kop’ev, and V. M. Ustinov, “Ingaas-gaas quantum-dot lasers,” *IEEE Journal of Selected Topics in Quantum Electronics*, vol. 3, no. 2, pp. 196–205, 1997.

[65] A. Nozik, “Quantum dot solar cells,” *Physica E: Low-dimensional Systems and Nanostructures*, vol. 14, no. 1, pp. 115 – 120, 2002.

[66] P. V. Kamat, J. A. Christians, and J. G. Radich, “Quantum dot solar cells: Hole transfer as a limiting factor in boosting the photoconversion efficiency,” *Langmuir*, vol. 30, no. 20, pp. 5716–5725, 2014. PMID: 24669885.

[67] H. Ishikuro and T. Hiramoto, “Quantum mechanical effects in the silicon quantum dot in a single-electron transistor,” *Applied Physics Letters*, vol. 71, no. 25, pp. 3691–3693, 1997.

[68] A. Shnirman, Y. Makhlin, Y. Makhlin, and G. Hön, “Noise and decoherence in quantum two-level systems,” *Physica Scripta*, vol. T102, no. 1, p. 147, 2002.

[69] Y. Yao, N. Zhou, and J. Prior, “Competition between diagonal and off-diagonal coupling gives rise to charge-transfer states in polymeric solar cells,” *Scientific Reports*, vol. 5, no. 14555, 2015.

[70] M. T. Allen, J. Martin, and A. Yacoby, “Gate-defined quantum confinement in suspended bilayer graphene,” *Nature communications*, vol. 3, p. 934, 2012.

[71] P. Recher, J. Nilsson, G. Burkard, and B. Trauzettel, “Bound states and magnetic field induced valley splitting in gate-tunable graphene quantum dots,” *Physical Review B*, vol. 79, pp. 085407–085411, 2009.

[72] G. M. Moy, J. J. Hope, and C. M. Savage, “Born and markov approximations for atom lasers,” *Phys. Rev. A*, vol. 59, pp. 667–675, 1999.

[73] G. Lindblad, “On quantum statistical mechanics of non - hamiltonian systems,” *Communications in Mathematical Physics*, vol. 48, pp. 119 – 130, 1976.

[74] A. Kossakowski, “On quantum statistical mechanics of non-hamiltonian systems,” *Reports on Mathematical Physics*, vol. 3, no. 4, pp. 247 – 274, 1972.

[75] V. Gorini, A. Kossakowski, and E. C. G. Sudarshan, “Completely positive dynamical semigroups of systems,” *Journa of Mathematical Physics*, vol. 17, no. 5, pp. 821–825, 1976.

[76] P. Dutta and P. M. Horn, “Low-frequency fluctuations in solids: 1f noise,” *Rev. Mod. Phys.*, vol. 53, no. 3, p. 497, 1981.

[77] M. B. Weissman, “1f noise and other slow, nonexponential kinetics in condensed matter,” *Rev. Mod. Phys.*, vol. 60, no. 2, p. 537, 1988.

[78] A. B. Zorin, F. J. Ahlers, J. Niemeyer, T. Weimann, H. Wolf, V. A. Krupenin, and L. S. V, “Background charge noise in metallic single-electron tunneling devices,” *Phys. Rev.*, vol. 53, no. 20, p. 13682, 1996.

[79] J. Bergli, Y. M. Galperin, and B. L. Altshuler, “Decoherence in qubits due to low-frequency noise,” *New Journal of Physics*, vol. 11, no. 2, p. 025002, 2009.

[80] M. T. Mitchison and M. B. Plenio, “Non-additive dissipation in open quantum networks out of equilibrium,” *New Journal of Physics*, vol. 20, no. 3, p. 033005, 2018.

[81] M. J. W. Hall, J. D. Cresser, L. Li, and E. Andersson, “Canonical form of master equations and characterization of non-Markovianity,” *Phys. Rev. A*, vol. 89, p. 042120, 2014.

[82] H. Grabert, P. Schramm, and G.-L. Ingold, “Quantum Brownian motion: The functional integral approach,” *Physics Reports*, vol. 168, no. 3, pp. 115 – 207, 1988.

[83] N. Makri and D. E. Makarov, “Tensor propagator for iterative quantum time evolution of reduced density matrices. I. theory,” *The Journal of Chemical Physics*, vol. 102, no. 11, pp. 4600–4610, 1995.

[84] A. Ishizaki and Y. Tanimura, “Quantum dynamics of system strongly coupled to low-temperature colored noise bath: reduced hierarchy equations approach,” *Journal of the Physical Society of Japan*, vol. 74, no. 12, pp. 3131–3134, 2005.

[85] Y. Tanimura, “Nonperturbative expansion method for a quantum system coupled to a harmonic-oscillator bath,” *Physical Review A*, vol. 41, no. 12, p. 6676, 1990.

[86] N. Makri, “Improved Feynman propagators on a grid and non-adiabatic corrections within the path integral framework,” *Chemical Physics Letters*, vol. 193, no. 5, pp. 435–445, 1992.

[87] A. O. Caldeira and A. J. Leggett, “Influence of dissipation on quantum tunneling in macroscopic systems,” *Phys. Rev. Lett.*, vol. 46, pp. 211–214, 1981.

[88] U. Weiss, H. Grabert, and S. Linkwitz, “Influence of friction and temperature on coherent quantum tunneling,” *Journal of Low Temperature Physics*, vol. 68, no. 3-4, pp. 213–244, 1987.

[89] D. Suess, A. Eisfeld, and W. T. Strunz, “Hierarchy of stochastic pure states for open quantum system dynamics,” *Phys. Rev. Lett.*, vol. 113, p. 150403, 2014.

[90] L. Keldysh, “Diagram technique for nonequilibrium processes,” *Soviet Physics(JETP)*, vol. 20, pp. 1515–1527, 1965.

[91] A. Kamenev, *Field Theory of Non-Equilibrium Systems.* Cambridge University Press, 2011.

[92] L. Pollet, “Recent developments in quantum monte carlo simulations with applications for cold gases,” *Reports on Progress in Physics*, vol. 75, no. 9, p. 094501, 2012.

[93] E. Gull, A. J. Millis, A. I. Lichtenstein, A. N. Rubtsov, M. Troyer, and P. Werner, “Continuous-time monte carlo methods for quantum impurity models,” *Rev. Mod. Phys.*, vol. 83, pp. 349–404, 2011.

[94] P. Nalbach, D. Braun, and M. Thorwart, “Exciton transfer dynamics and quantumness of energy transfer in the fenna-matthews-olson complex,” *Physical Review E*, vol. 84, no. 4, p. 041926, 2011.

[95] N. Makri and D. E. Makarov, “Tensor propagator for iterative quantum time evolution of reduced density matrices. II. numerical methodology,” *The Journal of Chemical Physics*, vol. 102, no. 11, pp. 4611–4618, 1995.

[96] P. Nalbach, J. Eckel, and M. Thorwart, “Quantum coherent biomolecular energy transfer with spatially correlated fluctuations,” *New Journal of Physics*, vol. 12, no. 6, p. 065043, 2010.

[97] T. Palm and P. Nalbach, “Quasi-adiabatic path integral approach for quantum systems under the influence of multiple non-commuting fluctuations,” *The Journal of Chemical Chysics*, vol. 149, no. 21, p. 214103, 2018.

[98] T. Palm and P. Nalbach, “Nonperturbative environmental influence on dephasing,” *Physical Review A*, vol. 96, no. 3, p. 032105, 2017.

[99] T. Palm and P. Nalbach, “Dephasing frustrates relaxation.” forthcoming.

[100] T. Palm and P. Nalbach, “Dephasing and relaxational polarized sub-ohmic baths acting on a two-level system,” *The Journal of Chemical Physics*, vol. 150, no. 23, p. 234108, 2019.

[101] A. Nitzan, *Chemical Dynamics in Condensed Phases*. Oxford, 2012.

[102] M. Thorwart, J. Eckel, and E. R. Mucciolo, “Non-Markovian dynamics of double quantum dot charge qubits due to acoustic phonons,” *Phys. Rev. B*, vol. 72, p. 235320, 2005.

[103] F. Shibata and N. Hashitsume, “Master equations for coupled systems,” *Zeitschrift für Physik B Condensed Matter*, vol. 34, no. 2, pp. 197–201, 1979.

[104] D. E. Makarov, *The Master Equation Approach to Problems in Chemical and Biological Physics*. John Wiley & Sons, 2017.

[105] H. Spohn and J. L. Lebowitz, *Irreversible Thermodynamics for Quantum Systems Weakly Coupled to Thermal Reservoirs*. John Wiley & Sons, 2007.

[106] H. Maguire, J. Iles-Smith, and A. Nazir, “Environmental nonadditivity and franck-condon physics in nonequilibrium quantum systems,” *Phys. Rev. Lett.*, vol. 123, p. 093601, 2019.

[107] E. T. Jaynes and F. W. C. Cummings, “Comparison of quantum and semiclassical radiation theories with application to the beam maser,” *Proceedings of the IEEE*, vol. 51, no. 1, pp. 89–109, 1963.

[108] C. Müller, J. Cole, and J. Lisenfeld, “Towards understanding two-level-systems in amorphous solids - insights from quantum devices,” *Reports on Progress in Physics*, vol. 82, 2017.

[109] A. Leggett and D. Vural, “The "tunneling two-level systems" model of the low-temperature properties of glasses: Are "smoking-gun" tests possible?,” *The journal of physical chemistry. B*, vol. 117, 2013.

[110] W. G. van der Wiel, T. Fujisawa, S. Tarucha, and L. P. Kouwenhoven, “A double quantum dot as an artificial two-level system,” *Japanese Journal of Applied Physics*, vol. 40, no. No 3B, p. 21002104, 2001.

[111] H.-G. Duan, P. Nalbach, R. J. D. Miller, and M. Thorwart, “Ultrafast energy transfer in excitonically coupled molecules induced by a nonlocal peierls phonon,” *The Journal of Physical Chemistry Letters*, vol. 10, no. 6, pp. 1206–1211, 2019.

[112] D. Wang, H. Kelkar, and D. Martin-Cano, “Turning a molecule into a coherent two-level quantum system,” *Nature Physics*, vol. 15, p. 483489, 2019.

[113] P. Nalbach and M. Thorwart, “Multiphonon transitions in the biomolecular energy transfer dynamics,” *The Journal of Chemical Physics*, vol. 132, no. 19, 2010.

[114] A. Würger, “Perturbation theory for the spin-phonon model,” *Journal of Physics: Condensed Matter*, vol. 9, no. 26, p. 5543, 1997.

[115] S. Chatterjee and N. Makri, “Real-time path integral methods, quantum master equations, and classical vs quantum memory,” *The Journal of Physical Chemistry B*, vol. 123, no. 49, pp. 10470–10482, 2019. PMID: 31721584.

[116] R. Feynman and A. Hibbs, *Quantum mechanics and path integrals*. International series in pure and applied physics, McGraw-Hill, 1965.

[117] R. P. Feynman and J. Shaham, *Statistical mechanics : a set of lectures / R.P. Feynman ; notes taken by R. Kikuchi and H.A. Feiveson, edited by Jacob Shaham*. W.A. Benjamin Reading, Mass, 1972.

[118] L. Schulman, *Techniques and Applications of Path Integration*. J. Wiley and Sons, 1981.

[119] M. Thorwart, P. Reimann, and P. Hänggi, “Iterative algorithm versus analytic solutions of the parametrically driven dissipative quantum harmonic oscillator,” *Phys. Rev. E*, vol. 62, pp. 5808–5817, 2000.

[120] C. Mujica-Martinez, P. Nalbach, and M. Thorwart, “Quantification of non-markovian effects in the fenna-matthews-olson complex,” *Physical Review. E, Statistical, nonlinear, and soft matter physics*, vol. 88, p. 062719, 2013.

[121] P. Nalbach, C. Mujica-Martinez, and M. Thorwart, “Vibronic speed-up of the excitation energy transfer in the fenna-matthews-olson complex,” *Physical Review. E, Statistical, nonlinear, and soft matter physics*, vol. 91, 2013.

[122] Y. Tanimura and R. Kubo, “Time evolution of a quantum system in contact with a nearly gaussian-markoffian noise bath,” *Journal of the Physical Society of Japan*, vol. 58, no. 1, pp. 101–114, 1989.

[123] D. Suess, A. Eisfeld, and W. T. Strunz, “Hierarchy of stochastic pure states for open quantum system dynamics,” *Phys. Rev. Lett.*, vol. 113, p. 150403, 2014.

[124] P.-P. Zhang, C. D. B. Bentley, and A. Eisfeld, “Flexible scheme to truncate the hierarchy of pure states,” *The Journal of Chemical Physics*, vol. 148, 2018.

[125] A. Strathearn, B. W. Lovett, and P. Kirton, “Efficient real-time path integrals for non-markovian spin-boson models,” *New Journal of Physics*, vol. 19, no. 9, p. 093009, 2017.

[126] P. Nalbach and M. Thorwart, “Ultraslow quantum dynamics in a sub-ohmic heat bath,” *Phys. Rev. B*, vol. 81, p. 054308, 2010.

[127] A. Winter, H. Rieger, M. Vojta, and R. Bulla, “Quantum phase transition in the sub-ohmic spin-boson model: Quantum monte carlo study with a continuous imaginary time cluster algorithm,” *Phys. Rev. Lett.*, vol. 102, p. 030601, 2009.

[128] A. Lucke, C. H. Mak, R. Egger, J. Ankerhold, J. Stockburger, and H. Grabert, “Is the direct observation of electronic coherence in electron transfer reactions possible?,” *The Journal of Chemical Physics*, vol. 107, no. 20, pp. 8397–8408, 1997.

Dankessagungen

Als erstes möchte ich mich bei Prof. Dr. Peter Nalbach bedanken, der mir dieses spannende Thema vorschlug und es mir ermöglichte an internationalen Konferenzen teilzunehmen, viele interessante Physiker kennen zu lernen und an den mir gestellten Aufgaben zu wachsen. Die vergangen Jahre waren eine schöne Zeit, für die vielen interessanten Gespräche und die neuen Blickwinkel auf die Physik und die Welt im Allgemeinen bin ich sehr dankbar bin. Ich hab dank ihm meine Sicht auf Nichtgleichgewichtsdynamik grundlegend geändert und eine verblüffend schöne Störungsrechnung kennengelernt. Peter Nalbach stand mir in den gesamten Zeitraum mit Rat und Tat sowie viel Geduld zur Seite und hat mich kontinuierlich unterstützt. Seine positive Natur und Hilfsbereitschaft sind inspirierend. Vielen Dank für alles!

Weiter möchte ich mich ausdrücklich bei Michael Thorwart bedanken, auch er stand mir immer mit Rat und Tat zur Seite. Durch ihn habe ich in meiner Masterarbeit QUAPI kennen gelernt und die Gespräche mit ihm über numerische Methoden und das Spin-Boson Problem waren immens hilfreich für diese Arbeit. Er hat mich herzlich in seiner Arbeitsgruppe in Hamburg aufgenommen und es mir ermöglicht eine breite Menge modernen Forschungsthemen kennen zu lernen, von Mayorana Fermionen und Skyrmionen hin zu getriebenen Systemen und molekularen Dynamiken. Die Vielfalt der Forschungsthemen in seiner Arbeitsgruppe erstaunt mich immernoch und Teil dieser gewesen zu sein, sehe ich als Privileg an, für das ich sehr dankbar bin.

Ausserdem möchte ich mich noch bei all den Mitgliedern dieser tollen Arbeitsgruppe bedanken, die ich kennenlernen durfte. Alle haben sich gerne Zeit genommen und ihre Forschungsthemen vorgestellt. Auch die vielen nicht physikbezogenen Gespräche haben mir Freude bereitet und ich werde das gemeinsame Mittagessen vermissen. Es war immer spannend Menschen mit so unterschiedlichen Hintergründen und Meinungen im offen Austausch zu erleben.

Ich hatte das Glück finanzielle Unterstützung durch das Projekt Nummer NA394/2-1 der Deutsche Forschungsgesellschaft zu Erhalten.

Schlußendlich danke ich meinen Freunden und meiner Familie, die mich auf meinem Weg begleiten und ohne deren Unterstützung diese Arbeit nicht möglich gewesen wäre.

Eidesstattliche Versicherung/ Declaration on oath

Hiermit versichere ich an Eides statt, die vorliegende Dissertationsschrift selbst verfasst und keine anderen als die angegebenen Hilfsmittel und Quellen benutzt zu haben.

Die eingereichte schriftliche Fassung entspricht der auf dem elektronischen Speichermedium.

Die Dissertation wurde in der vorgelegten oder einer ähnlichen Form nicht schon einmal in einem früheren Promotionsverfahren angenommen oder als ungenügend beurteilt.

Hamburg, den 02.03.2020

Timo Palm